Lectures on Detector Techniques
Stanford Linear Accelerator Center
September 1998 – February, 1999

Semiconductor Detectors
Part 2

Helmuth Spieler

Physics Division
Lawrence Berkeley National Laboratory

copies of these notes available at
http://www-physics.lbl.gov/~spieler/SLAC_Lectures

for more details see UC Berkeley Physics 198 course notes
at http://www-physics.lbl.gov/~spieler

Signal Acquisition

- Determine energy deposited in detector

- Detector signal generally a short current pulse

  Typical durations

Thin silicon detector (10 ... 300 m thick):	100 ps – 30 ns
Thick (~cm) Si or Ge detector:	1 – 10 μs
Proportional chamber (gas):	10 ns – 10 μs
Gas microstrip or microgap chamber:	10 – 50 ns
Scintillator + PMT/APD:	100 ps – 10 μs

  The total charge Q_s contained in the detector current pulse is $i_s(t)$ proportional to the energy deposited in the detector

  $$E \propto Q_s = \int i_s(t)\, dt$$

- Necessary to integrate the detector signal current.

  Possibilities: 1. Integrate charge on input capacitance

                       2. Use integrating ("charge sensitive") preamplifier

                       3. Amplify current pulse and use integrating ("charge sensing") ADC

Signal integration on Input Capacitance

$$R_i \cdot (C_{DET} + C_i) \gg \text{COLLECTION TIME } t_c$$

$$V_s = \frac{Q_s}{C_{DET} + C_i}$$

↑

System response depends on detector capacitance !
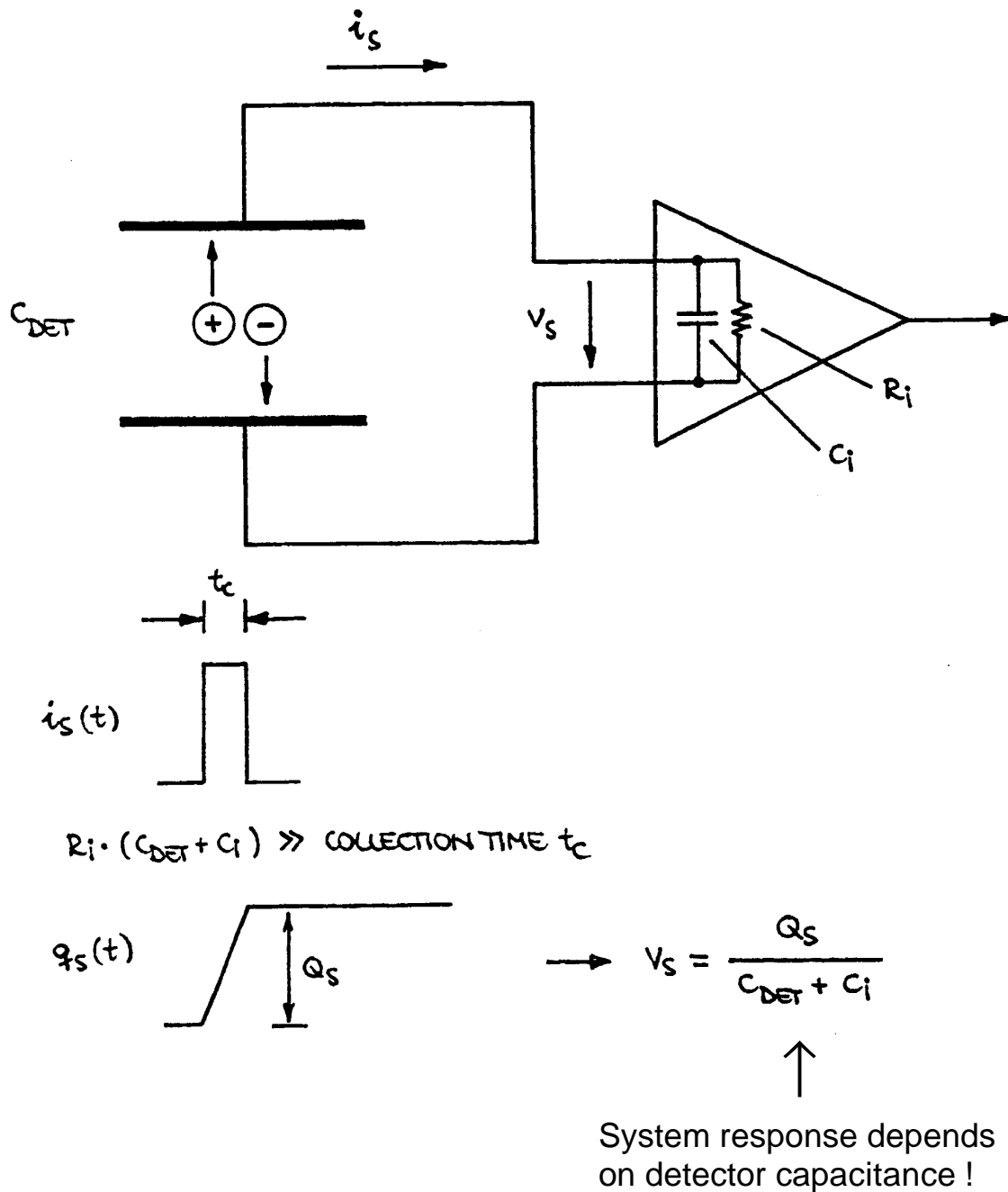
Detector capacitance may vary within a system or change with bias voltage (partially depleted semiconductor diode).

⇒   make system whose gain (dV_{out}/dQ_s) is independent of detector capacitance.

Active Integrator ("charge-sensitive amplifier")

Start with inverting voltage amplifier

Voltage gain $dV_o/dV_i = -A \implies v_o = -A\, v_i$

Input impedance $= \infty$ (i.e. no signal current flows into amplifier input)

Connect feedback capacitor C_f between output and input.
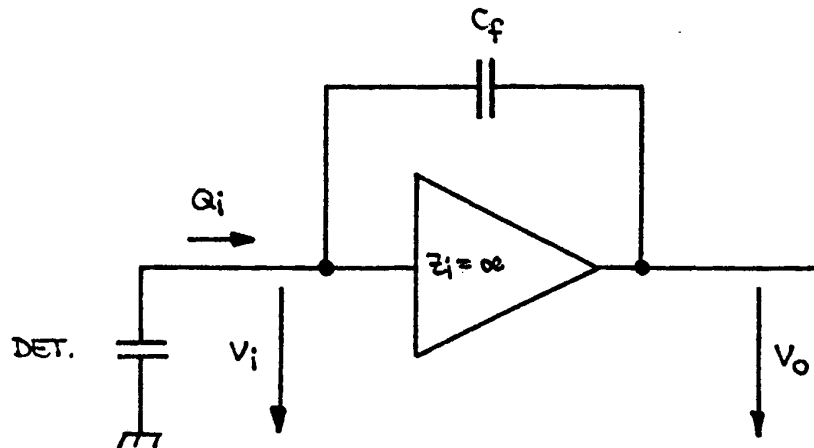
Voltage difference across C_f: $\qquad v_f = (A+1)\, v_i$

$\implies$ Charge deposited on C_f: $\qquad Q_f = C_f\, v_f = C_f(A+1)\, v_i$

$\qquad Q_i = Q_f \qquad$ (since $Z_i = \infty$)

$\implies$ Effective input capacitance

$$C_i = \frac{Q_i}{v_i} = C_f(A+1)$$

("dynamic" input capacitance)

Gain

$$A_Q = \frac{dV_o}{dQ_i} = \frac{A \cdot v_i}{C_i \cdot v_i} = \frac{A}{C_i} = \frac{A}{A+1} \cdot \frac{1}{C_f} \approx \frac{1}{C_f} \quad (A \gg 1)$$

Q_i is the charge flowing into the preamplifier ....

but some charge remains on C_{det}.

What fraction of the signal charge is measured?

$$\frac{Q_i}{Q_s} = \frac{C_i v_i}{Q_{det} + Q_i} = \frac{C_i}{Q_s} \cdot \frac{Q_s}{C_i + C_{det}}$$

$$= \frac{1}{1 + \dfrac{C_{det}}{C_i}} \approx 1 \ \ (\text{if } C_i \gg C_{det})$$

Example:

A = 10^3

C_f = 1 pF $\implies$ C_i = 1 nF

C_{det} = 10 pF: Q_i/Q_s = 0.99

C_{det} = 500 pF: Q_i/Q_s = 0.67

$\uparrow$

Si Det.: 50 µm thick
250 mm^2 area

Note: Input coupling capacitor must be >>C_i for high
charge transfer efficiency.

• Preamplifier must be tailored to detector

Calibration

Inject specific quantity of charge - measure system response

Use voltage pulse (can be measured conveniently with oscilloscope)
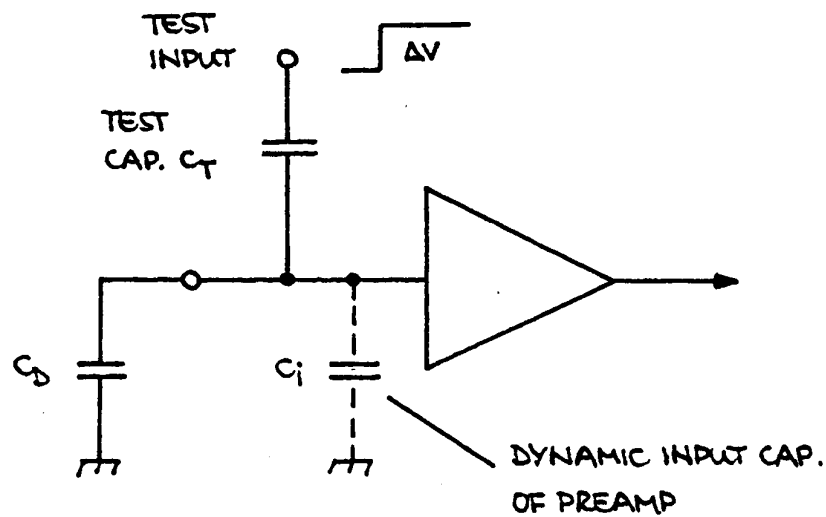
$$C_i \gg C_T \qquad \Rightarrow \qquad \text{Voltage step applied to test input develops over } C_T.$$

$$\Rightarrow \qquad Q_T = \Delta V \cdot C_T$$

Accurate expression:

$$Q_T = \frac{C_T}{1+\dfrac{C_T}{C_i}} \cdot \Delta V \approx C_T \left(1 - \frac{C_T}{C_i} \right) \Delta V$$

Typically: $C_T/C_i = 10^{-3} - 10^{-4}$

Summary of Amplifier Types

1. Simple Amplifiers
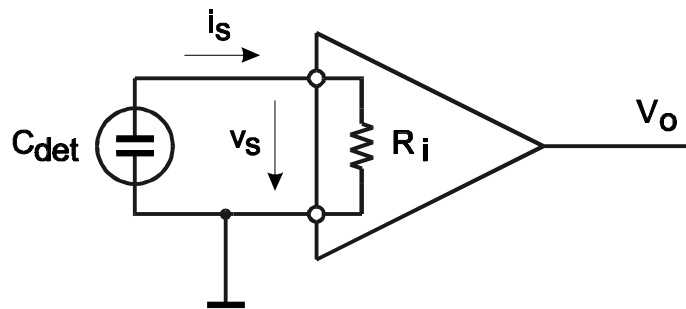
Output voltage V_o = voltage gain $A_v \times$ input voltage v_s.

Operating mode depends on charge collection time t_{coll} and the input time constant $R_i C_{det}$:

a)　　$R_i\, C_{det} \ll t_{coll}$　　detector capacitance discharges rapidly

$$\Rightarrow\quad V_o \propto i_s(t)$$

current sensitive amplifier

b)　　$R_i\, C_{det} \gg t_{coll}$　　detector capacitance discharges slowly

$$\Rightarrow\quad V_o \propto \int i_s(t)dt$$

voltage sensitive amplifier

• In both cases the ouput signal voltage is determined directly by the input voltage, but depending on the input time constant, the same amplifier can respond to current or charge.

2. Feedback Amplifiers

Basic amplifier as used above.

High input resistance: $R_i\, C_{det} >> \; t_{coll}$

Add feedback capacitance C_f
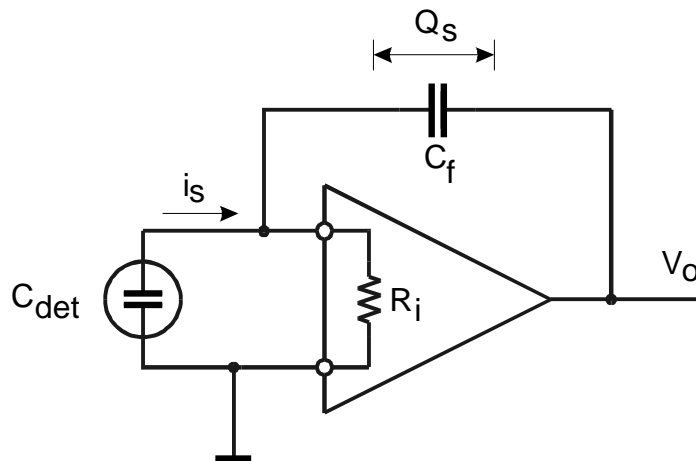
Signal current i_s is integrated on feedback capacitor C_f :

$$V_o \propto \; Q_s / C_f$$

Amplifier output directly determined by signal charge, insensitive to detector capacitance

$\Rightarrow$ charge-sensitive amplifier

Realistic Charge-Sensitive Preamplifiers

The preceding discussion assumed idealized amplifiers
with infinite speed.

- How do "real" amplifiers affect charge response?

- How does the detector affect amplifier response?

A Simple Amplifier
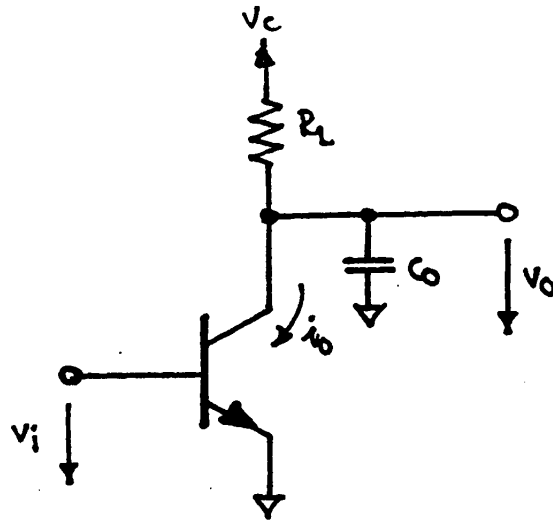
Voltage gain:

$$A_V = \frac{dv_o}{dv_i} = \frac{di_o}{dv_i} \cdot Z_L \equiv g_m Z_L$$

$g_m \equiv$ transconductance

$$Z_L = R_L \,//\, C_o$$

$$\frac{1}{Z_L} = \frac{1}{R_L} + i\omega\, C_o \qquad \Rightarrow \qquad A_V = g_m\left(\frac{1}{R_L} + i\omega\, C_o\right)^{-1}$$

$\uparrow$ $\uparrow$

low freq.   high freq.
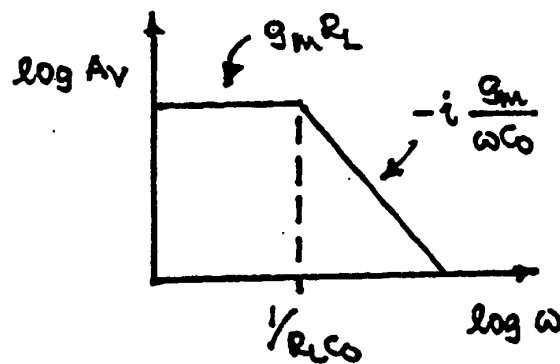
$\uparrow$ upper cutoff frequency $2\pi f_u$

Pulse Response of the Simple Amplifier

A voltage step $v_i(t)$ at the input causes a current step $i_o(t)$ at the output of the transistor.

For the output voltage to change, the stray capacitance C_o must first charge up.

$\Rightarrow$ The output voltage changes with a time constant $\tau = R_L C_o$

Frequency Domain   Time Domain
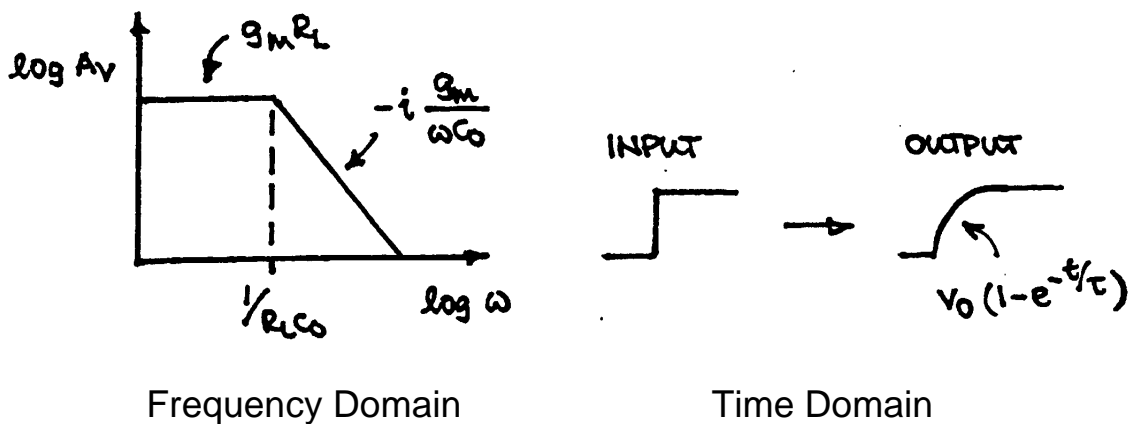
Note that τ is the inverse upper cutoff frequency $1/(2\pi f_u)$

Input Impedance of a Charge-Sensitive Amplifier

Input impedance

$$Z_i = \frac{Z_f}{A+1} \approx \frac{Z_f}{A} \quad (A \gg 1)$$

Amplifier gain vs. frequency
(beyond the upper cutoff
frequency)

$$A = -i \; \frac{\omega_0}{\omega}$$
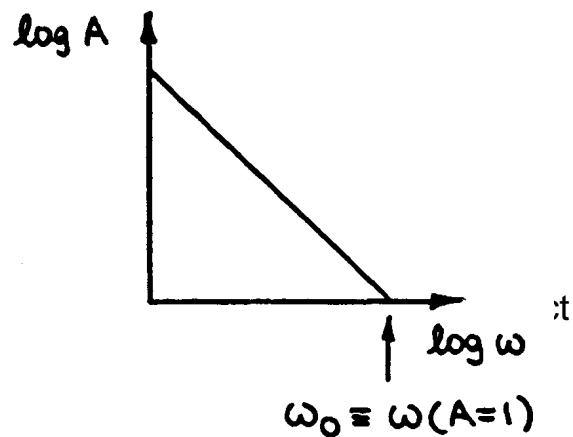
Feedback Impedance

$$Z_f = -i \; \frac{1}{\omega \, C_f}$$

$\Rightarrow$ Input Impedance

$$Z_i = -\frac{i}{\omega \, C_f} \cdot \frac{1}{-i\dfrac{\omega}{\omega_0}}$$

$$Z_i = \frac{1}{\omega_0 C_f}$$

*Imaginary component vanishes* $\Rightarrow$ *Resistance:* $Z_i \rightarrow R_i$

Time Response of a Charge-Sensitive Amplifier

Closed Loop Gain

$$A_f = \frac{C_D + C_f}{C_f} \quad (A_f \ll A_0)$$

$$A_f \approx \frac{C_D}{C_f} \quad (C_D \gg C_f)$$
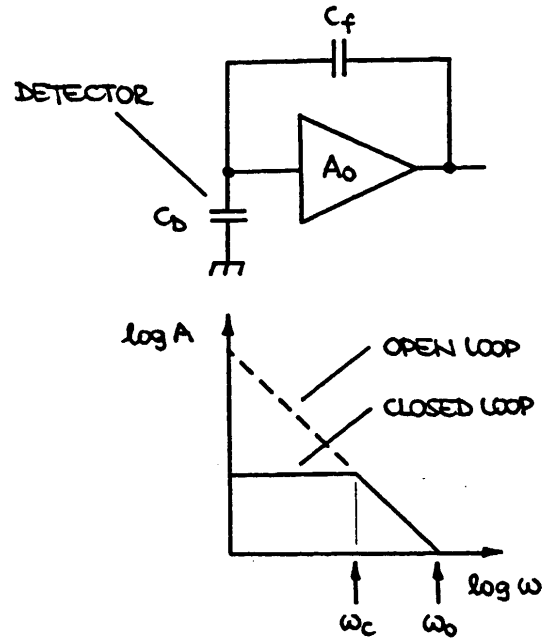
Closed Loop Bandwidth

$$\omega_C A_f = \omega_0$$

Response Time

$$\tau_{amp} = \frac{1}{\omega_C} = C_D \frac{1}{\omega_0 C_f}$$

Alternative Picture: Input Time Constant

$$\tau_i = R_i C_D$$

$$\tau_i = \frac{1}{\omega_0 C_f} \cdot C_D = \tau_{amp}$$

Same result as from conventional feedback theory.

Input impedance is critical in strip or pixel detectors:

Amplifiers must have a low input impedance to reduce transfer of charge through capacitance to neighboring strips
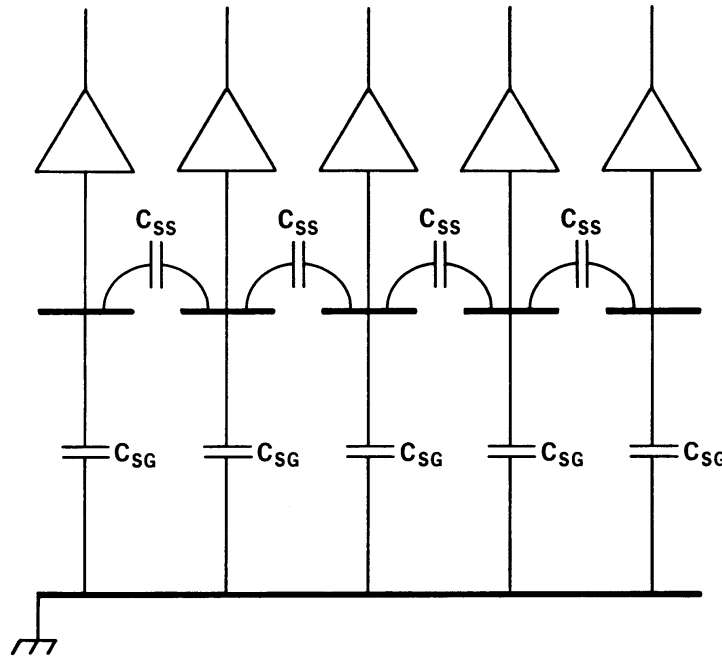
The capacitance is dominated by the fringing capacitance to the neighboring strips C_{SS}.

    Typically: $1 - 2$ pF/cm for strip pitches of $25 - 100$ µm.

The capacitance to the backplane C_{SG} is simple to calculate

$$C_{SG} = \varepsilon \frac{A}{d} = \varepsilon \frac{pl}{d}$$

where A is the area subtended by a strip element, d is the substrate thickness, p is the strip pitch (not width!) and l the strip length.

    The presence of the adjacent strips limits the fringing field to the centerline bewteen two strips, i.e. width = strip pitch.

The backplane capacitance is typically 20% of the strip-to-strip capacitance.

Negligible cross-coupling at times $t > (2 \ldots 3) \times R_i C_D$ and if $C_i \gg C_D$.

3. Resolution and Signal-to-Noise Ratio

Why?

a) Recognize structure in spectra

Comparison between NaI(Tl) and Ge detectors
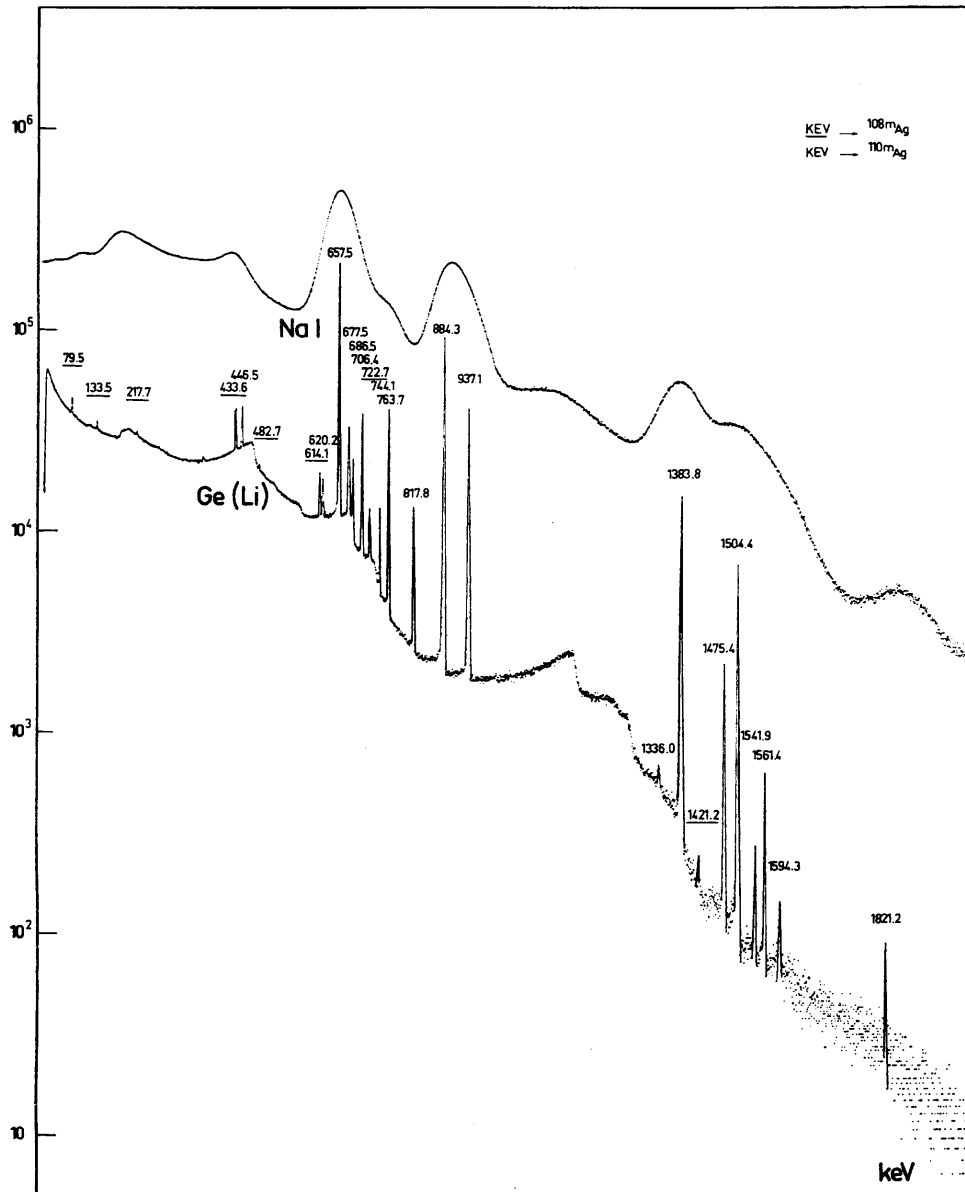
(J.Cl. Philippot, IEEE Trans. Nucl. Sci. **NS-17/3** (1970) 446)

b)   Improve sensitivity

Signal to background ratio improves with better resolution
(signal counts in fewer bins compete with fewer
background counts)
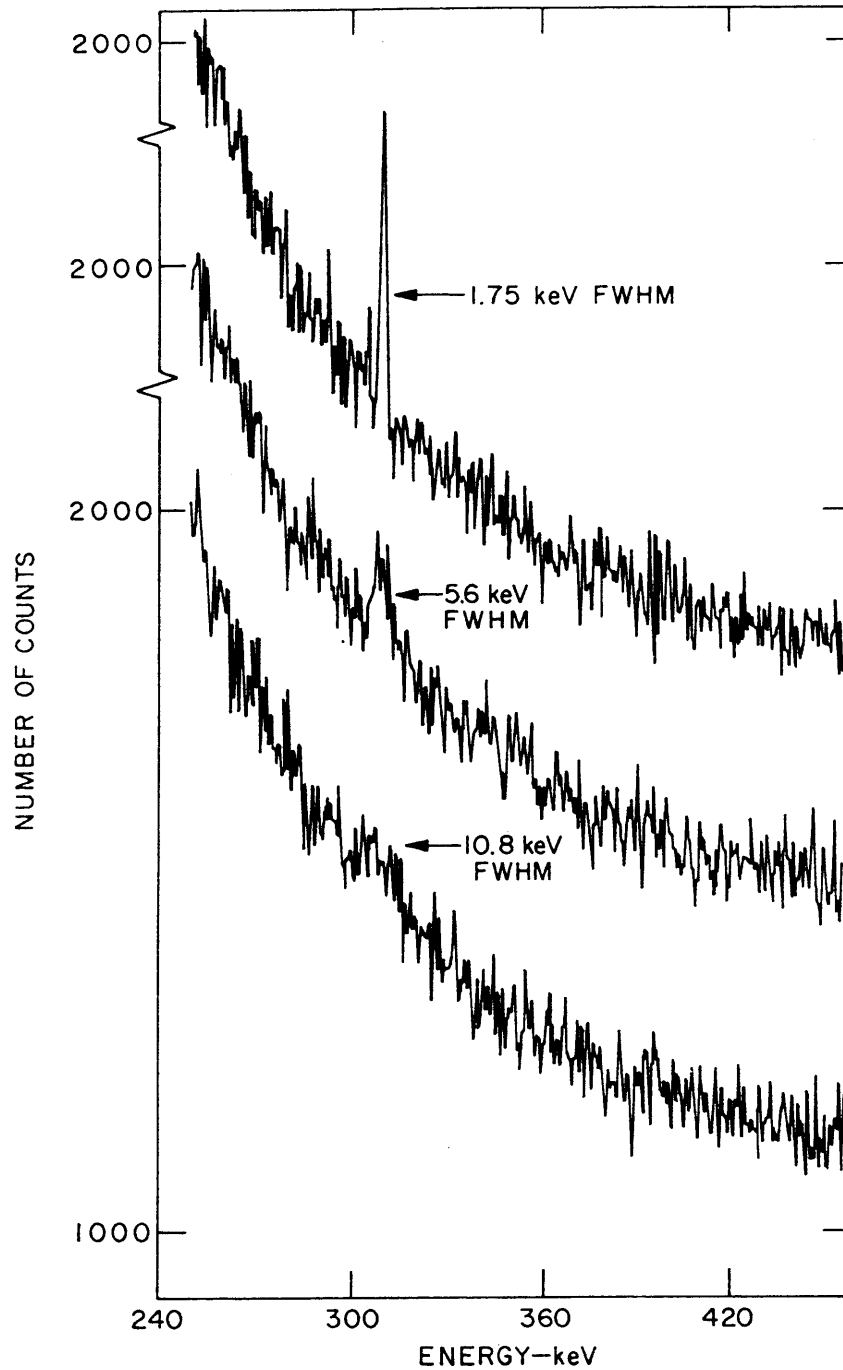
G.A. Armantrout, *et al.*, IEEE Trans. Nucl. Sci. **NS-19/1** (1972) 107

What determines Resolution?

1. Signal Variance >> Baseline Variance

SIGNAL $\oplus$ BASELINE NOISE $\Longrightarrow$ SIGNAL + NOISE

BASELINE BASELINE BASELINE
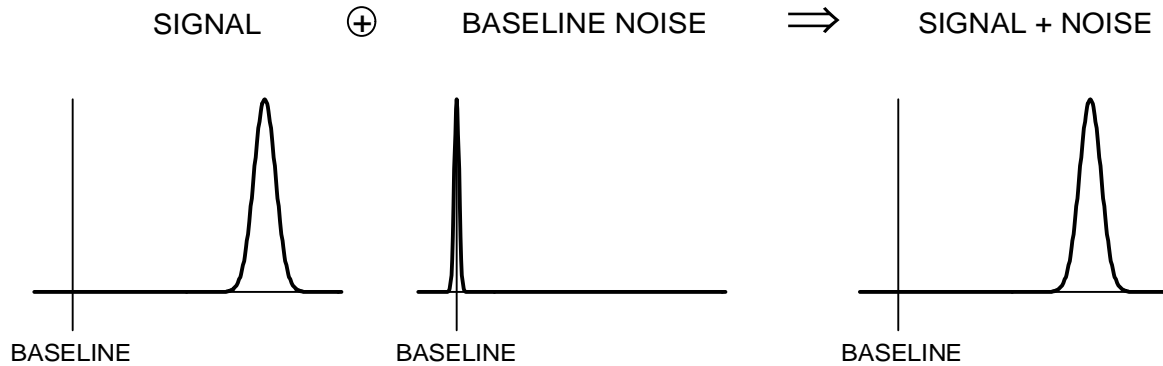
$\Longrightarrow$ Electronic (baseline) noise not important

Examples:

- High-gain proportional chambers

- Scintillation Counters with High-Gain PMTs

2. Signal Variance << Baseline Variance

SIGNAL $\oplus$ BASELINE NOISE $\Longrightarrow$ SIGNAL + NOISE

BASELINE BASELINE BASELINE
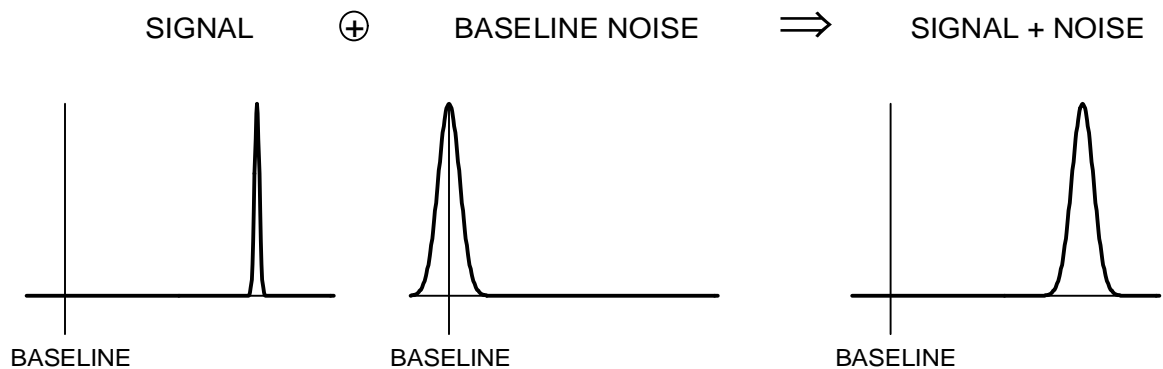
$\Longrightarrow$ Electronic (baseline) noise critical for resolution

Examples

- Gaseous ionization chambers (no internal gain)

- Semiconductor detectors

Low noise in tracking detectors is not necessary for resolution, but to reduce noise occupancy.

Energy loss distribution for minimum ionizing particles is broad:
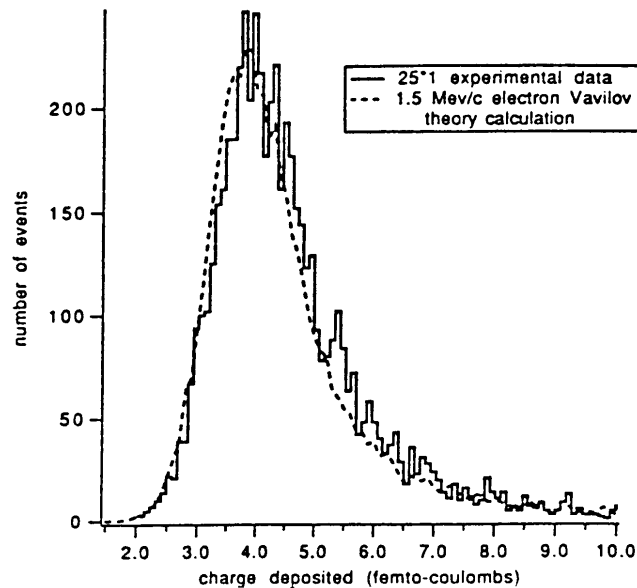
(Woods et al., Univ. Oklahoma)

Allowable noise level is determined by the noise occupancy, i.e.

noise rate << signal rate

Noise rate for a CR-RC shaper with time constant τ

$$f_n = \frac{1}{4\sqrt{3}\,\tau} \cdot e^{-Q_{th}^2/2Q_n^2}$$

where Q_{th}/Q_n is the threshold-to-noise ratio (derived later).

Magnitude of the noise must be sufficiently low that at the minimum signal level the rate of noise pulses still allows the required efficiency.

Baseline fluctuations can have many origins ...

pickup of external interference

artifacts due to imperfect electronics

… etc.,

but the (practical) fundamental limit is electronic noise.

Basic Noise Mechanisms

Consider n carriers of charge e moving with a velocity v through a sample of length l. The induced current i at the ends of the sample is

$$i = \frac{n\,e\,v}{l}\ .$$

The fluctuation of this current is given by the total differential

$$\langle di \rangle^2 = \left(\frac{ne}{l} \langle dv \rangle \right)^2 + \left(\frac{ev}{l} \langle dn \rangle \right)^2$$

where the two terms are added in quadrature since they are statistically uncorrelated.

Two mechanisms contribute to the total noise:

- velocity fluctuations, *e.g.*   thermal noise

- number fluctuations, *e.g.*   shot noise
  excess or '1/f' noise

Thermal noise and shot noise are both "white" noise sources, i.e.

power per unit bandwidth is constant:

($\equiv$ spectral density)
$$\frac{dV_{noise}^2}{df} = const. \equiv v_n^2$$

or
$$\frac{dP_{noise}}{df} = const.$$

whereas for "1/f" noise

$$\frac{dP_{noise}}{df} = \frac{1}{f^{\alpha}}$$

(typically $\alpha = 0.5 - 2$)

1. Thermal Noise in Resistors

The most common example of noise due to velocity fluctuations is the thermal noise of resistors. Transforming the current fluctuations from the time to the frequency domain yields:

Spectral noise power density vs. frequency f

$$\frac{dP_{noise}}{df} = 4kT$$

k = Boltzmann constant
T = absolute temperature

since

$$P = \frac{V^2}{R} = I^2 R$$

R = DC resistance

the spectral noise voltage density

$$\frac{dV^2_{noise}}{df} \equiv e^2_n = 4kTR$$

and the spectral noise current density

$$\frac{dI^2_{noise}}{df} \equiv i^2_n = \frac{4kT}{R}$$

The total noise depends on the bandwidth of the system. For example, the total noise voltage at the output of a voltage amplifier with the frequency dependent gain $A_v(f)$ is

$$v^2_{on} = \int_0^\infty e^2_n A^2_v(f)\, df$$

Note: Since spectral noise components are not correlated, one must integrate over the noise power.

2. Shot noise

A common example of noise due to number fluctuations is "shot noise", which occurs whenever carriers are injected into a sample volume independently of one another.

Example: current flow in a semiconductor diode
                    (emission over a barrier)

Spectral noise current density:

$$i_n^2 = 2q_e I$$

q_e = electron charge
I = DC current

A more intuitive interpretation of this expression will be given later.

Note: Shot noise does not occur in "ohmic" conductors. Since the number of available charges is not limited, the fields caused by local fluctuations in the charge density draw in additional carriers to equalize the total number.

Individual noise contributions add in quadrature
(additive in noise power)

$$P_{n,tot} = \sum_k P_{nk} \quad \Rightarrow \quad V_{n,tot} = \sqrt{\sum_k V_{nk}^2}$$

Both thermal and shot noise are purely random.

$\Rightarrow$ amplitude distribution is gaussian
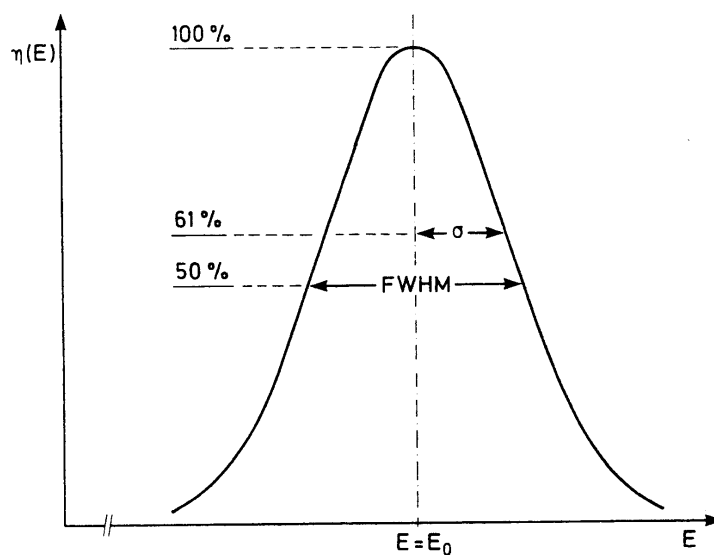
$\Rightarrow$ noise modulates baseline

$\Rightarrow$ baseline fluctuations superimposed on signal

$\Rightarrow$ output signal has gaussian distribution

Signal-to-Noise Ratio vs. Detector Capacitance

Voltage sensitive amplifier

Signal (at amplifier input)

$$v_s = \frac{Q_s}{C}$$

$C =$ total capacitance at input

Noise (referred to amplifier input)

$$v_{ni}$$

for a given preamplifier and shaper

$\Rightarrow$

$$\frac{S}{N} = \frac{v_s}{v_n} = \frac{1}{C} \; \frac{Q_s}{v_{ni}}$$

$$\uparrow$$

$$\boldsymbol{!}$$

Analagous result can be derived for current signal, but requires more knowledge of device noise mechanisms (to be discussed later).

In general

- *S/N* cannot be *improved* by feedback.

  This result is generally valid,

  i.e. it also holds for active integrators (charge-sensitive amplifiers).

Charge-Sensitive Preamplifier
Noise vs. Detector Capacitance

In a voltage-sensitive preamplifier the noise voltage at the output is essentially independent of detector capacitance,

i.e. the *equivalent input noise voltage* $v_{ni} = v_{no}/A_v$.

The signal-to-noise ratio depends on detector capacitance, since the input signal decreases with increasing input capacitance.

In a charge-sensitive preamplifier, the signal at the amplifier output is independent of detector capacitance (if $C_i >> C_{det}$).

What is the noise behavior?

Noise appearing at the output of the preamplifier is fed back to the input, decreasing the output noise from the open-loop value $v_{no}=v_{ni}A_{v0}$. The magnitude of the feedback depends on the shunt impedance at the input, i.e. the detector capacitance.

Note, that although specified as an equivalent input noise, the dominant noise sources are typically internal to the amplifier. Only in a fed-back configuration is some of this noise actually present at the input. In other words, the primary noise signal is not a physical charge (or voltage) at the amplifier input, to which the loop responds in the same manner as to a detector signal.

$\Rightarrow$ *S/N* **at the amplifier output depends on feedback.**

Noise in charge-sensitive preamplifiers

Start with an output noise voltage v_{no}, which is fed back to the
input through the capacitive voltage divider $C_f - C_d$.
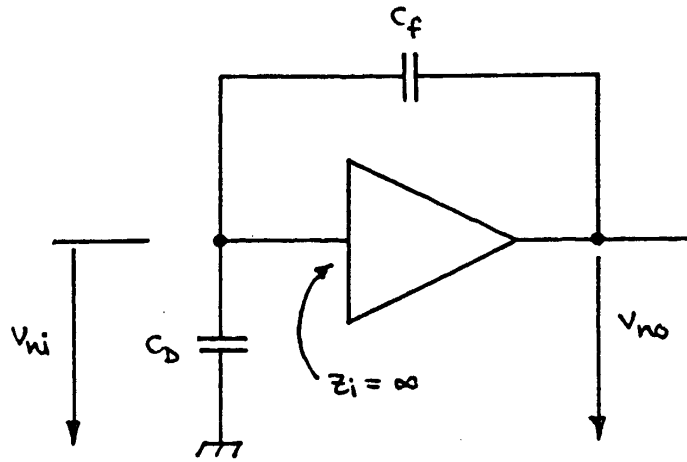
$$v_{no} = v_{ni} \frac{X_{C_f} + X_{C_D}}{X_{C_D}} = v_{ni} \frac{\dfrac{1}{\omega C_f} + \dfrac{1}{\omega C_D}}{\dfrac{1}{\omega C_D}}$$

$$v_{no} = v_{ni} \left(1 + \frac{C_D}{C_f}\right)$$

Equivalent input noise charge

$$Q_{ni} = \frac{v_{no}}{A_Q} = v_{no} C_f$$

$$Q_{ni} = v_{ni} \left(C_D + C_f \right)$$

Signal-to-noise ratio

$$\frac{Q_s}{Q_{ni}} = \frac{Q_s}{v_{ni}(C_D + C_f)} = \frac{1}{C} \frac{Q_s}{v_{ni}}$$

Same result as for voltage-sensitive amplifier,

but here noise grows with increasing C.

As shown previously, pulse rise time at the amplifier output also increases with total capacitive input load C, because of reduced feedback.

In contrast, the rise time of a voltage sensitive amplifier is not affected by the input capacitance, although the noise increases with C just as for the charge-sensitive amplifier.

Pulse Shaping

Two conflicting objectives:

1. Improve Signal-to-Noise Ratio *S/N*

     Restrict bandwidth to match measurement time

     $\Longrightarrow$ Increase Pulse Width

2. Improve Pulse Pair Resolution

     $\Longrightarrow$ Decrease Pulse Width

Pulse pile-up
distorts amplitude
measurement
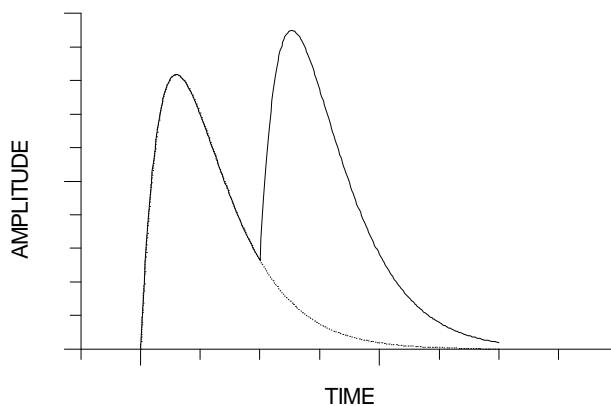
Reducing pulse
shaping time to
1/3 eliminates
pile-up.
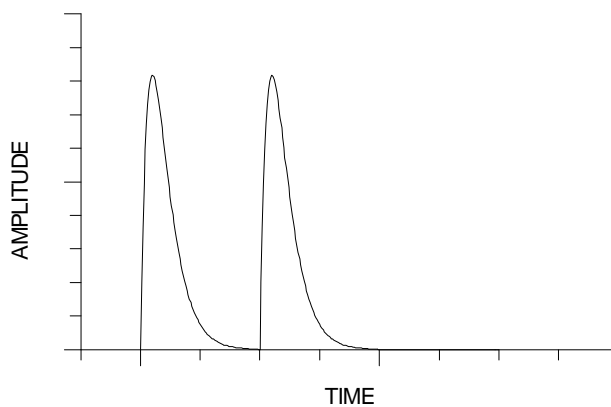
Necessary to find balance between these conflicting requirements. Sometimes minimum noise is crucial, sometimes rate capability is paramount.

Usually, many considerations combined lead to a "non-textbook" compromise.

- *"Optimum shaping" depends on the application!*

- Shapers need not be complicated –
    Every amplifier is a pulse shaper!

    (see "A Simple Amplifier")

Simple Example: CR-RC Shaping

Preamp   "Differentiator"   "Integrator"

High-Pass Filter   Low-Pass Filter
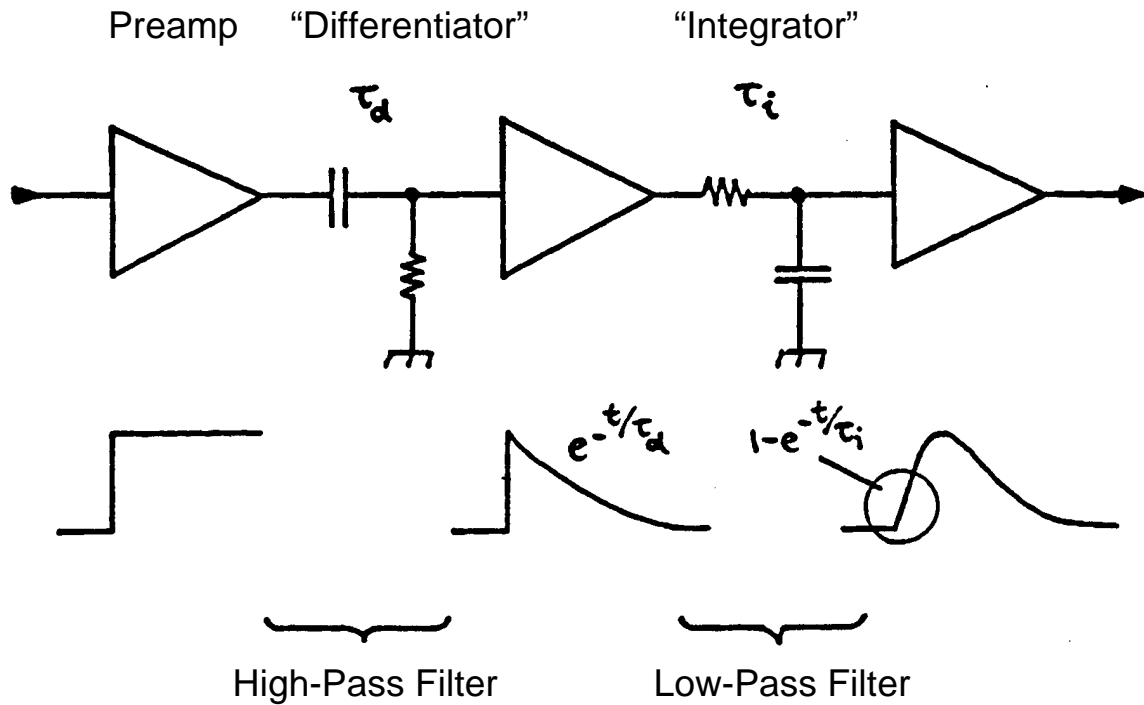
Simple arrangement: Noise performance only 36% worse than
                      optimum filter with same time constants.

$\Rightarrow$ Useful for estimates, since simple to evaluate

Pulse Shaping and Signal-to-Noise Ratio

Pulse shaping affects both the

- total noise

and

- peak signal amplitude

at the output of the shaper.

Equivalent Noise Charge

Inject known signal charge into preamp input
(either via test input or known energy in detector).

Determine signal-to-noise ratio at shaper output.

Equivalent Noise Charge $\equiv$ Input charge for which $S/N = 1$

Measurement of Equivalent Noise Charge

Inject an input signal with known charge using a pulse generator set to approximate the detector signal (possible ballistic deficit). Measure the pulse height spectrum.

| peak centroid | $\Rightarrow$ | signal magnitude |
| peak width | $\Rightarrow$ | noise (FWHM= 2.35 rms) |

or

measure width of x-ray or γ-ray peak

Analytical Analysis of a Detector Front-End
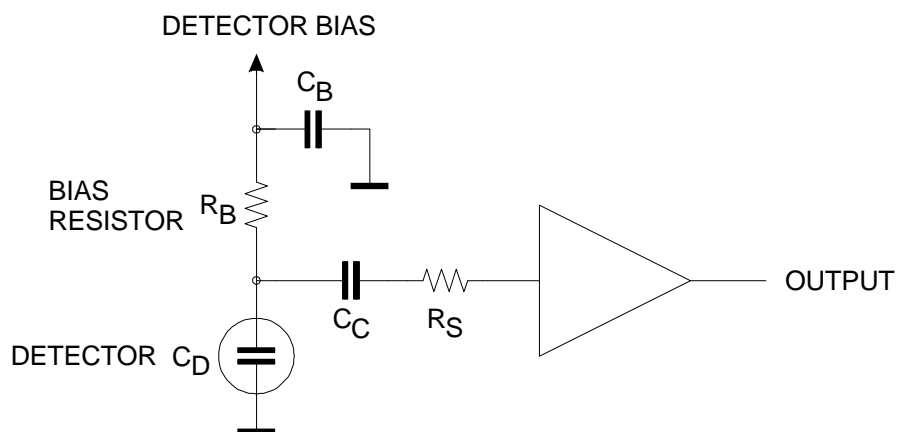
Detector bias voltage is applied through the resistor R_B. The bypass capacitor C_B serves to shunt any external interference coming through the bias supply line to ground. For AC signals this capacitor connects the "far end" of the bias resistor to ground, so that R_B appears to be in parallel with the detector.

The coupling capacitor C_C in the amplifier input path blocks the detector bias voltage from the amplifier input (which is why a capacitor serving this role is also called a "blocking capacitor"). Since this capacitor passes AC signals, it can be neglected.

The series resistor R_S represents any resistance present in the connection from the detector to the amplifier input. This includes

- the resistance of the detector electrodes

- the resistance of the connecting wires

- any resistors used to protect the amplifier against large voltage transients ("input protection")

- ... etc.

Equivalent circuit for noise analysis
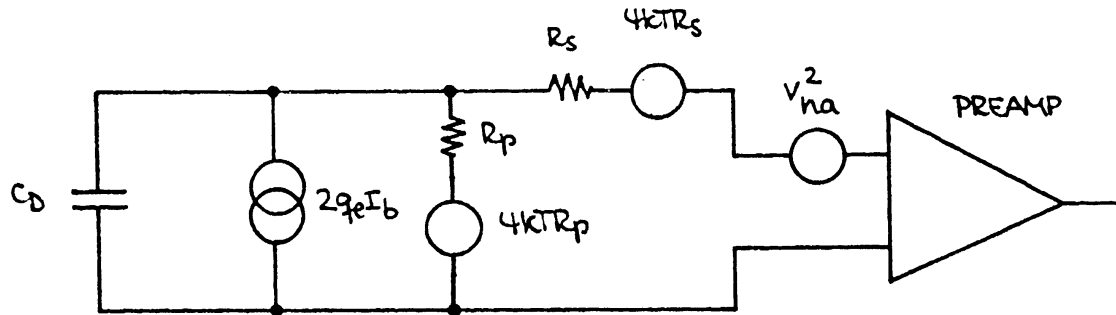
| detector | bias current shot noise | shunt resistance thermal noise | series resistance thermal noise | equivalent input noise voltage of amplifier |

In this example a voltage-sensitive amplifier is used, so all noise contributions will be calculated in terms of the noise voltage applied to the amplifier input.

Steps in the analysis:

1. Determine the frequency distribution of the noise voltage presented to the amplifier input from all individual noise sources

2. Integrate over the frequency response of a CR-RC shaper to determine the total noise output.

3. Determine the equivalent noise charge

Noise Contributions

1. Detector bias current
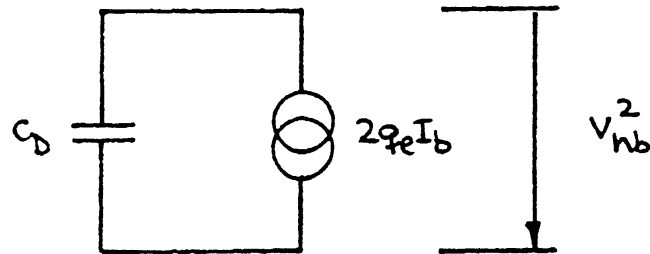
This model results from two assumptions:

1. The input impedance of the amplifier is infinite

2. The shunt resistance R_P is much larger than the capacitive reactance of the detector in the frequency range of the pulse shaper.

    Does this assumption make sense?

    If R_P is too small, the signal charge on the detector capacitance will discharge before the shaper output peaks. To avoid this

    $$R_P C_D \gg t_P \approx \frac{1}{\omega_P}$$

    where ω_P is the midband frequency of the shaper. Therefore,

    $$R_P \gg \frac{1}{\omega_P C_D}$$

    as postulated.

Under these conditions the noise current will flow through the detector capacitance, yielding the voltage

$$v_{nb}^2 = i_{nb}^2 \frac{1}{(\omega\, C_D)^2} = 2 q_e I_b \frac{1}{(\omega\, C_D)^2}$$

$\Rightarrow$ the noise contribution decreases with increasing frequency (shorter shaping time)

Note: Although shot noise is "white", the resulting noise spectrum is strongly frequency dependent.

In the time domain this result is more intuitive. Since every shaper also acts as an integrator, one can view the total shot noise as the result of "counting electrons".

Assume an ideal integrator that records all charge uniformly within a time T. The number of electron charges measured is

$$N_e = \frac{I_b T}{q_e}$$

The associated noise is the fluctuation in the number of electron charges recorded

$$\sigma_n = \sqrt{N_e} \propto \sqrt{T}$$

Does this also apply to an AC-coupled system, where no DC current flows, so no electrons are "counted"?

Since shot noise is a fluctuation, the current suffers both positive and negative excursions. Although the DC component is not passed through an AC coupled system, the excursions are. Since, on the average, each fluctuation requires a positive and a negative zero crossing, the process of "counting electrons" is actually the counting of zero crossings, which in a detailed analysis yields the same result.

2. Parallel Resistance

Shunt components:

1. bias noise current source
   (infinite resistance by definition)

2. detector capacitance

Current due to the noise voltage from R_P can only flow through the detector capacitance C_D.

$\Rightarrow$ equivalent circuit
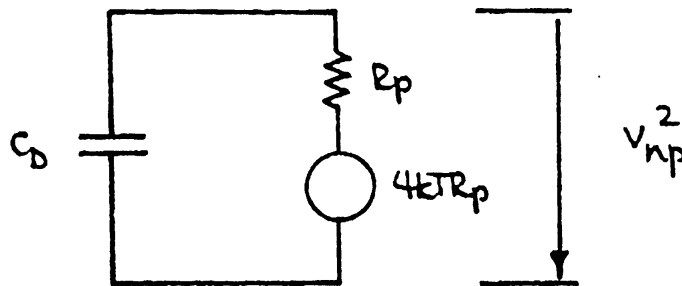
The noise voltage applied to the amplifier input is

$$v_{np}^2 = 4kTR_P \left(\frac{-i/\omega C_D}{R_P - i/\omega C_D} \right)^2$$

$$v_{np}^2 = 4kTR_P \frac{1}{1+(\omega R_P C_D)^2}$$

Comment:

Integrating this result over all frequencies yields

$$\int\limits_0^\infty v_{np}^2(\omega)\,d\omega = \int\limits_0^\infty \frac{4kTR_P}{1+(\omega\,R_PC_D)^2}\,d\omega = \frac{kT}{C_D}$$

which is independent of R_P. Commonly referred to as "kTC" noise, this contribution is often erroneously interpreted as the "noise of the detector capacitance". An ideal capacitor has no thermal noise; all noise originates in the resistor.
So, why is the result independent of R_P?

R_P determines the primary noise, but also the noise bandwidth of this subcircuit. As R_P increases, its thermal noise increases, but the noise bandwidth decreases, making the total noise independent of R_P.

However,
If one integrates v_{np} over a bandwidth-limited system

$$V_n^2 = \int\limits_0^\infty 4kTR_P\left|\frac{G(i\omega)}{1-i\omega\,R_PC_D}\right|^2 d\omega$$

the total noise decreases with increasing R_P.

3. Series Resistance

The noise voltage generator associated with the series resistance R_S is in series with the other noise sources, so it simply contributes

$$v_{nr}^2 = 4kTR_S$$

4. Amplifier input noise voltage density

The amplifier noise sources usually are not physically present at the amplifier input. Instead the amplifier noise originates within the amplifier, appears at the output, and is referred to the input by dividing the output noise by the amplifier gain. Here, the output noise is referred to a voltage-sensitive input, so it appears as a noise voltage generator.

$$v_{na}^2 = v_{nt}^2 \; + \; \frac{A_f}{f}$$

$$\uparrow \qquad \uparrow$$

"white $1/f$ noise
noise"   (can also originate in
                external components)

This noise voltage generator also adds in series with the other sources.

Amplifiers generally also exhibit input current noise, which is physically present at the input. However, its effect is the same as for the detector bias current, so the analysis given in 1. can be applied.

Equivalent noise charge at the shaper output

1. Assume a CR-RC shaper

2. Equal differentiation and integration time constants
$\tau_d = \tau_i = \tau$.

Integrating over frequency for all noise contributions and
accounting for the signal transmission through the shaper yields
the equivalent noise charge

$$Q_n^2 = \left(\frac{e^2}{8}\right)\left[\left(2q_e I_b + \frac{4kT}{R_P}\right)\cdot\tau + \left(4kTR_S + v_{na}^2\right)\cdot\frac{C_D^2}{\tau} + 4A_f C_D^2\right]$$

↑	↑	↑
current noise	voltage noise	1/f noise
∝ τ	∝ 1/τ	independent
independent of C_D	∝ C_D^2	of τ
		∝ C_D^2

- Current noise is independent of detector capacitance,
  consistent with the notion of "counting electrons".

- Voltage noise increases with detector capacitance
  (reduced signal voltage)

- 1/f noise is independent of shaping time.
  In general, the total noise of a 1/f depends on the
  ratio of the upper to lower cutoff frequencies, not on the
  absolute noise bandwidth. If τ_d and τ_i are scaled by the
  same factor, this ratio remains constant.

Q_n assumes a minimum when the current and voltage noise contributions are equal.

dominated by   voltage   current noise
$\downarrow$ $\downarrow$

For a CR-RC shaper the noise minimum obtains for $\tau_d = \tau_i = \tau$.

This is usually not true for other shapers.

Note:

Although the parallel resistor was analyzed as a noise voltage source, it appears as a current noise source.

$\Rightarrow$ Modeling the parallel resistor as a noise current source is more appropriate.

$\Rightarrow$ judicious choice of model simplifies calculation.

   For sources connected in parallel, currents are additive.

   For sources connected in series, voltages are additive.

$\Rightarrow$ In the detector community voltage and current noise are often called "series" and "parallel" noise.

   The rest of the world uses equivalent noise voltage and current. Since they are physically meaningful, use of these widely understood terms is preferable.

Numerical expression for the noise of a CR-RC shaper

(note that some units are "hidden" in the numerical factors)

$$Q_n^2 = 12\, I_B\, \tau \ + \ 6\cdot 10^5\, \frac{\tau}{R_P} \ + \ 3.6\cdot 10^4\, v_n^2\, \frac{C^2}{\tau} \quad \text{[rms electrons]}$$

where

τ shaping time constant [ns]

I_B detector bias current + amplifier input current [nA]

R_P input shunt resistance [kΩ]

v_n equivalent input noise voltage spectral density [nV/$\sqrt{\text{Hz}}$]

C total input capacitance [pF]

Q_n= 1 *el*   corresponds to   3.6 eV in Si
                                              2.9 eV in Ge

(see Spieler and Haller, IEEE Trans. Nucl. Sci. **NS-32** (1985) 419)

Another form of pulse shaping: Correlated Double Sampling
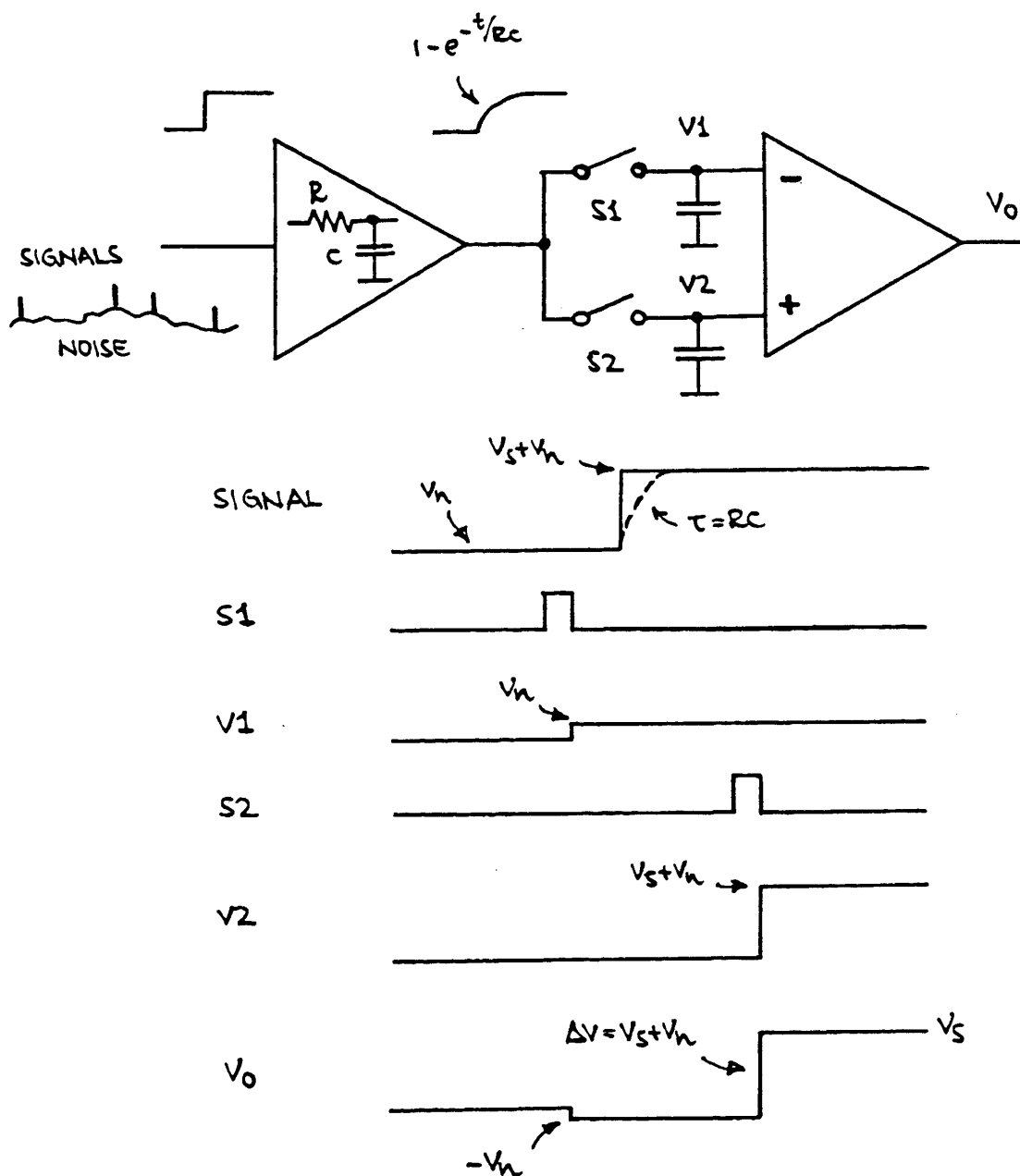
1. Signals are superimposed on a (slowly) fluctuating baseline

2. To remove baseline fluctuations the baseline is sampled prior to the arrival of a signal.

3. Next, the signal + baseline is sampled and the previous baseline sample subtracted to obtain the signal

Correlated Double Sampling

Equivalent noise charge due to the current noise

$$Q_{ni}^2 = i_n^2 \ \tau \ \frac{\dfrac{2T}{\tau} + e^{-T/\tau} - e^{-2T/\tau} + 1}{4\left(1 - e^{-T/\tau}\right)^2}$$

The voltage noise contribution is

$$Q_{nv}^2 = C_i^2 \ v_n^2 \ \frac{1}{\tau} \ \frac{2 - e^{-2T/\tau}}{4\,(1 - e^{-T/\tau})^2}$$

and the total equivalent noise charge

$$Q_n = \sqrt{Q_{ni}^2 + Q_{nv}^2}$$

Optimal choice of

prefilter time constant τ vs.

sampling interval T

depends on the relative contributions of voltage and current noise sources.

Optimization

1. Noise current negligible

Parameters: $T=$ 100 ns
                          $C_d=$ 10   pF
                          $v_n=$ 2.5 nV/√Hz

        ● $i_n=$ 6   fA/√Hz   ($I_b=$ 0.1 nA)
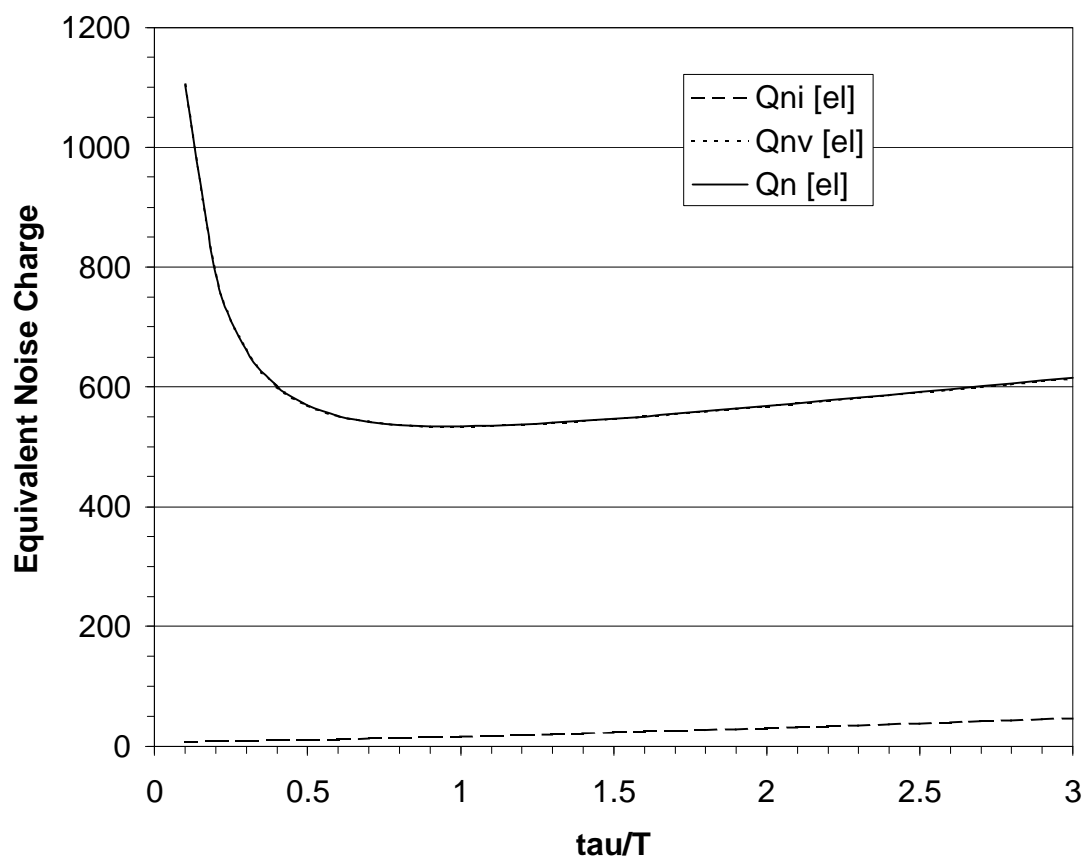
Noise attains shallow minimum for $\tau = T$.

2. Significant current noise contribution

Parameters: $T=$ 100 ns

$C_d=$ 10   pF

$v_n=$ 2.5 nV/√Hz

● $i_n=$ 600 fA/√Hz   ($I_b=$ 1 μA)
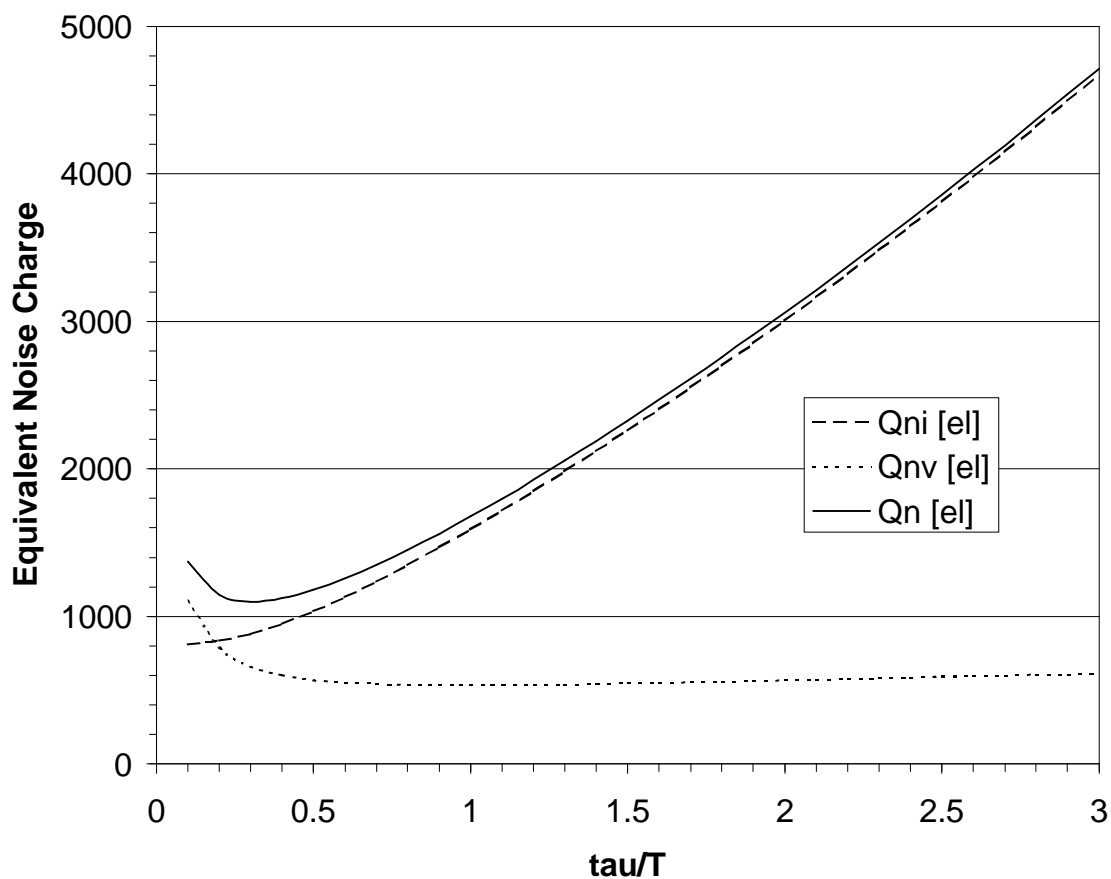
Noise attains minimum for $\tau = 0.3\ T$.

Summary

Two basic noise mechanisms: input noise current i_n

input noise voltage v_n

Equivalent Noise Charge:

$$Q_n^2 = i_n^2 \, T_s \, F_i \; + \; C_i^2 \, v_n^2 \, \frac{F_v}{T_s}$$

where T_s Characteristic shaping time (*e.g.* peaking time)

F_i, F_v "Form Factors" that are determined
by the shape of the pulse.

C_i Total capacitance at the input node
(detector capacitance + input capacitance of
preamplifier + stray capacitance + ...)

Typical values of F_i , F_v

CR-RC shaper	F_i = 0.924	F_v = 0.924
CR-(RC)^4 shaper	F_i = 0.45	F_v = 1.02
CR-(RC)^7 shaper	F_i = 0.34	F_v = 1.27
CAFE chip	F_i = 0.4	F_v = 1.2

Note that $F_i < F_v$ for higher order shapers.

Shapers can be optimized to reduce current noise contribution
relative to the voltage noise (mitigate radiation damage!).

Radiation Damage

Two basic radiation damage mechanisms:

- Displacement Damage

    Incident radiation displaces silicon atoms from lattice sites. Also referred to as bulk damage.

- Ionization Damage

    Energy absorbed by electronic ionization in insulating layers, typically SiO_2, liberates charge, which drifts or diffuses and is eventually trapped either in the insulator layer at interfaces. Also referred to as surface damage.

Both types of damage occur both in detectors and transistors/ICs.

Minute concentrations of defects and impurities have significant on diode characteristics even without additional radiation damage.

Reverse bias current vs. voltage (S. Holland, LBNL)
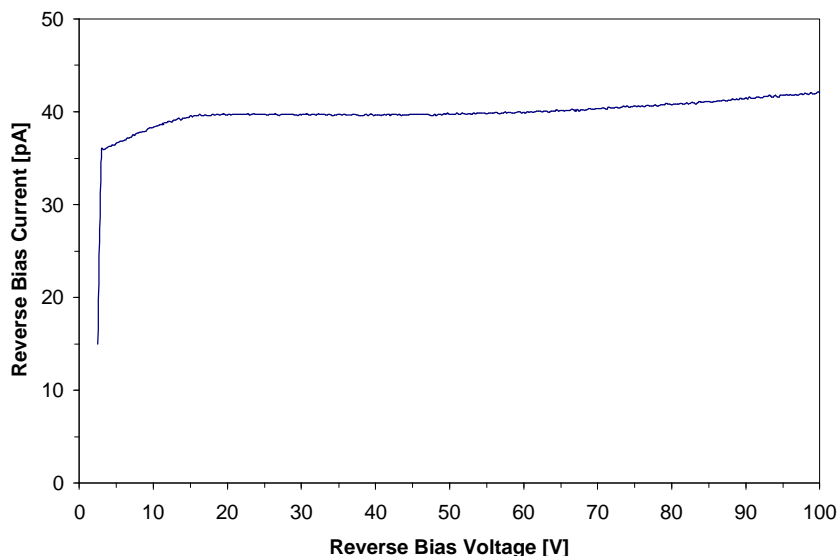
Even this state-of-the-art diode (450 pA/cm^2) has leakage current 10x larger than the theoretical value.

Displacement Damage

An incident particle or photon capable of imparting an energy of about 20 eV to a silicon atom can dislodge it from its lattice site.

Displacement damage creates defect clusters.

> For example, a 1 MeV neutron transfers about 60 to 70 keV to the Si recoil atom, which in turn displaces roughly 1000 additional atoms in a region of about 0.1 μm size.

Displacement damage is proportional to non-ionizing energy loss, which is not proportional to the total energy absorbed, but depends on the particle type and energy.

> X-rays do not cause direct displacement damage, since momentum conservation sets a threshold energy of 250 keV for photons.

> ^{60}Co γ rays cause displacement damage primarily through Compton electrons and are about three orders of magnitude less damaging per photon than a 1 MeV neutron.

Relative displacement damage for various particles and energies:

Particle	proton	proton	neutron	electron	electron
Energy	1 GeV	50 MeV	1 MeV	1 MeV	1 GeV
Relative Damage	1	2	2	0.01	0.1

Defects introduce intermediate states in the bandgap.
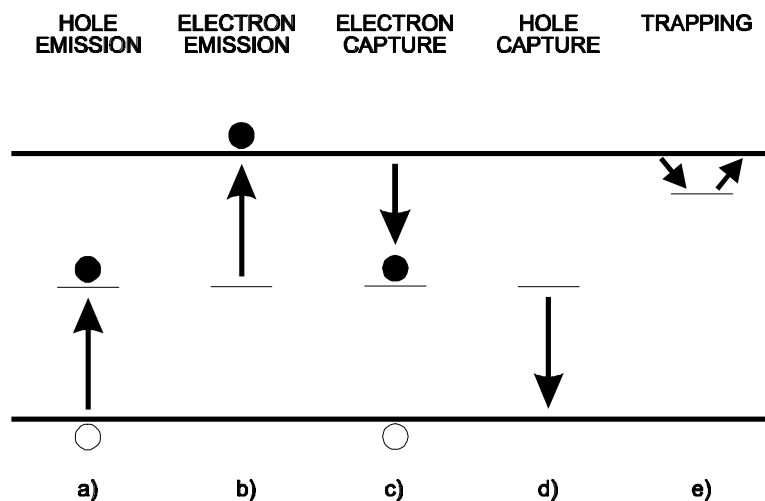
a) Hole emission

 electron promoted from valence band to defect state

b) Electron emission

 electron transition from defect state to conduction band

 a) + b)   ⇒   additional charge carriers in conduction band
            "generation current"

c) Electron capture

 electron captured from conduction band

d) Hole capture

 electron transition to valence band

 c) + d)   ⇒   charge carriers removed from conduction
            band
            "recombination"

e) trapping: charge captured and released after some time

Displacement damage manifests itself in three important ways:

1. Increase in reverse bias current

The bias current after irradiation has been shown to be

$$I_R = I_0 + \alpha \cdot \Phi \cdot Ad$$

where I_0 is the bias current before irradiation, α is a damage coefficient dependent on particle type and fluence, Φ is the particle fluence, and the product of detector area and thickness Ad is the detector volume.

For   650 MeV protons $\alpha \approx 3 \cdot 10^{-17}$ A/cm

           1 MeV neutrons $\alpha \approx 2 \cdot 10^{-17}$ A/cm.
                (characteristic of the albedo emanating
                from a calorimeter)

The parametrization used is quite general, as it merely assumes a spatially uniform formation of electrically active defects in the detector volume, without depending on the details of energy levels or states.

The coefficients given above apply to room temperature operation. The reverse bias current of silicon detectors depends strongly on temperature.

Even after rather low fluences the generation current dominates, so the reverse bias current

$$I_R(T) \propto v_{th} n_i \propto v_{th} \sqrt{N_c N_v} \; e^{-E/2k_BT} \propto T^2 e^{-E/2k_BT}$$

The effective activation energy $E = 1.2$ eV for radiation damaged samples, whereas unirradiated samples usually exhibit $E = 1.12$ eV.

The ratio of currents at two temperatures T_1 and T_2 is

$$\frac{I_R(T_2)}{I_R(T_1)} = \left(\frac{T_2}{T_1}\right)^2 \exp\left[-\frac{E}{2k_B}\left(\frac{T_1-T_2}{T_1 T_2}\right)\right]$$

Cooling to 0 °C typically reduces the reverse bias current to 1/6 of its value at room temperature.

After irradiation the leakage current initially decreases with time. Pronounced short term and long term annealing components are observed and precise fits to the annealing curve require a sum of exponentials.

In practice, the variation of leakage current with temperature is very reproducible from device to device, even after substantial doping changes due to radiation damage. The leakage current can be used for dosimetry and diodes are offered commercially specifically for this purpose.

2. Changes in Effective Doping

The processes leading to a change in effective doping are extremely complex and poorly understood, so the results are only summarized briefly.

It has been observed by many groups that the effective doping of n-type silicon initially decreases with fluence, becomes intrinsic (i.e. undoped) and then turns p-like, where the space charge increases with fluence.

This phenomenon is consistent with the notion that acceptor sites are formed by the irradiation, although this does not mean that mobile holes are created. Instead, the defect sites trap electrons and build up a space charge whose field must be overcome by the applied detector bias to sweep signal charge through the detector thickness.

Initially, the effective doping level N_d -N_a decreases as new acceptor states neutralize original donor states. At some fluence the two balance, creating "intrinsic" material, and beyond this fluence the acceptor states dominate.
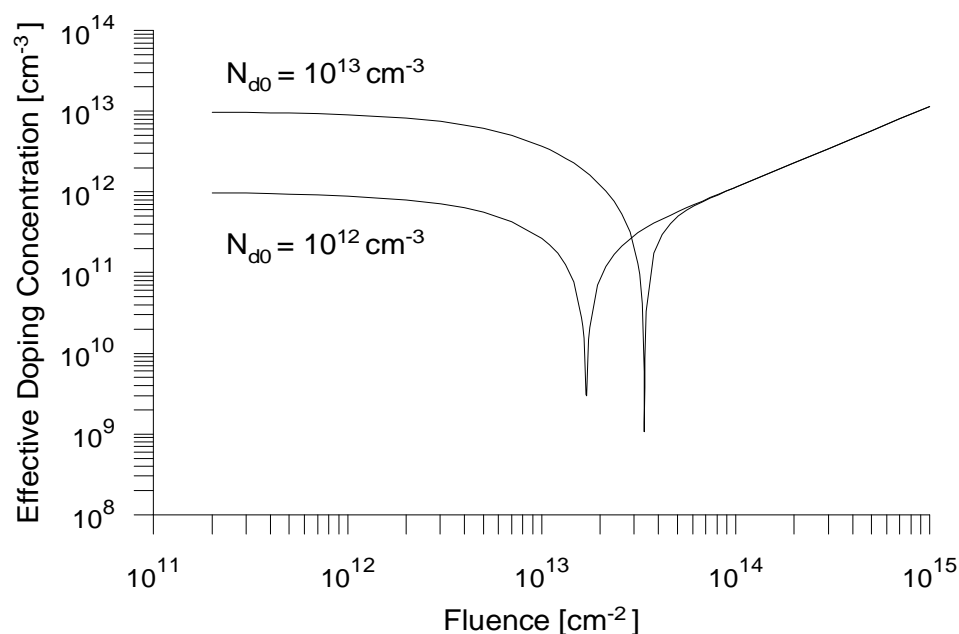
Type inversion from n- to p-like space charge typically occurs at a fluence of about 10^{13} cm^{-2}.

Very high resistivity silicon ($\rho >10$ kΩcm or $N_d < 4 \cdot 10^{11}$ cm^{-3}) is often highly compensated, $N_{eff} = N_d - N_a$ with $N_d \sim N_a >> N_{eff}$, so that minute changes to either donors or acceptors can alter the net doping concentration significantly. Moderate resistivity n-type material ($\rho = 1$ to 5 kΩcm) used in large area tracking detectors is usually dominated by donors.

In addition to acceptor formation, there is evidence for a concurrent process of donor removal.

After defect states are formed by irradiation, their electronic activity changes with time.

A multitude of processes contribute, some leading to beneficial annealing, i.e. a reduction in acceptor-like states, and some increasing the acceptor concentration.

The most deleterious is the increase in effective acceptor concentration, called "anti-annealing"

The *relative effect* of anti-annealing increases strongly with

- fluence and
- temperature.

Fluence [cm^{-2}]	$N_a(t=100\text{h}) / N_a(t=0) =$ $V(t=100\text{h}) / V(t=0)$		
	0 °C	20 °C	40 °C
10^{13}	1.00	1.02	1.39
10^{14}	1.01	1.21	4.71

Effect of anti-annealing on acceptor concentration and required operating voltage vs. fluence and temperature.

Anti-annealing is a concern because of its effect on detector depletion voltage, i.e. the voltage required to collect charge from the complete thickness of the silicon detector. Since this voltage increases with the space charge concentration, anti-annealing can easily exceed the safe operating range, especially at high fluences.

Clearly, low temperature operation is beneficial. Nevertheless, even a low temperature system will require maintenance at room temperature and warm up periods must be controlled very carefully.

3. Charge loss due to trapping

Data on charge collection efficiency are still rather sketchy. The primary mechanism is expected to be trapping of signal charge at defect sites, i.e. a decrease in carrier lifetime τ.

Since the loss in signal charge is proportional to $exp(-t_c/\tau)$, reducing the collection time t_c mitigates the effect.

Since either the operating voltage is increased or depletion widths are reduced at damage levels where charge trapping is appreciable, fields tend to be higher and collection times decrease automatically with radiation damage, provided the detector can sustain the higher fields.

The lifetime can be described by

$$1/\tau = \gamma \Phi ,$$

where for holes $\gamma_p = 2.7 \cdot 10^{-7}$ cm^{2}s and for electrons $\gamma_e = 1.2 \cdot 10^{-6}$ cm^{2}s for $\Phi > 10^{13}$ cm^{-2} of 1 MeV equivalent neutrons.

For a fluence $\Phi = 5 \cdot 10^{13}$ cm^{-2}s^{-1}, a 400 μm thick detector with a depletion voltage of 130V operated at a bias voltage of 200V would show a decrease in signal charge of 12%.

Ionization Damage

schematic cross section of MOSFET
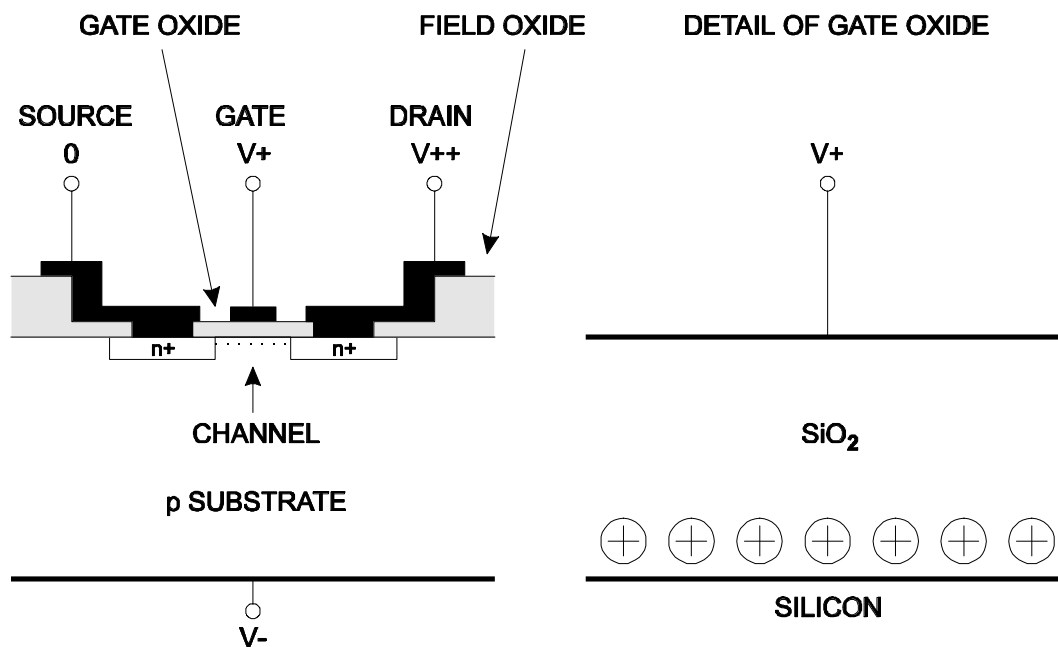
Electron-hole pairs created in oxide

- electrons mobile and flow through contact

- hole transport by slow hopping mechanism

    holes are trapped and released in oxide

    holes move to interface and are trapped

    $\Rightarrow$ charge buildup at oxide-silicon interface

    $\Rightarrow$ attracts electrons to silicon surface

    gate voltage must be adjusted more negative

Trapped oxide charge can be mobile

$\Rightarrow$ charge distribution changes with time

$\Rightarrow$ charge distribution changes with varying electric field

In addition

• annealing effects

Time dependende of total charge and distribution of charge buildup very complicated!

Strong dependence on dose rate!

Similar effects in field oxide

thicker, so trapping exacerbated

$\Rightarrow$ surface channels

Ionization effects in devices determined by

- interface trapped charge

- oxide trapped charge

- mobility of trapped charge

- time and field dependence of charge states

Strongly dependent on

- rate of irradiation

- applied voltages and variation in time
    devices must be tested under voltage

- time variation of the radiation

- temperature

Dominant damage mechanism in MOS transistors
   (threshold shifts and decrease in surface mobility)

Also affects interelectrode isolation and capacitance in detectors.

For many details see:
Ma and Dressendorfer, *Ionizing Radiation in MOS Devices and Circuits*, Wiley, 1989, TK 7871.99.M44I56

Radiation damage is a critical problem in semiconductor detectors.

Dominant effects and mitigation techniques:

a) detector leakage current

$$I_R = I_{R0} + \alpha \Phi A d$$

⇒ shot noise

$$Q_{ni}^2 = 2 q_e I_R F_i T_S$$

⇒ self-heating of detector (thermal runaway possible)

• reduce current by cooling

$$I_R(T) \propto T^2 e^{-E/2k_B T}$$

• reduce shaping time

• reduce area of detector element

b) Increase in depletion voltage

• thin detector

• allow for operation below full depletion

⇒ less signal

Requires lower noise to maintain minimum S/N

• decrease area of detector element
(capacitance)

⇒ pixel detectors

Use of a highly-developed technology, i.e. Si rather than "exotic" materials, provides performance reserves and design flexibility to cope with radiation damage.

for more information: Tutorial at http://www-physics.lbl.gov/~spieler

Example: Photodiode Readout
(S. Holland, N. Wang, I. Kipnis, B. Krieger, W. Moses, LBNL)

Medical Imaging (Positron Emission Tomography)
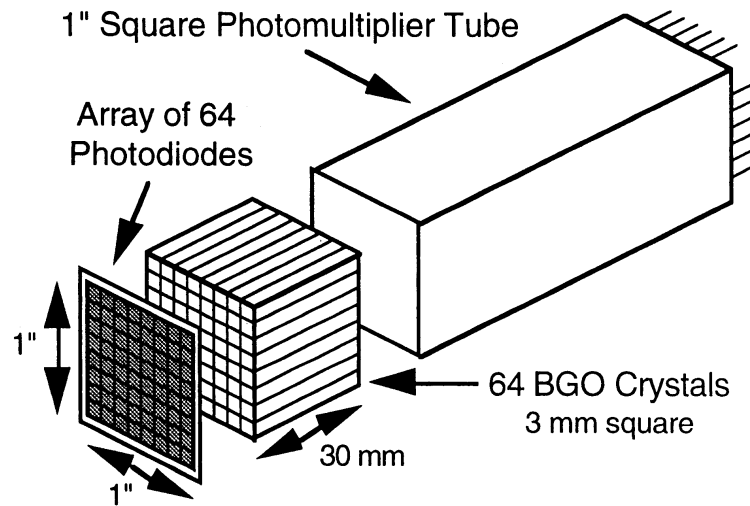
Read out 64 BGO crystals with one PMT (timing, energy) and tag crystal by segmented photodiode array.

Requires then dead layer on photodiode to maximize quantum efficiency.
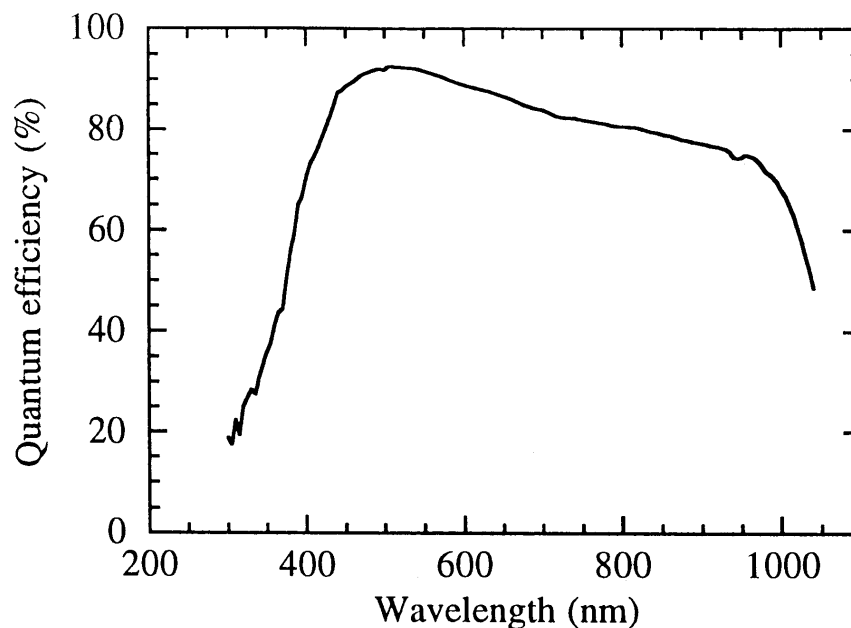
Thin electrode must be implemented with low resistance to avoid significant degradation of electronic noise.

Furthermore, low reverse bias current critical to reduce noise.
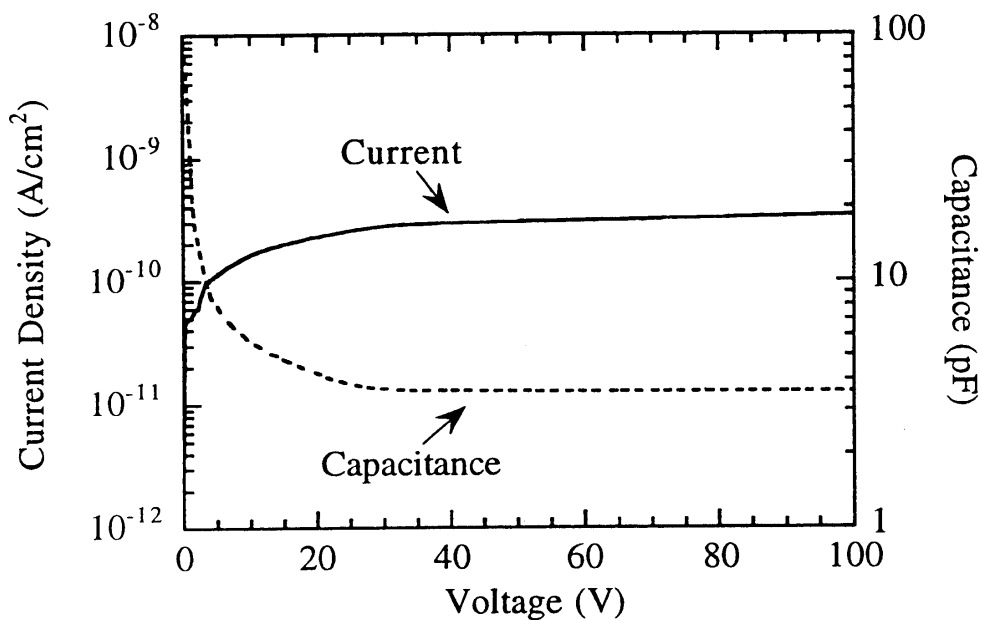
Photodiodes designed and fabricated in LBNL Microsystems Lab.

Front-end chip (preamplifier + shaper):

    16 channels per chip

    die size: 2 x 2 mm^2,
                  1.2 μm CMOS

    continuously adjustable shaping time (0.5 to 50 μs)

    gain: 100 mV per 1000 el.

Noise vs. shaping time
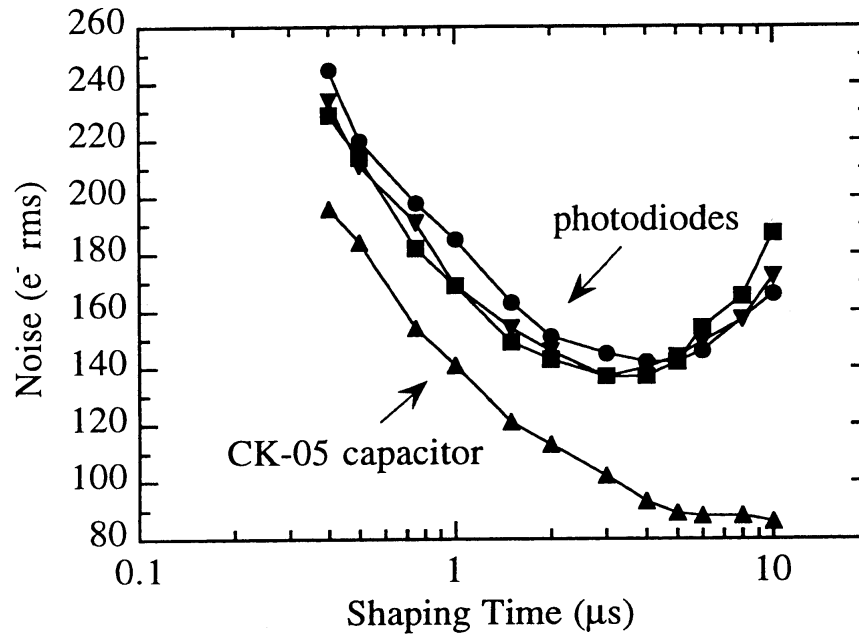
Energy spectrum with BGO scintillator
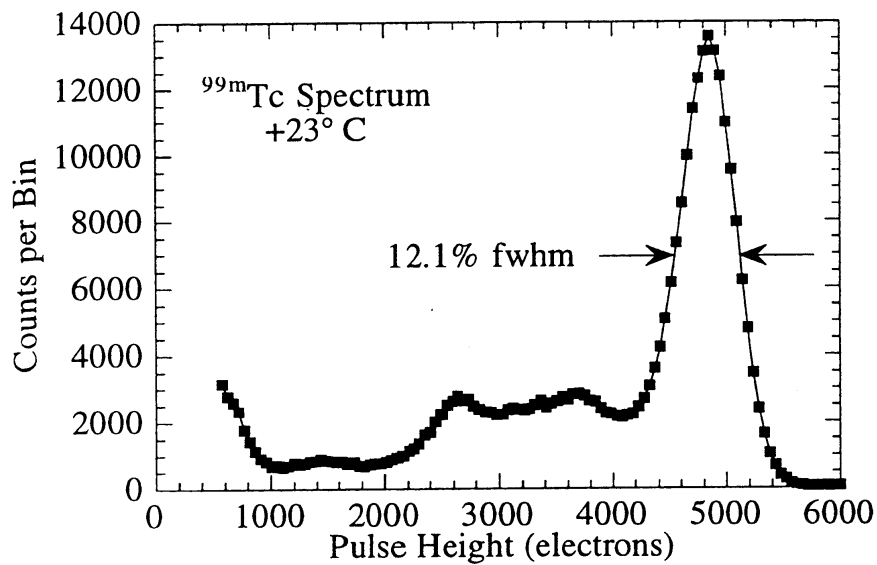
Example: High-Rate X-Ray Spectroscopy
(B. Ludewigt, C. Rossington, I. Kipnis, B. Krieger, LBNL)

Use strip detector

      not for position resolution

but for

      segmentation $\Rightarrow$ distribute rate over many channels

                           $\Rightarrow$ reduced capacitance

                           $\Rightarrow$ low noise at short shaping time

                           $\Rightarrow$ higher rate per detector element

For x-ray energies 5 – 25 keV $\Rightarrow$ photoelectric absorption
                                                   dominates
                                                   (signal on 1 or 2 strips)

Strip pitch: 100 μm   Strip Length: 2 mm (matched to ALS)
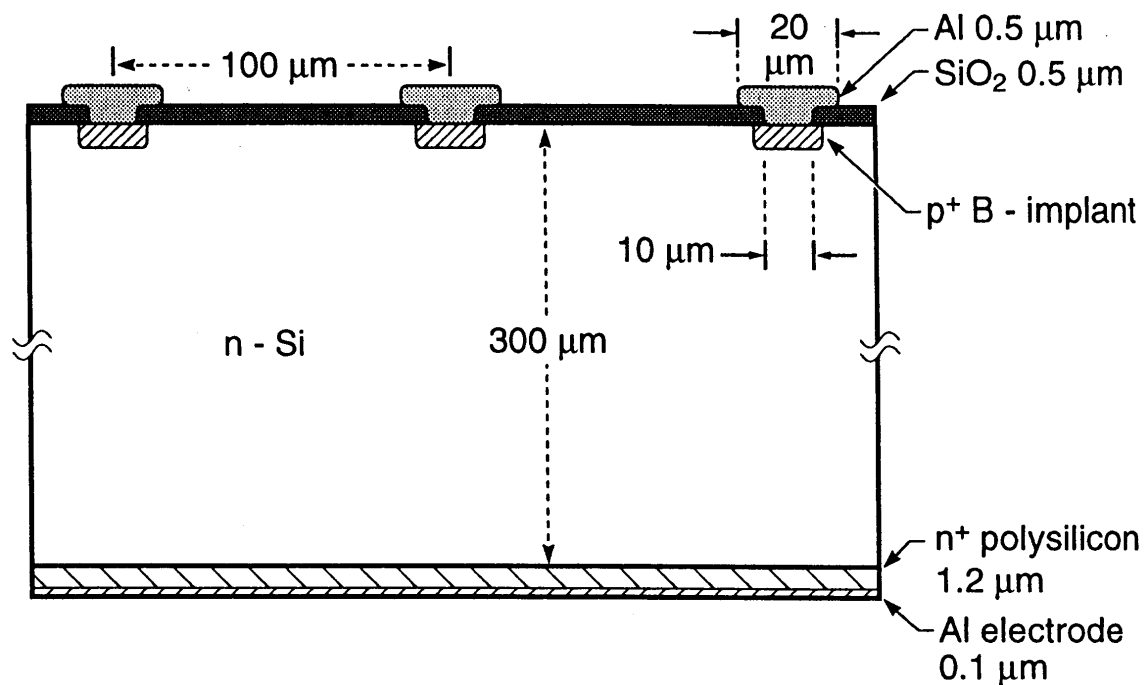
Readout IC tailored to detector

Preamplifier + CR-RC^2 shaper + cable driver to bank of parallel ADCs
(M. Maier, et al.)

Preamplifier with pulsed reset.

Shaping time continuously variable 0.5 to 20 μs.
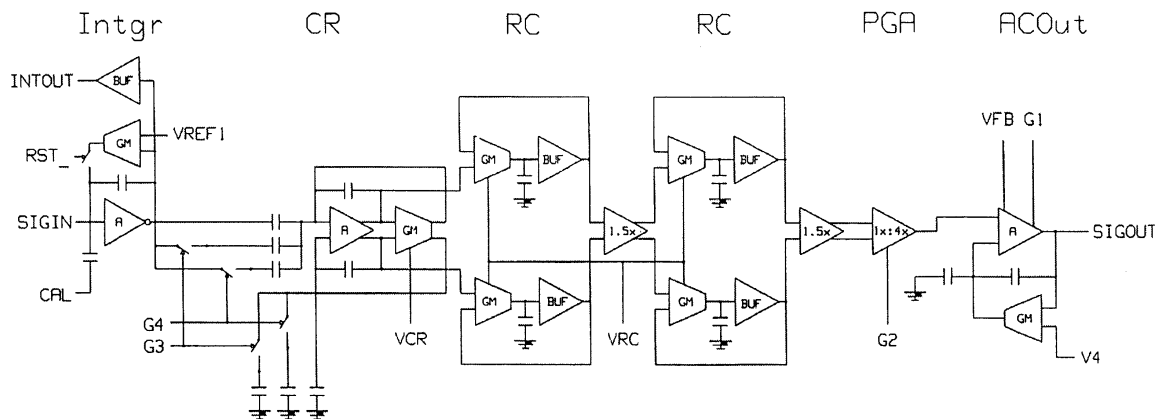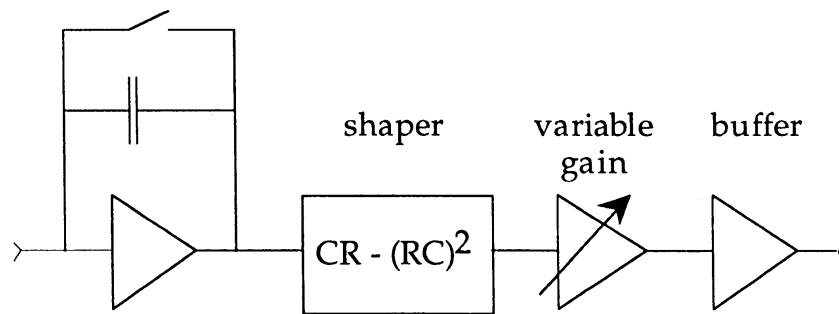
Chip wire-bonded to strip detector
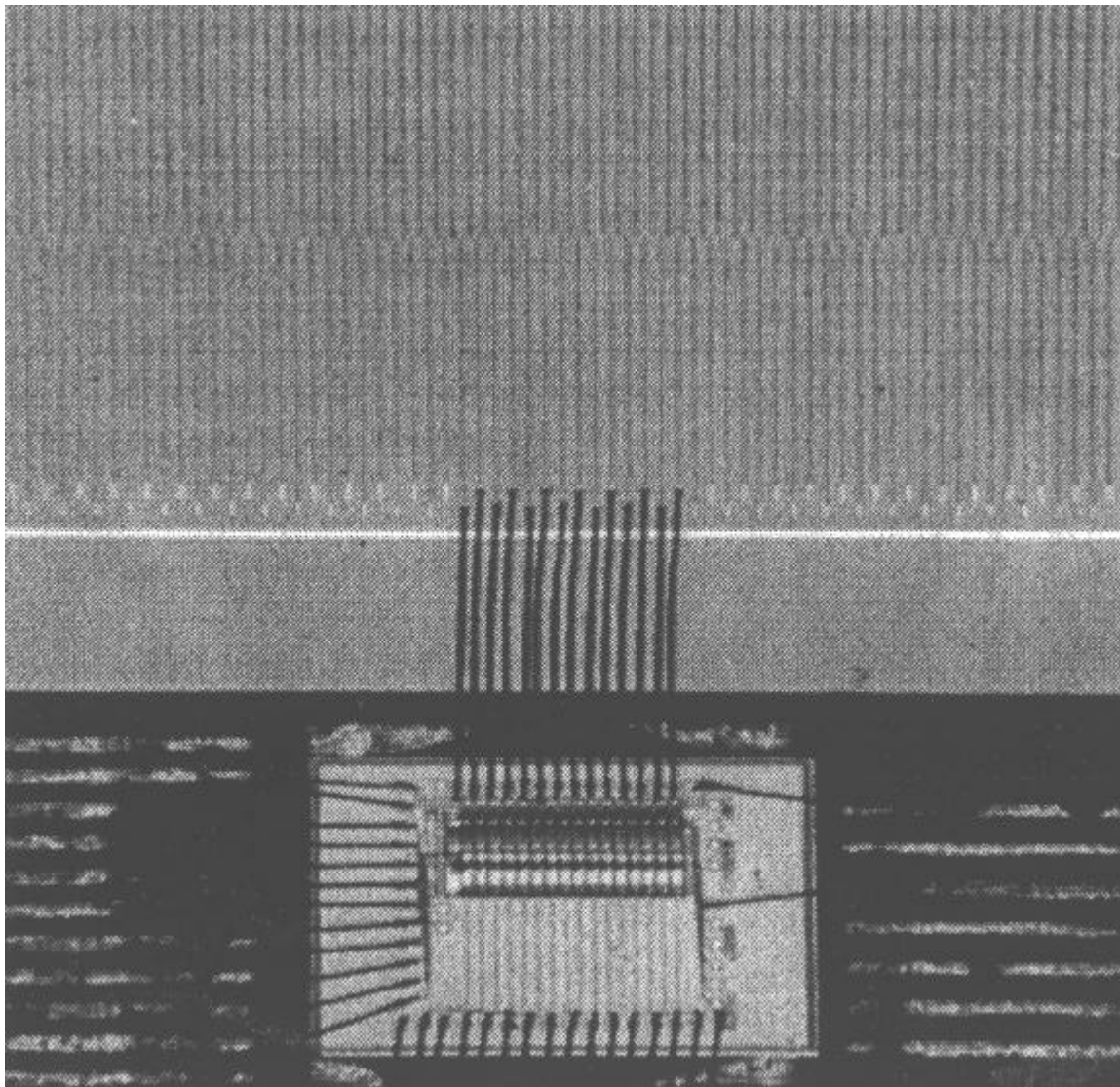
Initial results
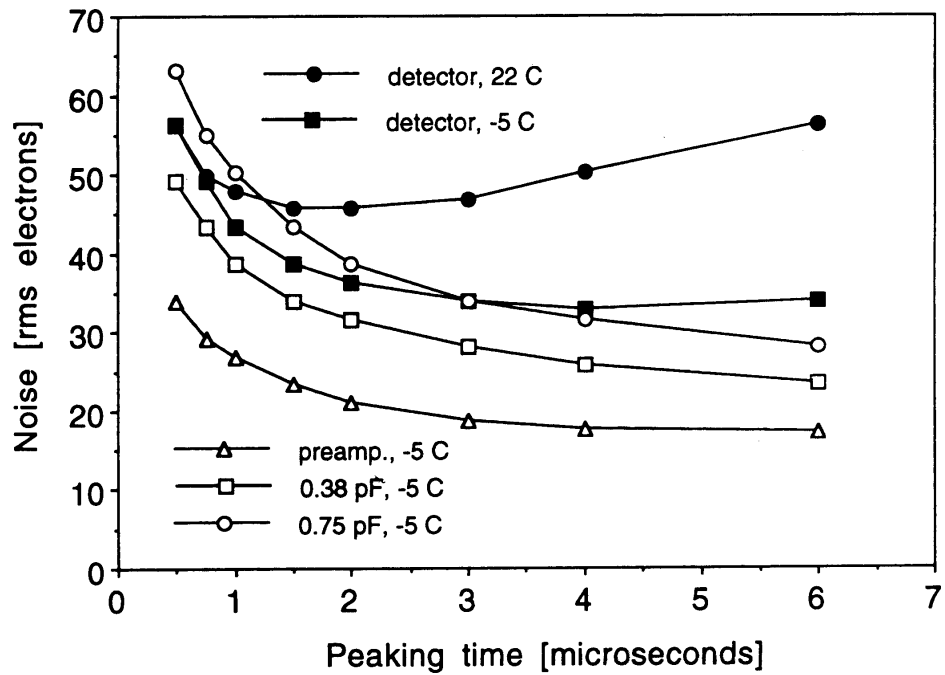
Detector shot noise requires moderate cooling of detector.

Second prototype
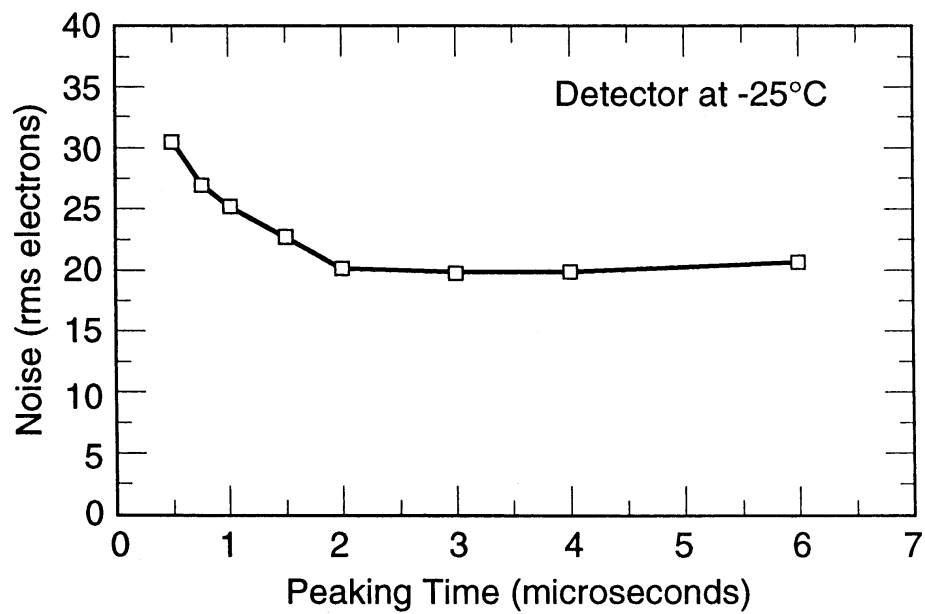
Measured spectra

^{55}Fe
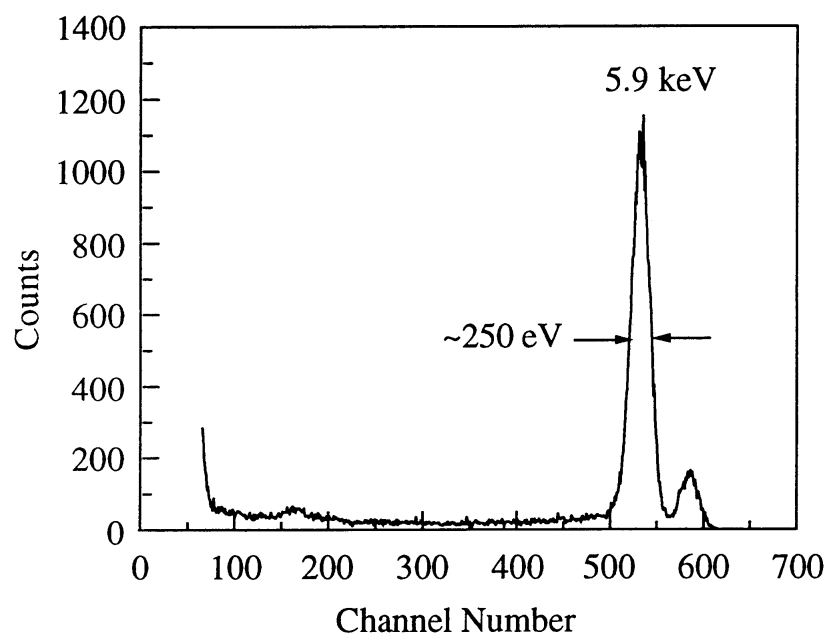
^{241}Am
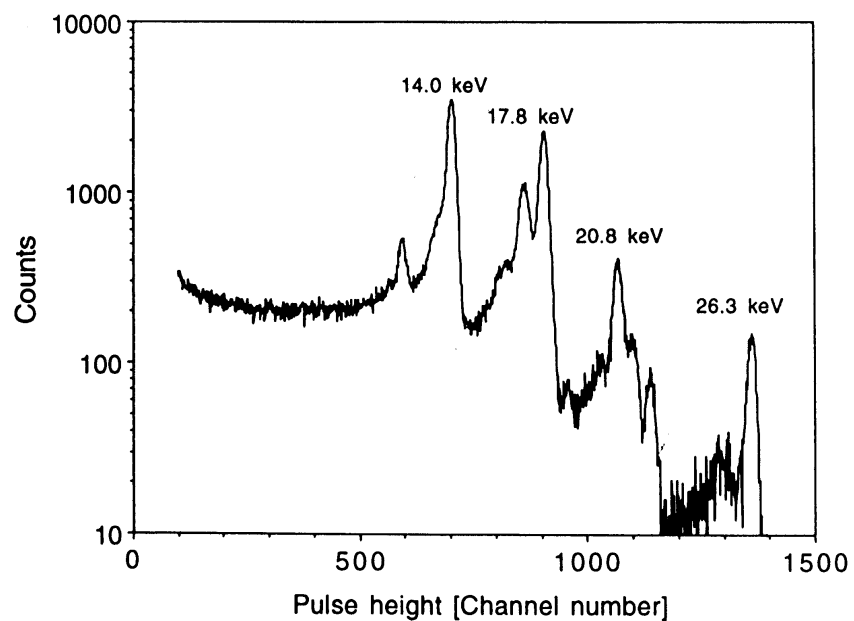
Some detector optimization still necessary

Backside incidence
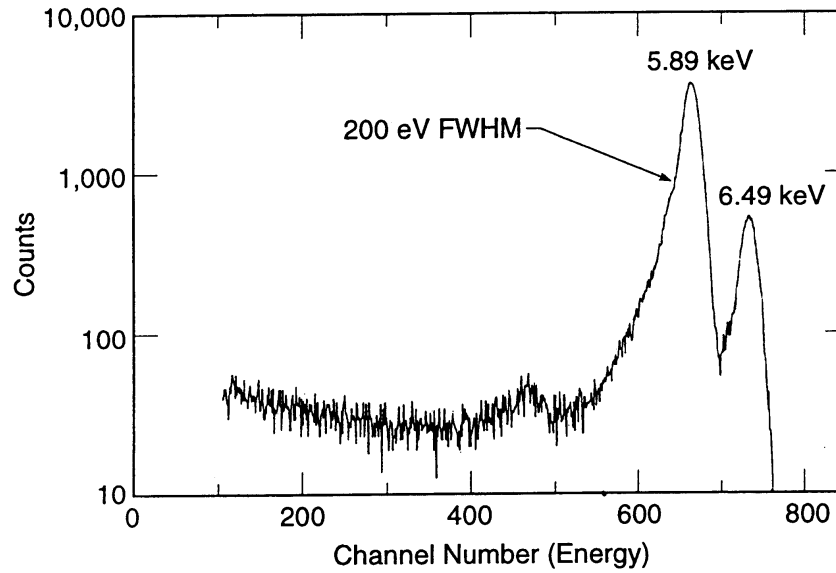
Strip-side incidence
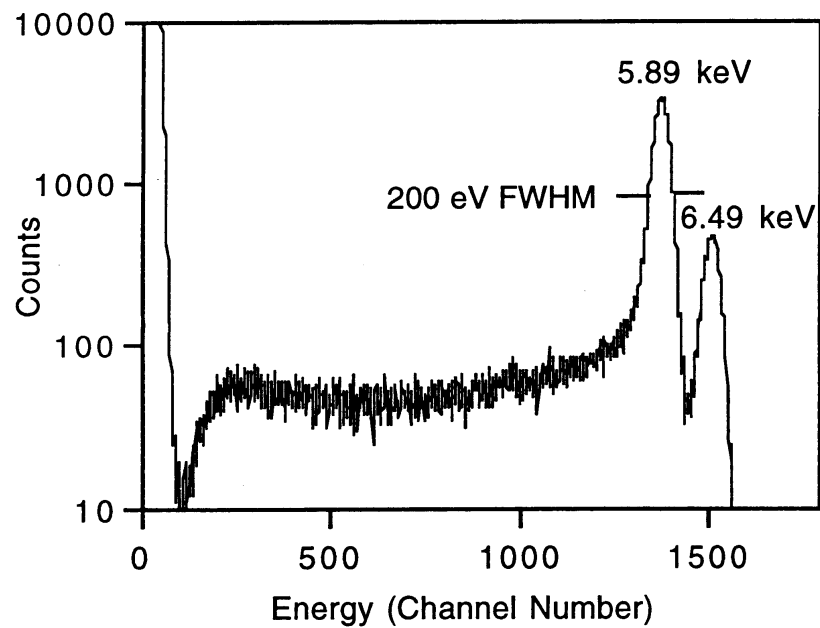
Energy Measurement via Phonons

Energy required to excite phonons much smaller than for ionization. Since a given absorbed energy will produce many more phonons than electron-hole pairs, the statistical fluctuations will be much smaller. Also increased sensitivity to weakly or non-ionizing particles.

Assume thermal equilibrium:

If all absorbed energy E is converted into phonons, the temperature of the sample will increase by

$$\Delta T = \frac{E}{C}$$

where C the heat capacity of the sample (specific heat x mass).

At room temperature the specific heat of Si is 0.7 J/gK, so

$$E = 1 \text{ keV}, m = 1 \text{ g} \quad \Rightarrow \quad \Delta T = 2 \cdot 10^{-16} \text{ K},$$

which isn't practical.

What can be done?

a) reduce mass

b) reduce temperature to reduce heat capacity
"freeze out" any electron contribution, so phonon excitation dominates

Debye model of heat capacity: $C \propto \left(\dfrac{T}{\Theta}\right)^3$

Example $m = 15 \text{ μg}$

$T = 0.1 \text{ K}$

Si $\Rightarrow$ $C = 4 \cdot 10^{-15} \text{ J/K}$

$E = 1 \text{ keV}$ $\Rightarrow$ $\Delta T = 0.04 \text{ K}$

How to measure temperature rise?

Couple thermistor to sample and measure resistance change
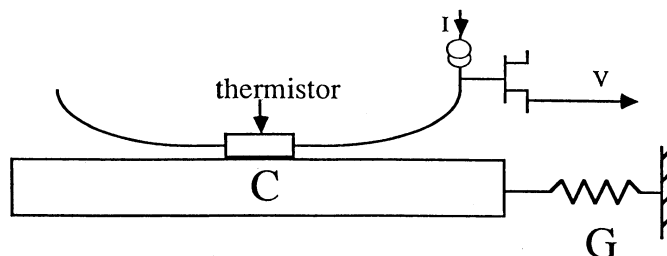
(from Sadoulet at al.)

Thermistors made of very pure semiconductors (Ge, Si) can exhibit responsivities of order 1 V/K, so a 40 mK change in temperature would yield a signal of 40 mV.

Signal Fluctuations

number of phonons

$$\overline{N} = \frac{E}{\overline{E}_{phonon}} = \frac{CT}{k_B T}$$

Fluctuation in the number of phonons

$$\Delta E = \Delta N \cdot \overline{E}_{phonon} = \sqrt{\overline{N}} \cdot \overline{E}_{phonon} = \sqrt{\frac{CT}{k_B T}} \cdot k_B T = \sqrt{k_B T^2 C}$$

so for $T = 0.1$ K and $C = 4 \cdot 10^{-15}$ J/K

$$\Delta E = 0.15 \text{ eV}$$

Theoretical limit of Si ionization detector at 1 keV: ~20 eV rms

Experimental Results

Monolithic Si calorimeter: 0.25 mm wide x 1 mm long x 15 μm thick
(D. McCammon et al., NIM A326 (1993) 157-165)
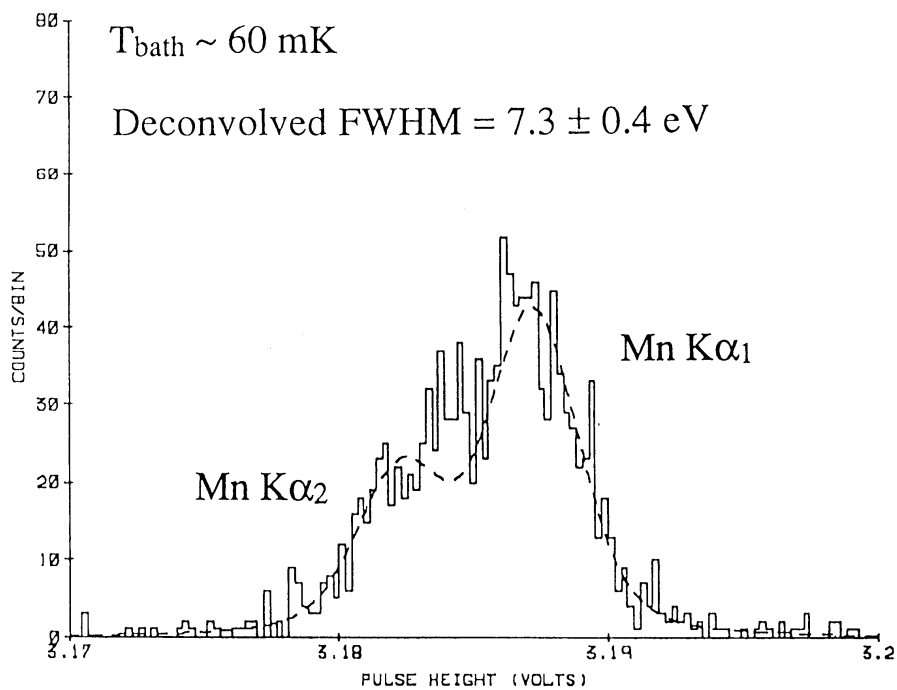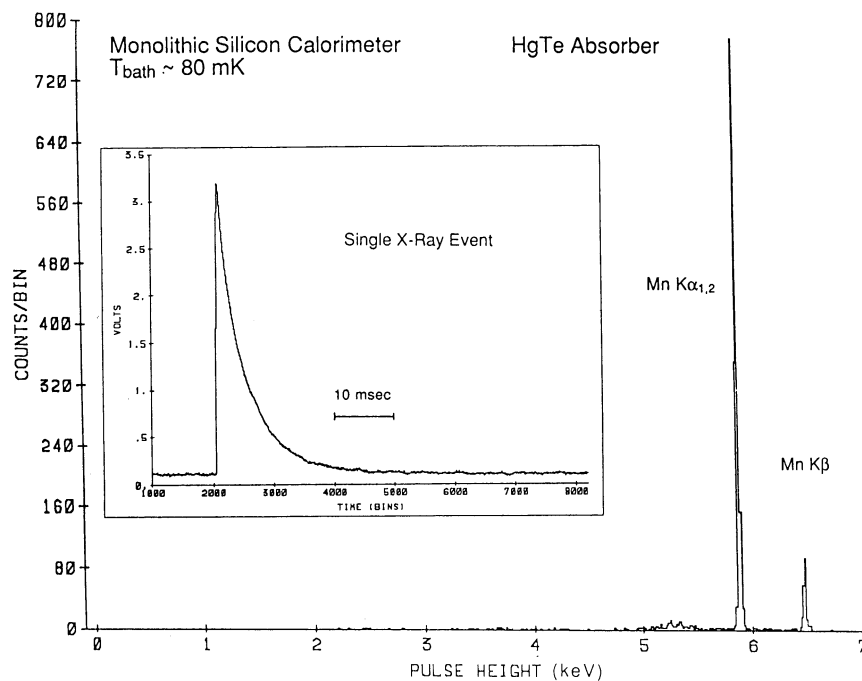
Recent results from NIST group
(Martinis et al., see Physics Today, July, 1998)
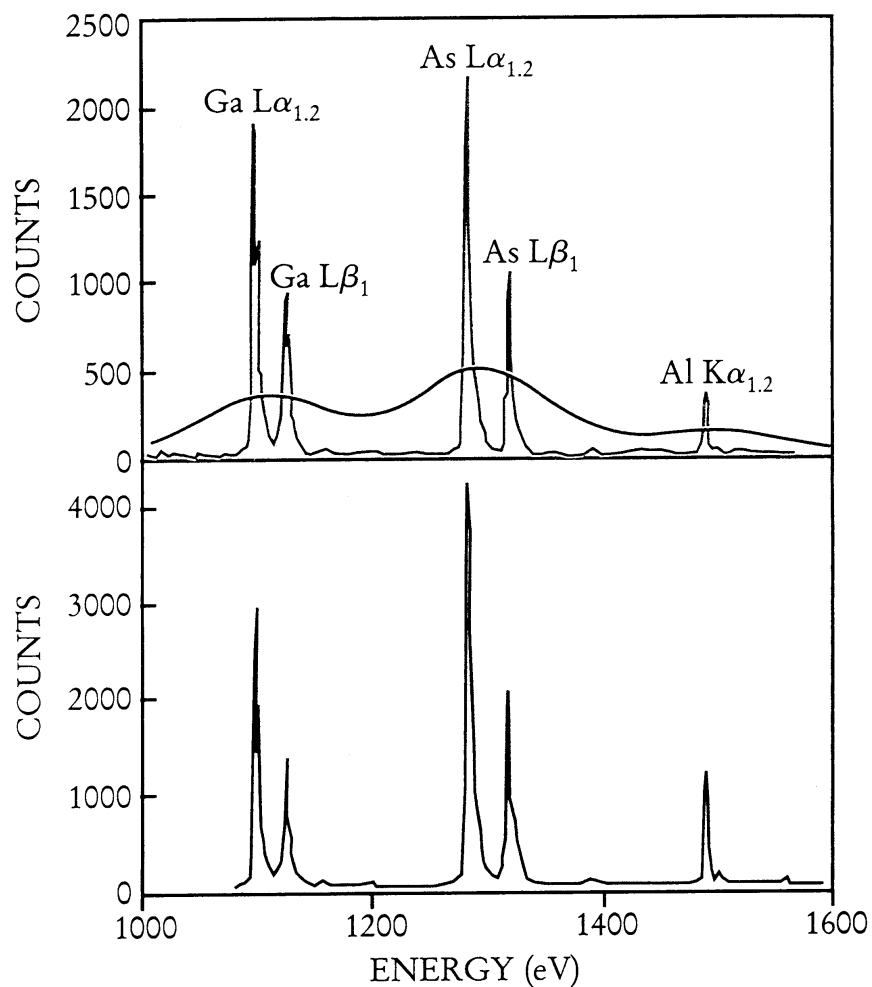
Upper plot: microcalorimeter spectrum (4 eV resolution) with superimposed spectrum from conventional Si detector

Lower plot: crystal diffraction spectrometer

Noise optimization

Absorber coupled to cold finger through thermal conductance G.

The signal pulse will rise rapidly by ΔT and decay exponentially

$$T(t) = \Delta T e^{-t/\tau}$$

with the decay time

$$\tau = \frac{C}{G}$$

Single X-Ray Event

10 msec
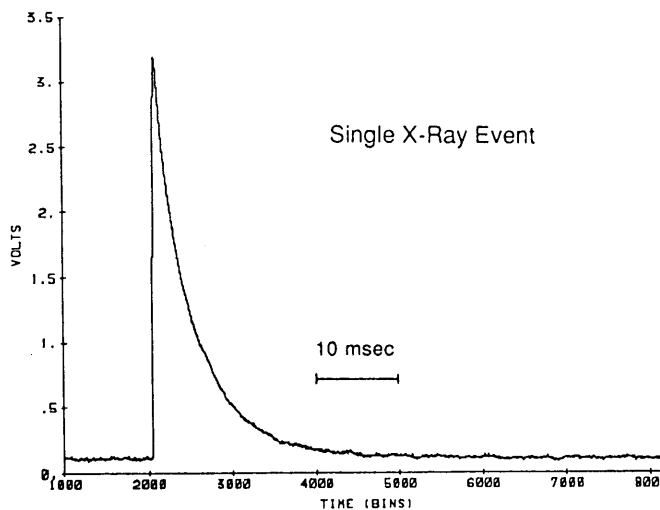
Fluctuations in the phonon number in the absence of incident radiation will give rise to noise pulses with the same shape.

$\Rightarrow$ both the signal and the noise have the same frequency spectrum

$\Rightarrow$ S/N *of sensor alone* is independent of shaping time

However, this does not apply to external noise sources, for example

- resistive sensor

- input transistor

- noise induced by mechanical vibrations

Ideally, front-end and shaper designed to contribute negligible noise, while providing suppression of low-frequency pickup.

Furthermore, phonon fluctuations are increased by fluctuations in signal going into ionization and ionization losses (e.g. trapping).

Silicon sensor can also be configured to measure ionization simultaneously with phonon excitation (P. Luke, LBNL)
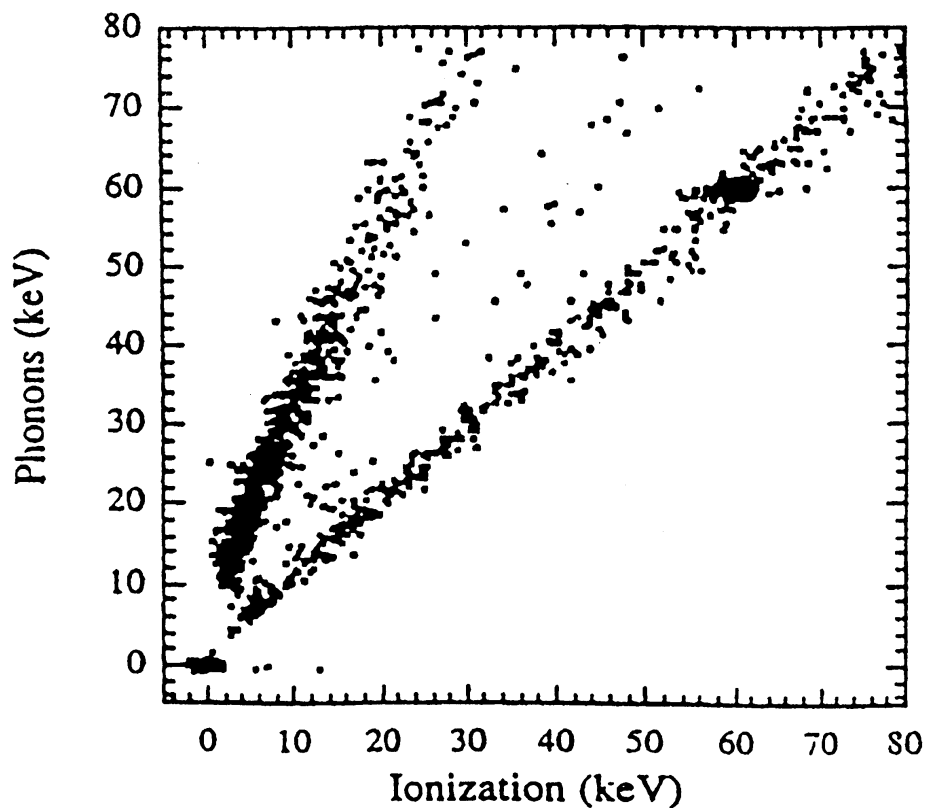
(from Sadoulet et al.)

Upper branch: weakly ionizing nuclear recoils

Lower branch: compton electrons from incident gamma rays

Can be used for background suppression

# Tracking Detectors: Required Signal-to-Noise Ratio

Acceptable noise level established by signal level and noise occupancy

1. Signal Level
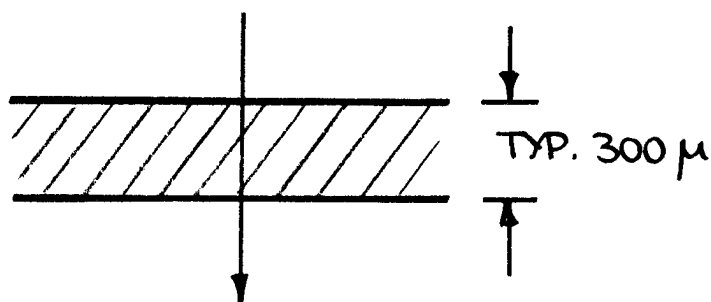
For minimum ionizing particles: Q_s= 22000 el (3.5 fC)

Signals vary event-by-event according to Landau distribution
(calculation by G. Lynch)
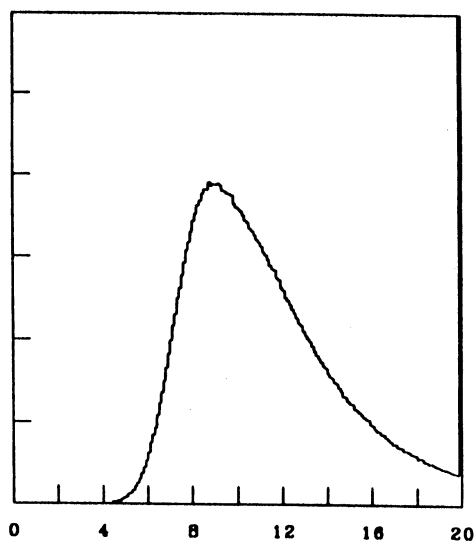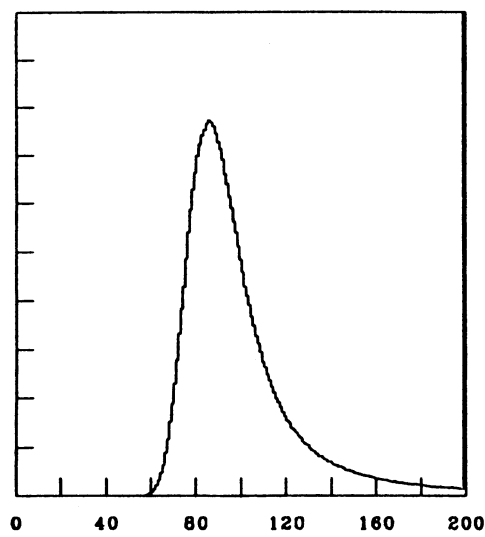
Si : 40 µm thick   Si : 300 µm thick

Width of distribution decreases with increasing energy loss.

Measured Landau distribution in a 300 μm thick Si detector
(Wood et al., Univ. Oklahoma)
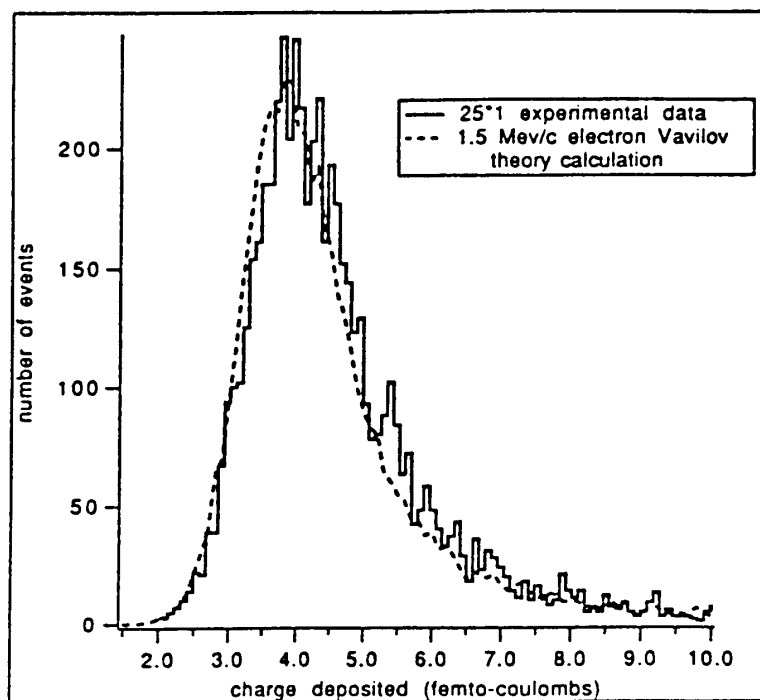
The Landau distribution peaks at the most probable energy loss Q_0 and extends down to about 0.5 Q_0 for 99% efficiency.

Assume that the minimum energy is $f_L Q_0$.

Tracks passing between two strips will deposit charge on both strips. If the fraction of the signal to be detected is f_{sh}, the circuit must be sensitive signal as low as

$$Q_{\min} = f_{sh} f_L Q_0$$

2. Threshold Setting

It would be desirable to set the threshold much lower than Q_{min}, to be insensitive to threshold variations across the chip.

A lower limit is set by the need to suppress the noise rate to an acceptable level that still allows efficient pattern recognition.

The threshold-to-noise ratio required for a desired noise rate f_n in a system with shaping time T_S is (see Physics 198 course notes)

$$\frac{Q_T}{Q_n} = \sqrt{-2\log(4\sqrt{3}f_n T_S)}$$

Expressed in terms of occupancy P_n in a time interval Δt

$$\frac{Q_T}{Q_n} = \sqrt{-2\log\left(4\sqrt{3}_n T_S \frac{P_n}{\Delta t}\right)}$$

In the strip system the average hit occupancy is about 5×10^{-3} in a time interval of 25 ns. If we allow an occupancy of 10^{-3} at a shaping time of 20 ns, this corresponds to

$$\frac{Q_T}{Q_n} = 3.2$$

The threshold uniformity is not perfect. The relevant measure is the threshold uniformity referred to the noise level. For a threshold variation ΔQ_T, the required threshold-to-noise ratio becomes

$$\frac{Q_T}{Q_n} = \sqrt{-2\log\left(4\sqrt{3}_n T_S \frac{P_n}{\Delta t}\right)} + \frac{\Delta Q_T}{Q_n}$$

If $\Delta Q_T / Q_n = 0.5$, the required threshold-to-noise ratio becomes $Q_T / Q_n = 3.7$.

To maintain good timing, the signal must be above threshold by at least Q_n, so $Q_T / Q_n > 4.7$.

Combining the conditions for the threshold

$$\left(\frac{Q_T}{Q_n}\right)_{\min} Q_n \leq Q_{\min}$$

and signal

$$Q_{\min} = f_{sh} f_L Q_0$$

yields the required noise level

$$Q_n \leq \frac{f_{sh} f_L Q_0}{(Q_T / Q_n)_{\min}}$$

If charge sharing is negligible $f_{sh} = 1$, so with $f_L = 0.5$, $Q_0 = 3.5$ fC and $(Q_T / Q_n)_{\min} = 4.7$

$$Q_n \leq 0.37 \text{ fC} \text{ or } Q_n \leq 2300 \, el$$

If the system is to operate with optimum position resolution, i.e. equal probability of 1- and 2-hit clusters, then $f_{sh} = 0.5$ and

$$Q_n \leq 0.19 \text{ fC} \text{ or } Q_n \leq 1150 \, el$$

Examples

1. CDF Vertex Detector Upgrade: SVX2

Expand coverage of existing vertex detector

a) side view (z = beam axis)
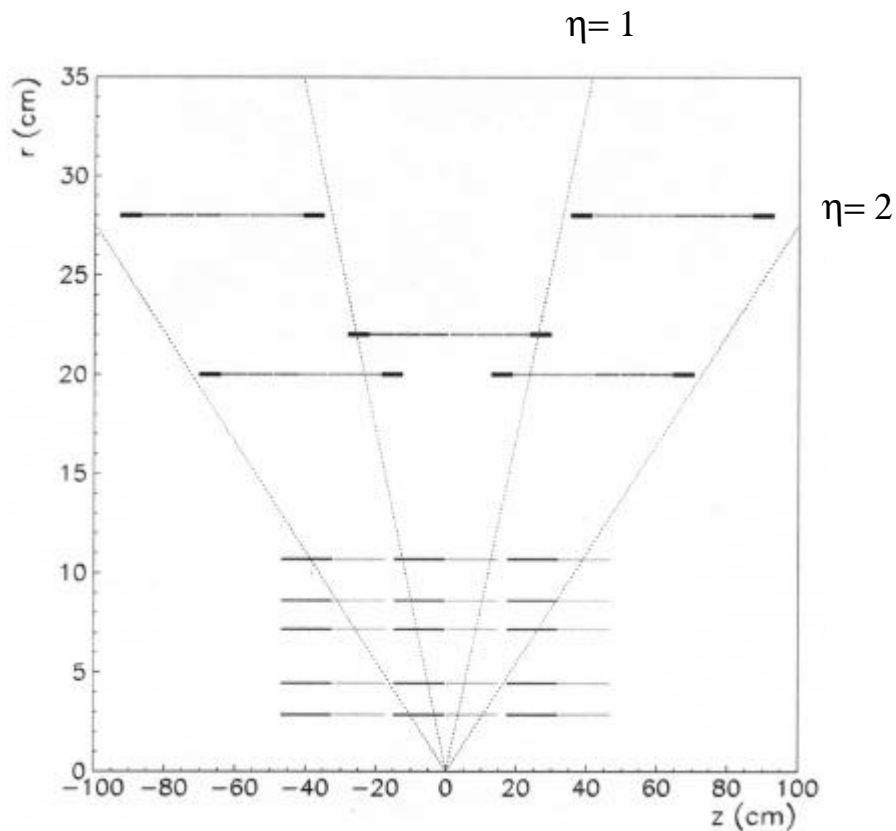
    Inner 5 layers: SVX2

    Outer 2 layers: ISL

b) Axial view of vertex detector
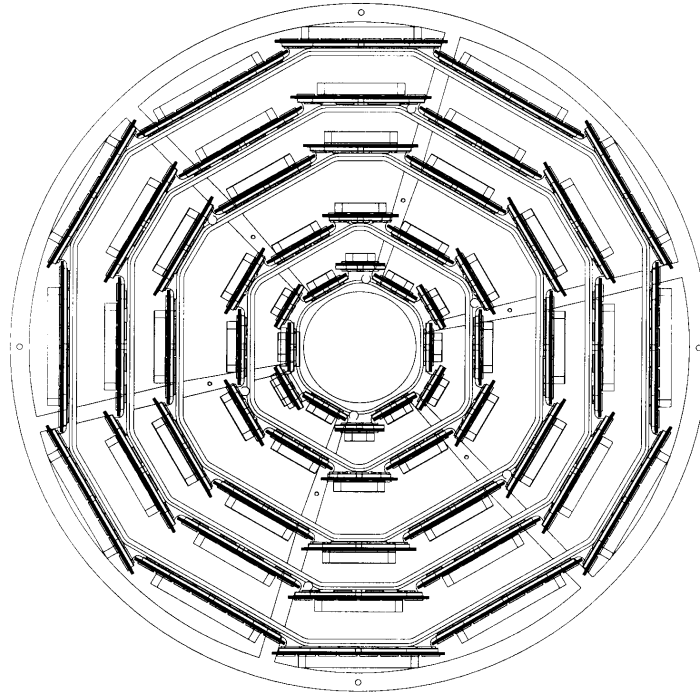
Property	Layer 0	Layer 1	Layer 2	Layer 3	Layer 4
Radial distance (cm)	2.45	4.67	7.02	8.72	10.6
Stereo angle (degrees)	90	90	+1.2	90	-1.2
$r\phi/z$ readout channels	256/512	384/576	640/640	768/512	896/896
$r\phi/z$ readout chips	2/2	3/3	5/5	6/4	7/7
$r\phi/z$ strip pitch (μm)	60/141	62/125.5	60/60	60/141	65/65
Total width (mm)	17.14	25.59	40.30	47.86	60.17
Total length (mm)	74.3	74.3	74.3	74.3	74.3

Layers 0, 1 and 3 use 90° stereo angle, whereas layers 4 and 5 use 1.2° stereo angle to reduce ghosting.

Electronic Readout

SVX2 uses the SVX3 chip, which is a further development of the SVX2 chip used by D∅.

Include on-chip digitization of analog signal

Threshold, calibration via on-chip DACs

All communication to and from chip via digital bus

Block diagram of SVX2
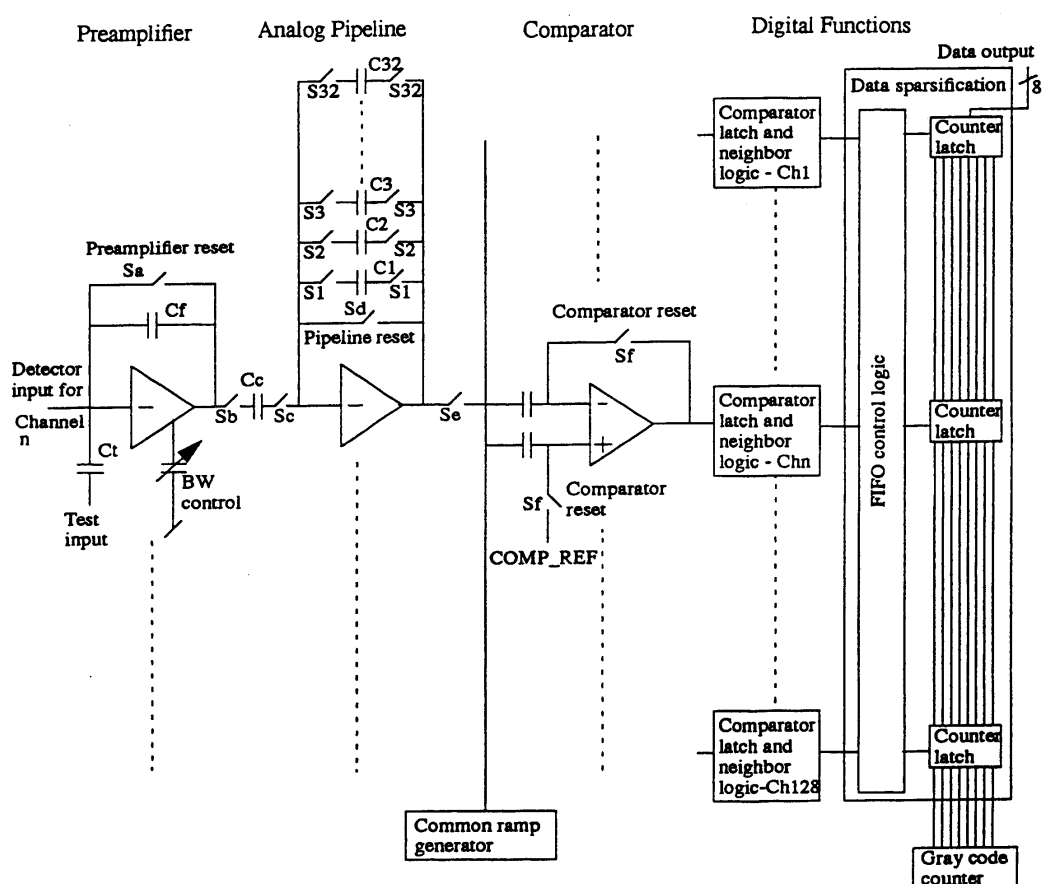
Wilkinson ADC integrated with pipeline + comparator required for sparsification. Adds 100 μm to length and 300 μW/ch power.

ADC clock runs at 106 MHz in experiment, tested to 400 MHz

Total power: 3 mW/ch

SVX2 die layout

Dimensions: 6.3 x 8.7 mm

0.8 μm, triple-metal rad-hard CMOS

Input Pads

Preamplifiers

Analog Pipeline

ADC Comparator

Neighbor Logic

Sparsification +
Readout

ADC Ramp +
Counter, I/O
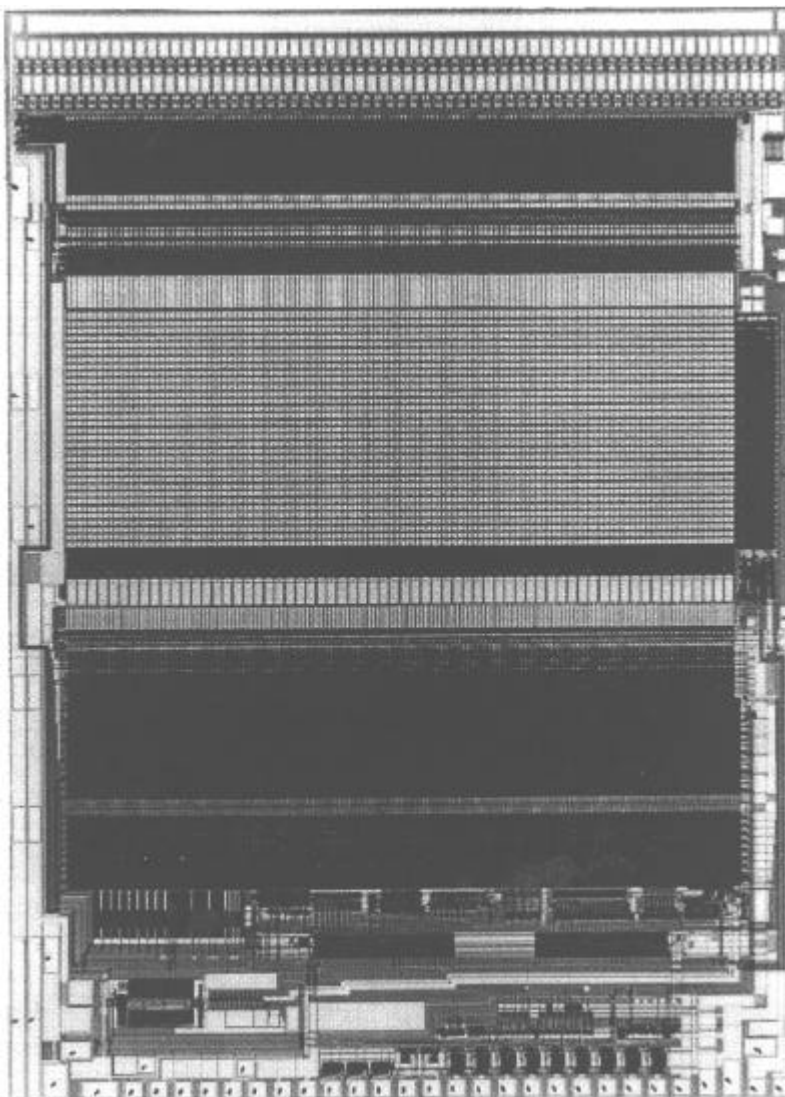
SVX2 (used by D∅) is designed for sequential signal acquisition and readout.

SVX3 (used by CDF) allows concurrent read-write, i.e. signal acquisition and readout can proceed concurrently.

SVX3 Floor Plan

SVX3FE — SVX3BE

Pipeline Control Logic

Integrators (128 channels)

Analog Pipeline

128 Channels

47 Storage cells / channel

ADC Comparators

Sparsification FIFO

I/O

ADC ramp and Counter

Analog Section — **Digital Section**
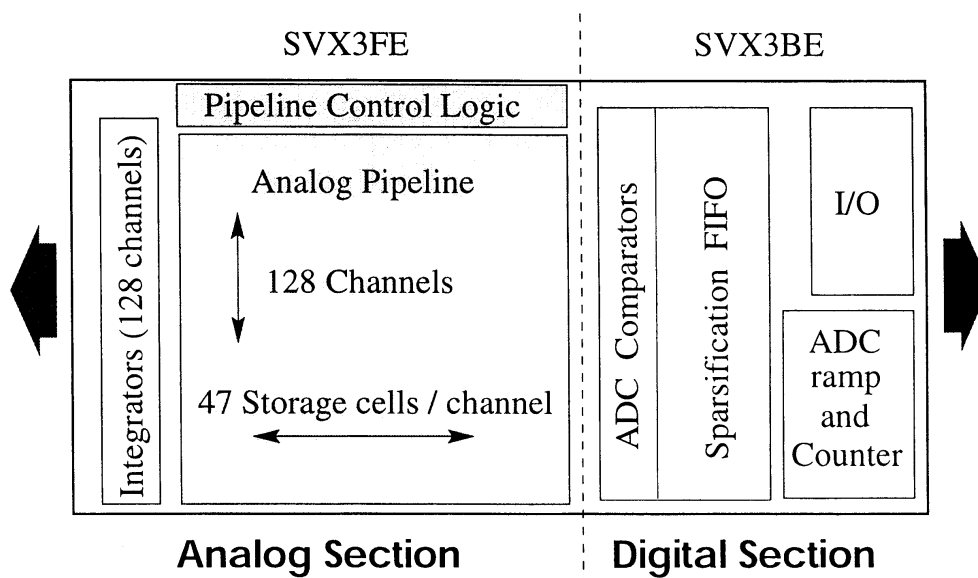
Analog section: 6.26 x 8.06 mm^2
Digital section: 6.26 x 4.97 mm^2

Combined in 1 chip: 6.26 x 12 mm^2

Measured Noise: Q_n= 500 el + 60 el/pF rms

Both chips fabricated in rad-hard CMOS.

SVX2 and SVX3 utilize correlated double sampling for pulse shaping
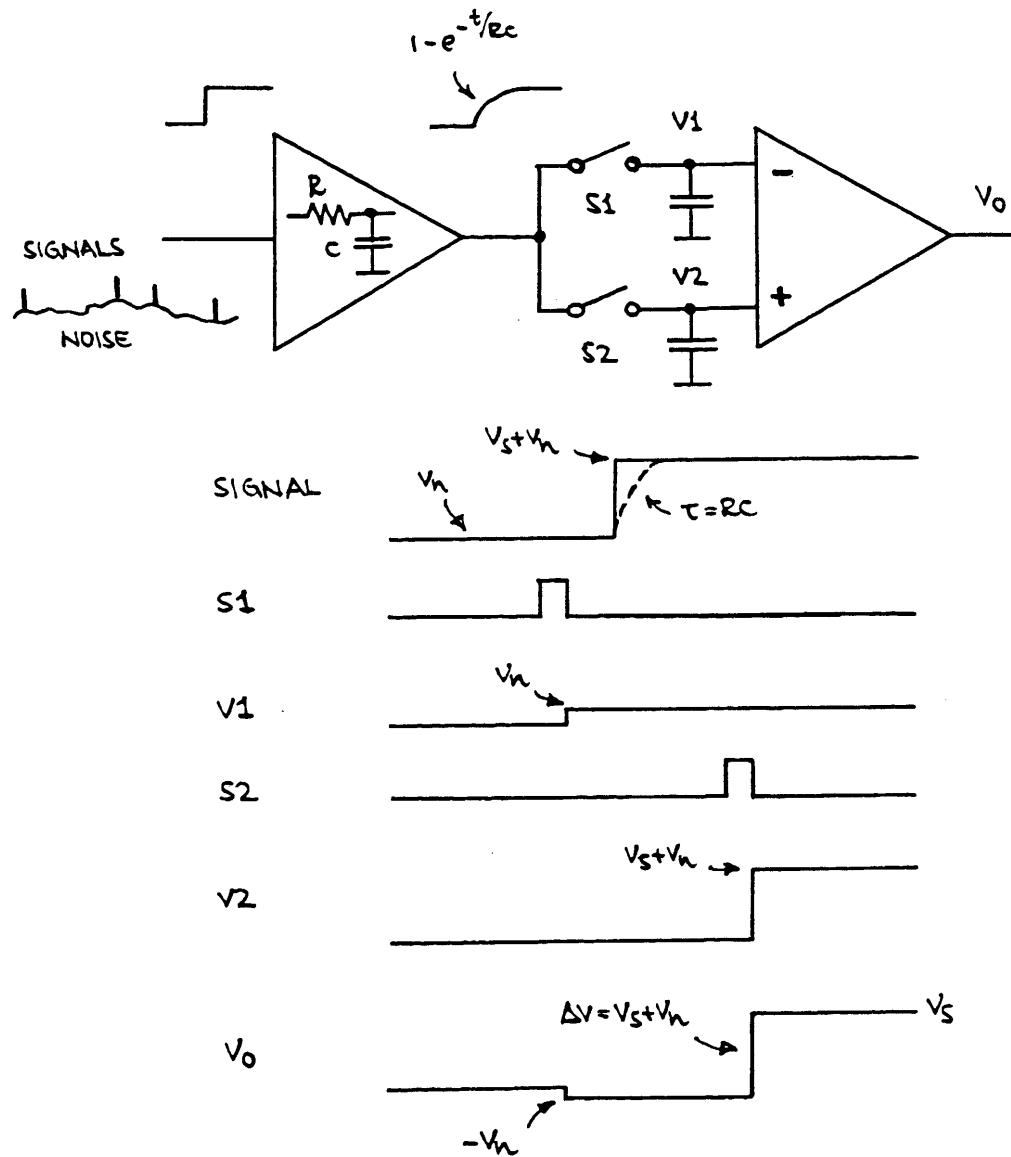
Correlated double sampling requires prior knowledge of signal arrival.

OK for colliders if $\Delta T_{beam} > T_{shaper}$, but not for random signals.

High luminosity colliders (SLAC B Factory, LHC) have much shorter beam crossing intervals

$\Rightarrow$ continuous shaping required

2. BaBar Silicon Vertex Tracker

B mesons from $\Upsilon(4S)$ production have low momentum.

Asymmetry in beam energies (9 GeV e$^-$ on 3.1 GeV e$^+$) used to provide boost ($\beta\gamma = 0.56$) that allows conventional vertex detectors to cope with short B meson lifetime.

Vertex detector must provide resolution in boost direction, i.e. parallel to beam axis, rather than in $r\varphi$.

Resolution requirement not stringent:

> Less than 10% loss in precision in the asymmetry measurement if the separation of the B vertices is measured with a resolution of ½ the mean separation (250 µm at PEPII)

> $\Rightarrow$ 80 µm vertex resolution required for both CP eigenstates and tagging final states.

Resolution is multiple-scattering limited

> beam pipe: 0.6% X_0

Use crossed strips

> z-strips for vertex resolution

> $r\varphi$ strips for pattern recognition

Measurement does not utmost position resolution

> $\Rightarrow$ use binary readout

Position resolution for analog and binary readout vs dip angle λ.

Analog readout (50 and 100 μm pitch)

Analog Centroid

Noise=4.3 keV, D=300
Threshold 4 x Noise
+ Pitch=50
O Pitch=100
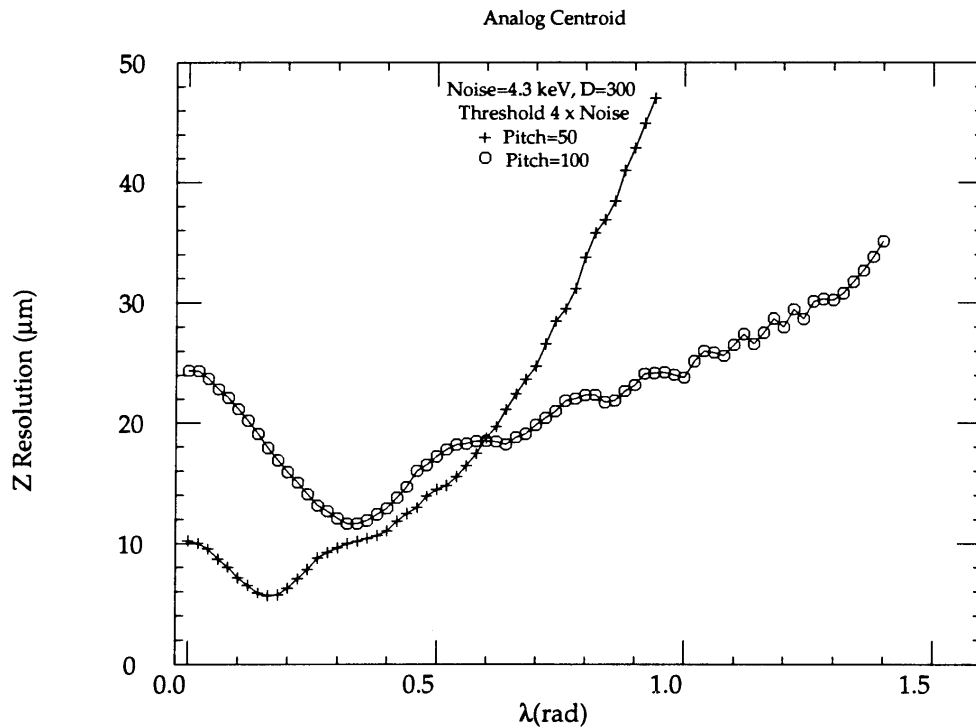
Binary readout (50 and 100 μm pitch)

Digital Centroid

Noise=4.3 keV, D=300
Threshold 4 x Noise
+ Pitch=50
O Pitch=100
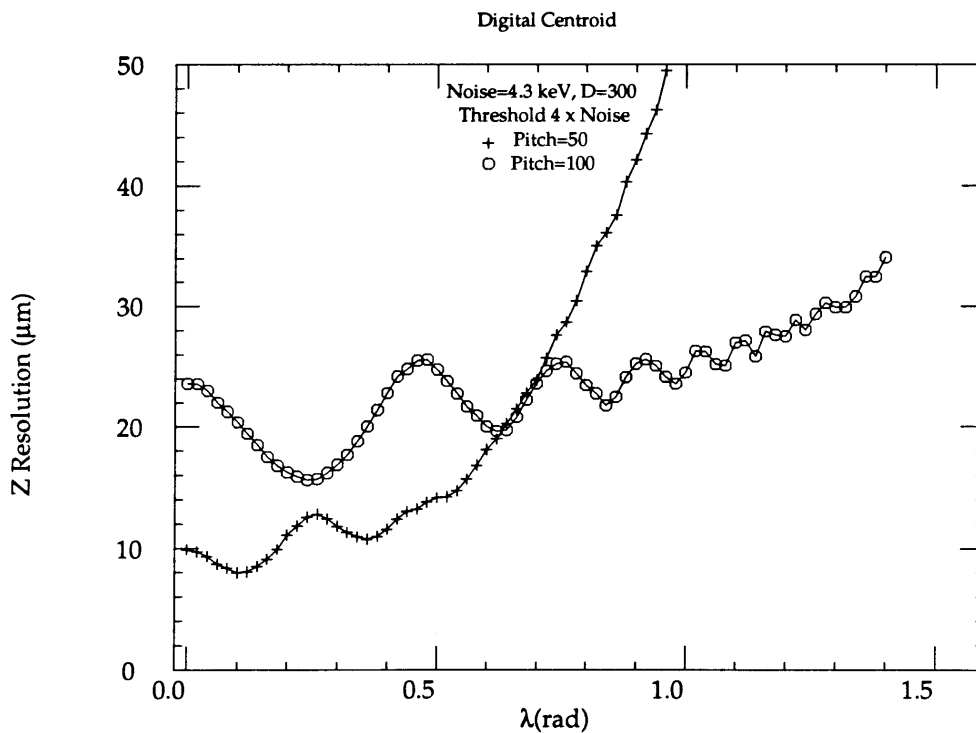
Why does 100 mm pitch yield better resolution at large dip angles?

Signal in z-strips degrades at large dip angles

$$Q_s = d\,\frac{dE}{dx} \qquad\qquad Q_s = p\cos\Theta\cdot\frac{dE}{dx}$$
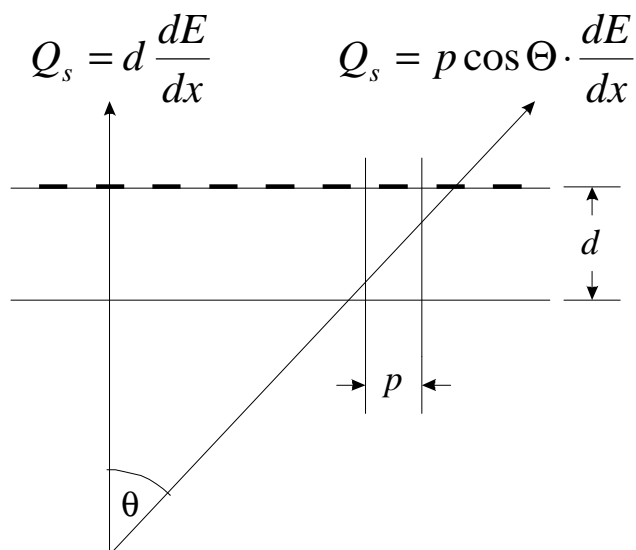
Change strip pitch at $\lambda > 0.7$ radians

Furthermore ….

   add coarse analog information (3 – 4 bits adequate)

Mechanical arrangement of detector

Axial view

14 cm
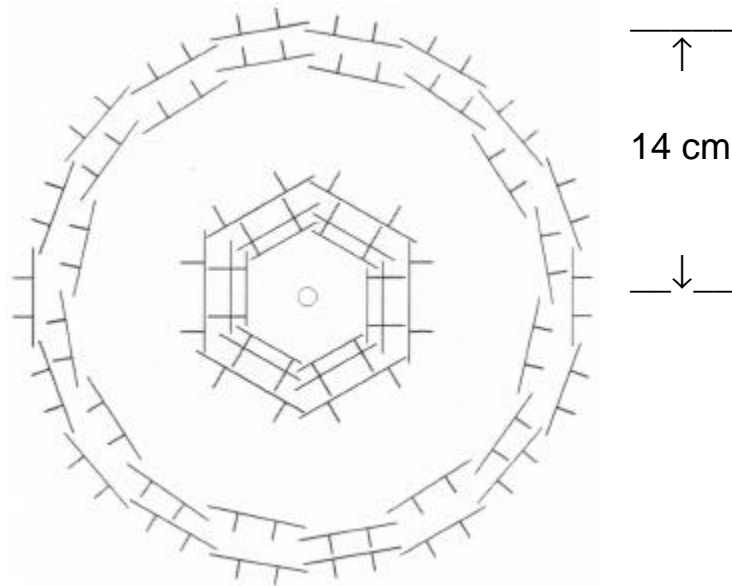
Side view
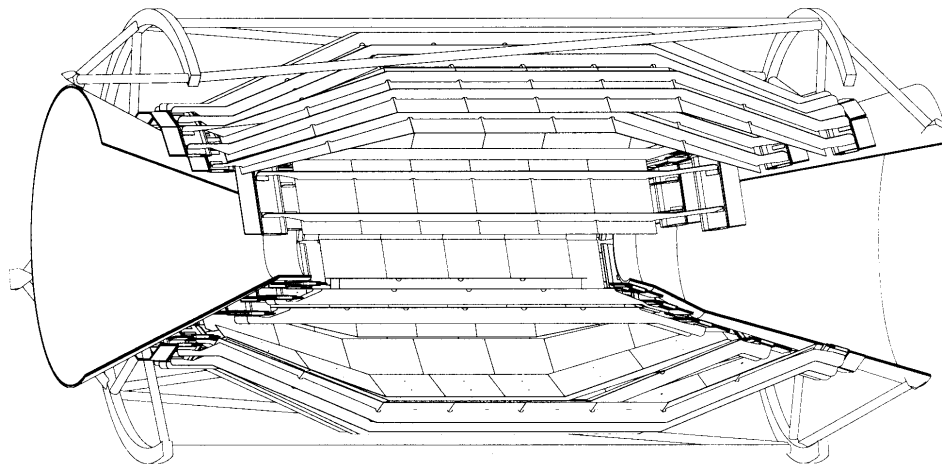
Outer layers use "lampshade" geometry instead of disks
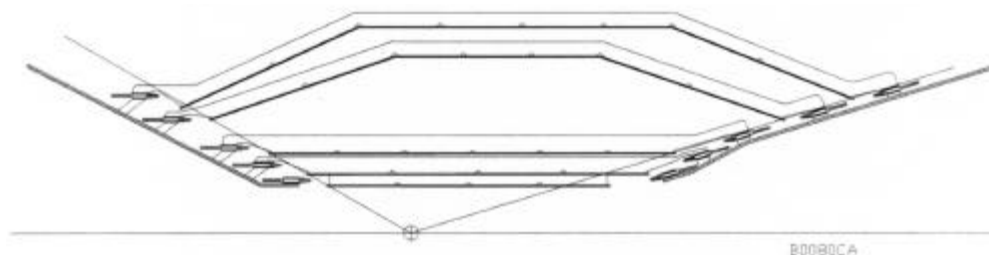
Electronics mounted outside of active region
(connected to detectors by kapton cables)

$\Rightarrow$ long strips (high capacitance) in outer layers

| Layer	Fanout Type	Length (cm)	Number of Readout Strips	Channels	Typical Pitch at Input (μm)	Output (μm)	Number of Circuits
1	z, F+B	12.5	950	768	100	50	12
	ϕ, F+B	3.0	768	768	50	50	12
2	z, F+B	14.5	1150	1024	100	50	12
	ϕ, F+B	3.0	960	1024	50	50	12
3	z, F+B	15.6	1360	1280	100	50	12
	ϕ, F+B	2.0	1280	1280	50	50	12
4a	z, F	19.7	885	512	200	50	8
	z, B	24.3	1115	512	200	50	8
	ϕ, F+B	2.0	512	512	65	50	16
4b	z,F	20.6	930	512	200	50	8
	z,B	24.2	1160	512	200	50	8
	ϕ, F+B	2.0	512	512	65	50	16
5a	z, F	25.2	1160	512	200	50	9
	z, B	25.1	1205	512	200	50	9
	ϕ, F+B	2.0	512	512	65	50	18
5b	z, F+B	26.1	1205	512	200	50	18
	ϕ, F+B	2.0	512	512	65	50	18

z-strips are connected at ends, to avoid cables in middle of detector.

Kapton connecting cables that connect multiple detector segments
(use $r\varphi$ resolution to disentangle ambiguities)

Connections made along diagonals:
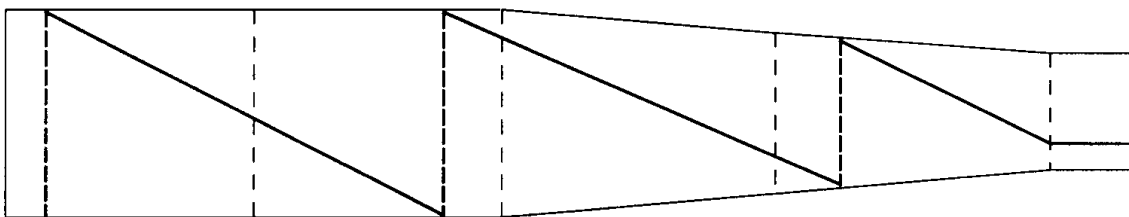
AToM – Readout IC for BaBar Vertex Detector
(LBNL, Pavia, UCSC)

AToM Block Diagram
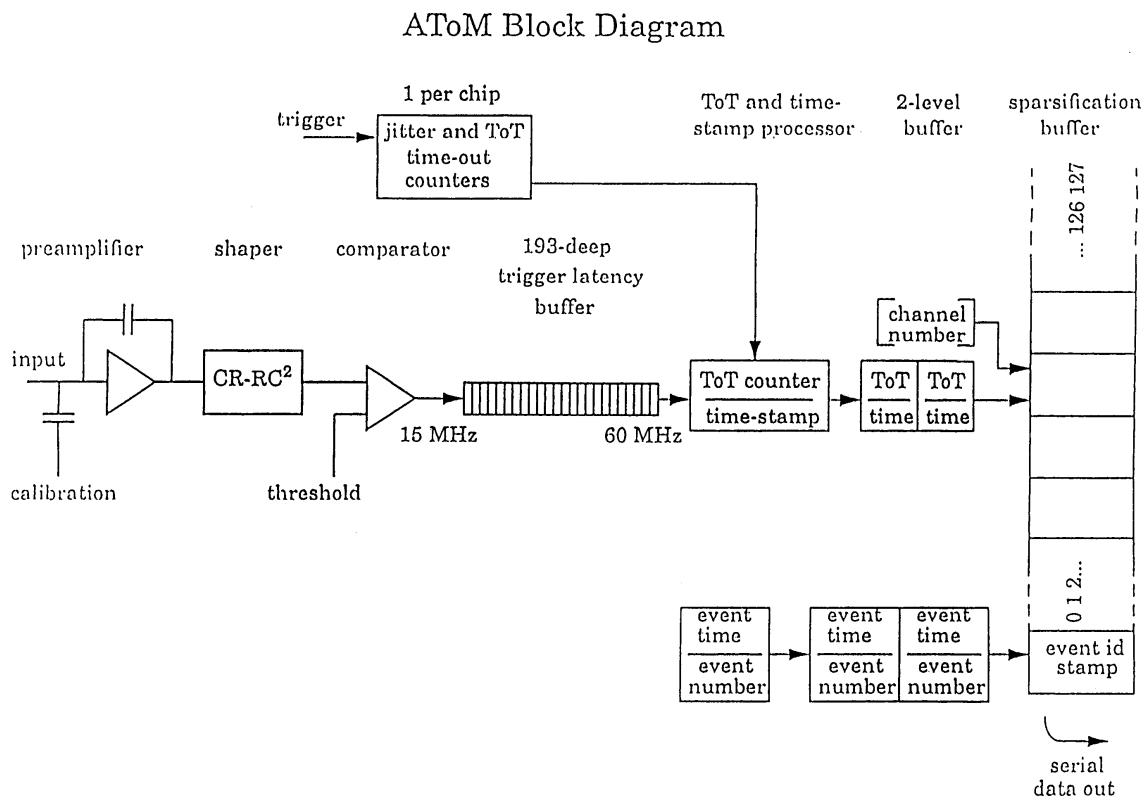
Preamplifier with continuous reset

CR-RC^2 shaper with selectable shaping times (100, 200 and 400 ns)

> Outer layers of tracker have longer strips (higher capacitance) than inner layers. Lower occupancy allows use of longer shaping time to maintain electronic noise.

Coarse digitization via Time-Over-Threshold
> (analog information for position interpolation only requires 3 – 4 bit resolution)

Measured noise (pre-production run) for 3 shaping times

100 ns:	Q_n= 350 el + 42 el/pF
200 ns:	Q_n= 333 el + 35 el/pF
400 ns:	Q_n= 306 el + 28 el/pF

Simulated vertex resolution
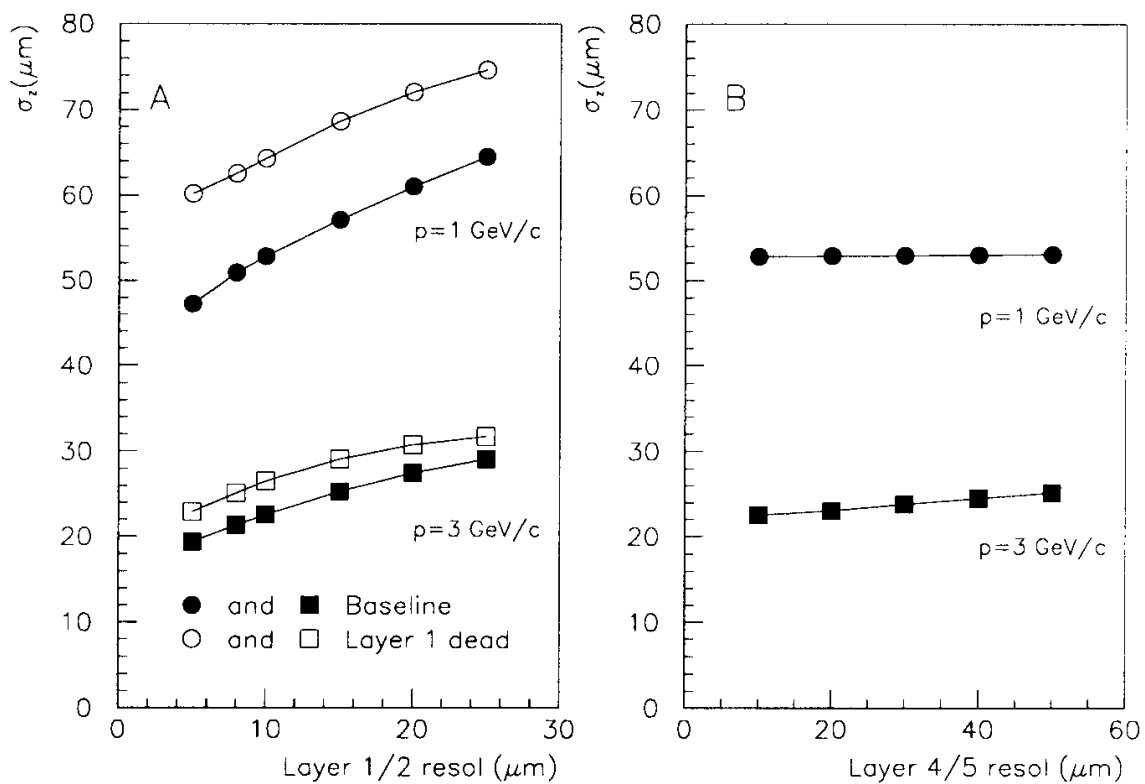
ATLAS Semiconductor Tracker (LHC)

Total rate of tracks in the detector: ~ $3 \cdot 10^{10}$ s^{-1}
     (hit rate at $r_\perp = 14$ cm: ~ 10^7 cm^{-2}s^{-1})

Pixels at small radii (4, 11, 14 cm) to cope with
- high event rate (2D non-projective structure)
- radiation damage
     small capacitance ~ 100 fF $\Rightarrow$ low noise $Q_n \approx 200$ el

Strips at larger radii (30, 37, 45, 52 cm) - minimize material, cost

Pixels and strips provide primary pattern recognition capability

Straw drift chambers at outer radius (56 – 107 cm)
    ~70 layers yield 40 space points at large r and augment pattern
    recognition by continuous tracking (least expensive solution)
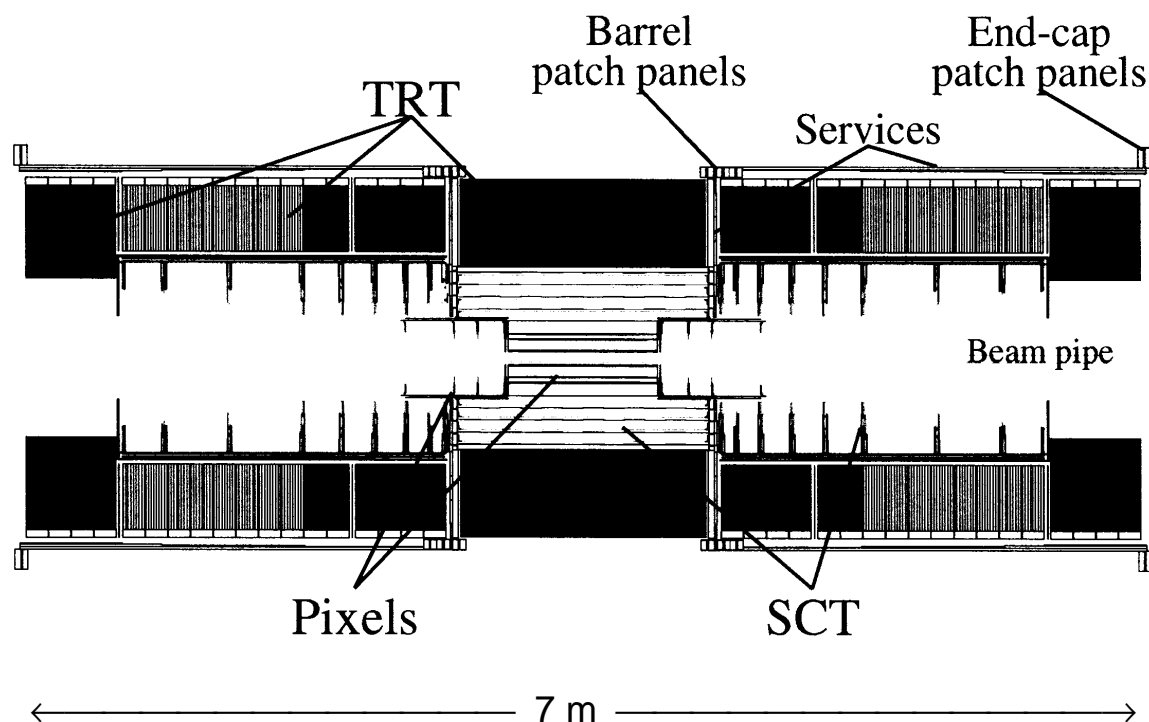
Strip modules use back-to-back single-sided detectors with small-angle stereo (40 mr) to provide z-resolution with negligible "ghosting".

Resolution provided by 3 detector types in barrel

	$R\phi$	z
Pixels	12 μm	66 μm
Strips	16 μm	580 μm
Straws	170 μm	—

Segmentation $\Rightarrow$ Large number of data channels

Total number of channels and area

Pixels	1.4×10^8 channels	2.3 m^2
Strips	6.2×10^6 channels	61 m^2
Straws	4.2×10^5 channels	

But, ...
only a small fraction of these channels are struck in a given crossing

Occupancy for pixels, 50 μm x 300 μm:

4 cm Pixel Layer	4.4×10^{-4}
11 cm Pixel Layer	0.6×10^{-4}

Occupancy for strip electrodes with 80 μm pitch, 12 cm length:

30 cm Strip Layer	6.1×10^{-3}
52 cm Strip Layer	3.4×10^{-3}

Strips + Pixels: many channels

    Essential to minimize

        power
        material (chip size, power cables, readout lines)
        cost (chip size)
   failure rate (use simple, well controlled circuitry)

    Goal is to obtain adequate position resolution, rather than the best possible

    $\Rightarrow$ Binary Readout

   detect only presence of hits

        identify beam crossing

Architecture of ATLAS strip readout

    Pipeline clocked at LHC crossing frequency of 40 MHz
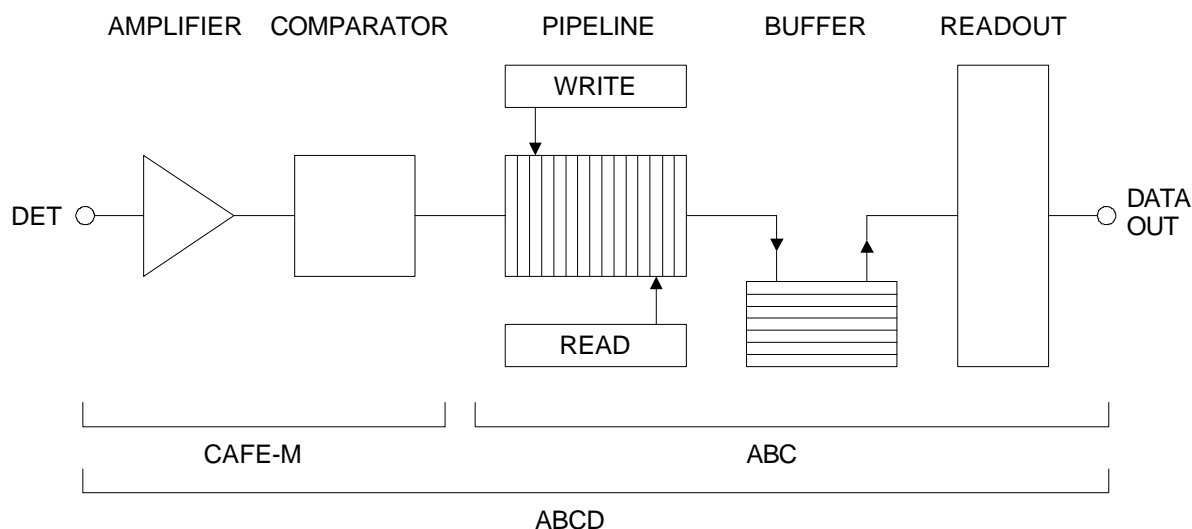
Two implementations with same functionality:

    2 chips: CAFE-M   (analog, BJT)   LBNL, UCSC
        + ABC   (digital, CMOS)   RAL, UCSC, LBNL

    1 chip: ABCD   (analog + digital, BiCMOS)
        Cracow, CERN

ATLAS SCT test detector module

readout ICs   wire-bonds   silicon detector
↓   ↓   ↓
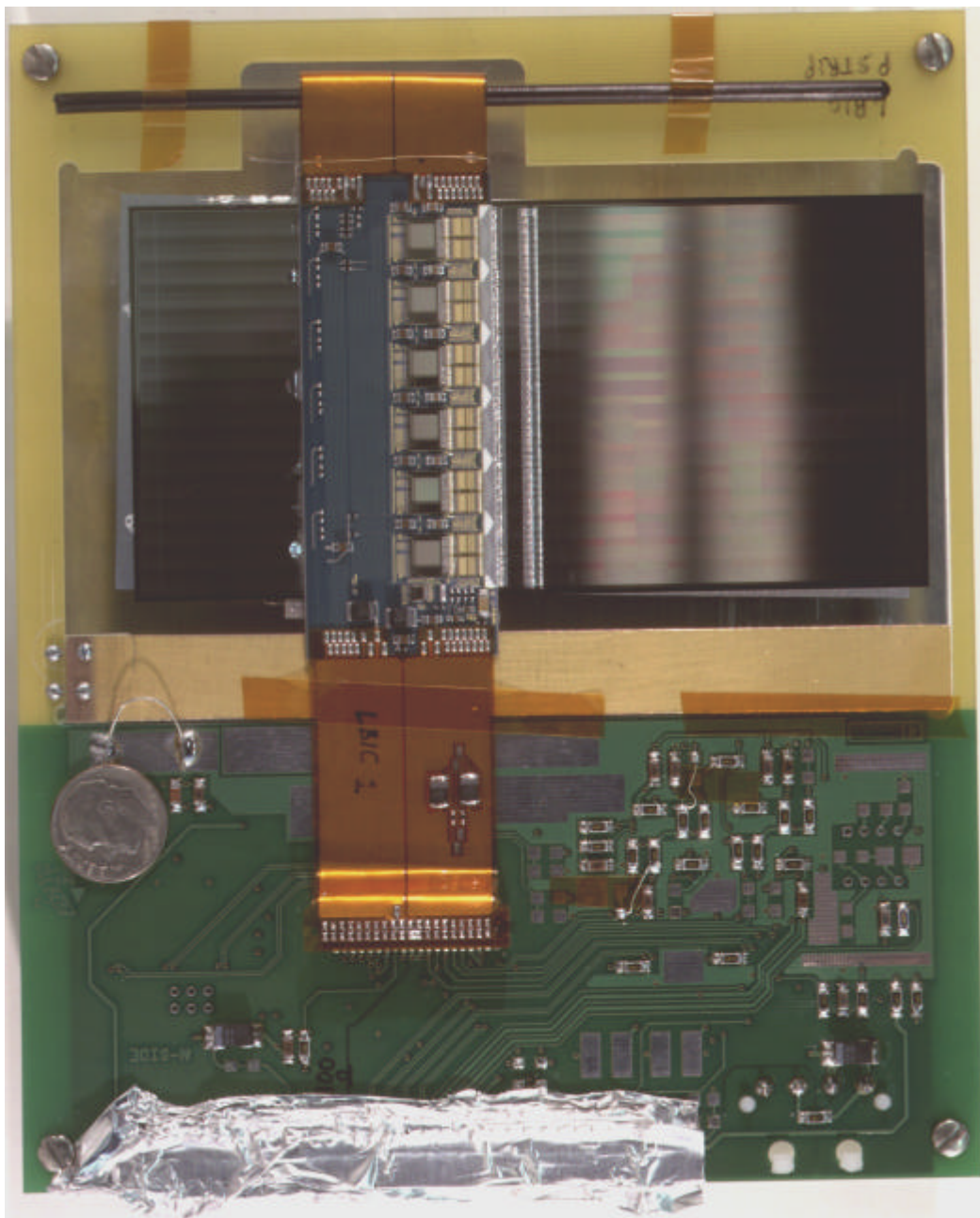
The module is mounted in a pc-board support frame to facilitate handling during test. The module itself is the rectangular object in the upper half of the picture.

Block diagram of CAFE chip
(LBNL, UCSC)

PREAMP   GAIN/SHAPER   COMPARATOR

DET.   OUTPUT

TEST INPUT   THRESHOLD
                                     ADJUST
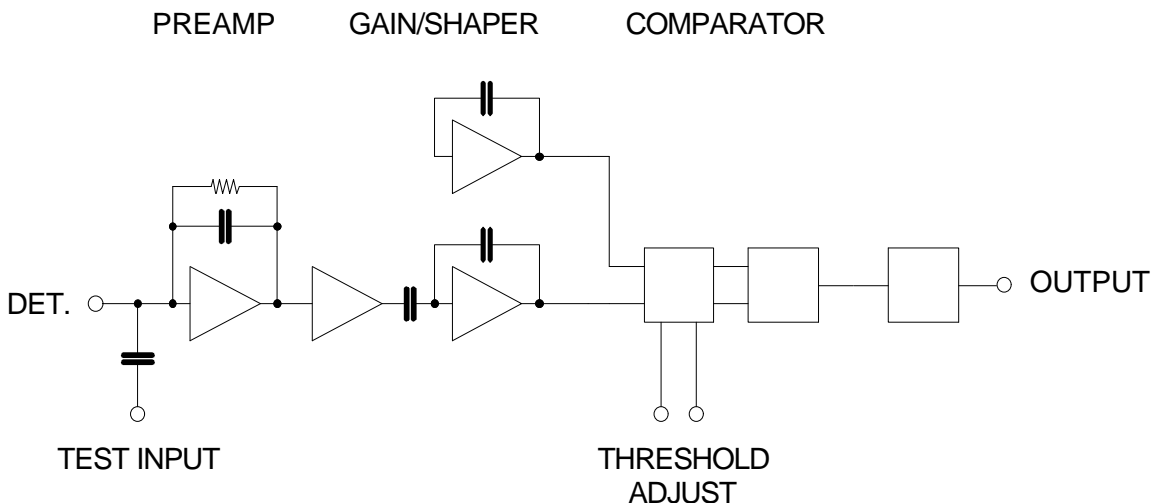
- 128 ch, bondable to 50 μm strip pitch

- bipolar transistor technology, rad-hard
    $\Rightarrow$ minimum noise independent of shaping time*

- peaking time: 25 ns (equivalent CR-RC^4)

- double-pulse resolution (4 fC – 4 fC):   50 ns

- noise, timing: following slides

- 1.3 to 1.8 mW/ch (current in input transistor adjustable)

- die size: 6.4 x 4.5 mm^2

see: I. Kipnis, H. Spieler and T. Collins, IEEE Trans. Nucl. Sci.
    NS-41/4 (1994) 1095-1103
    and http://www-atlas.lbl.gov/strips/strips.html for more info.

* see http://www-physics.lbl.gov/~spieler/physics_198_notes

Detector Model for Noise Simulations
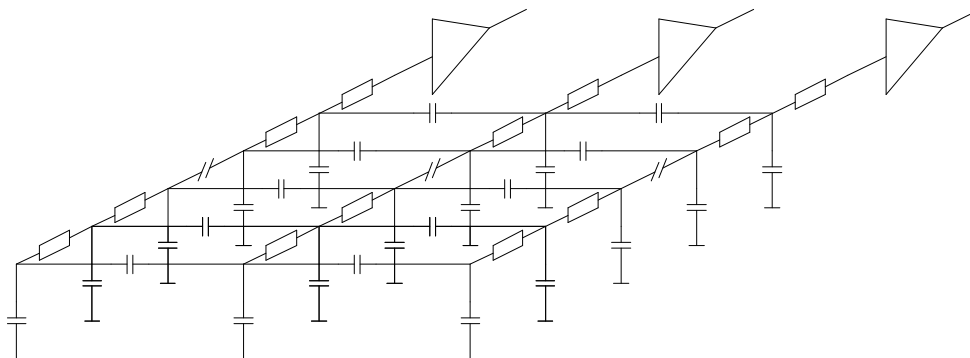
Analyze signal and noise in center channel.

Includes: Noise contributions from neighbor channels
             Signal transfer to neighbor channels
             Noise from distributed strip resistance
   Full SPICE model of preamplifier

Measured Noise of Module

Simulation Results
(p-strips on n-bulk)

1460 el (150 μA)

1230 el (300 μA)

(before irradiation)
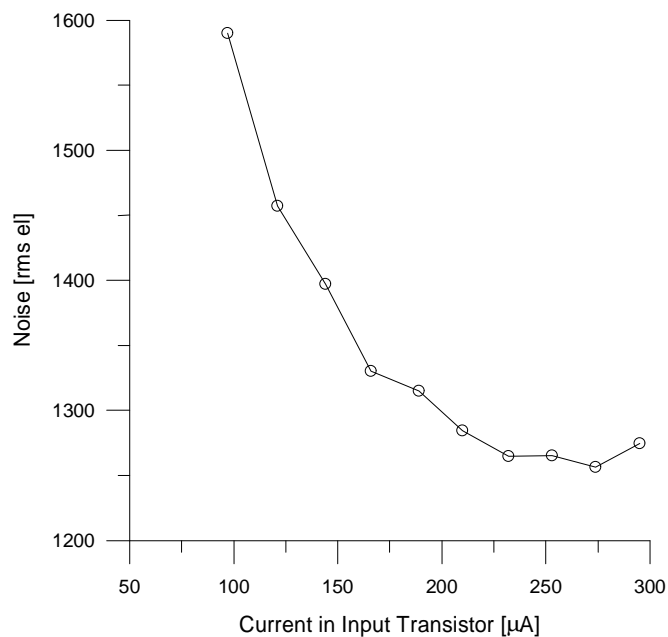
Noise Occupancy vs. Threshold

Module with CAFE chip in test beam position at KEK

Q$_n$ = 1320 el

Noise Occupancy (y-axis)

Threshold Squared [fC^2] (x-axis)
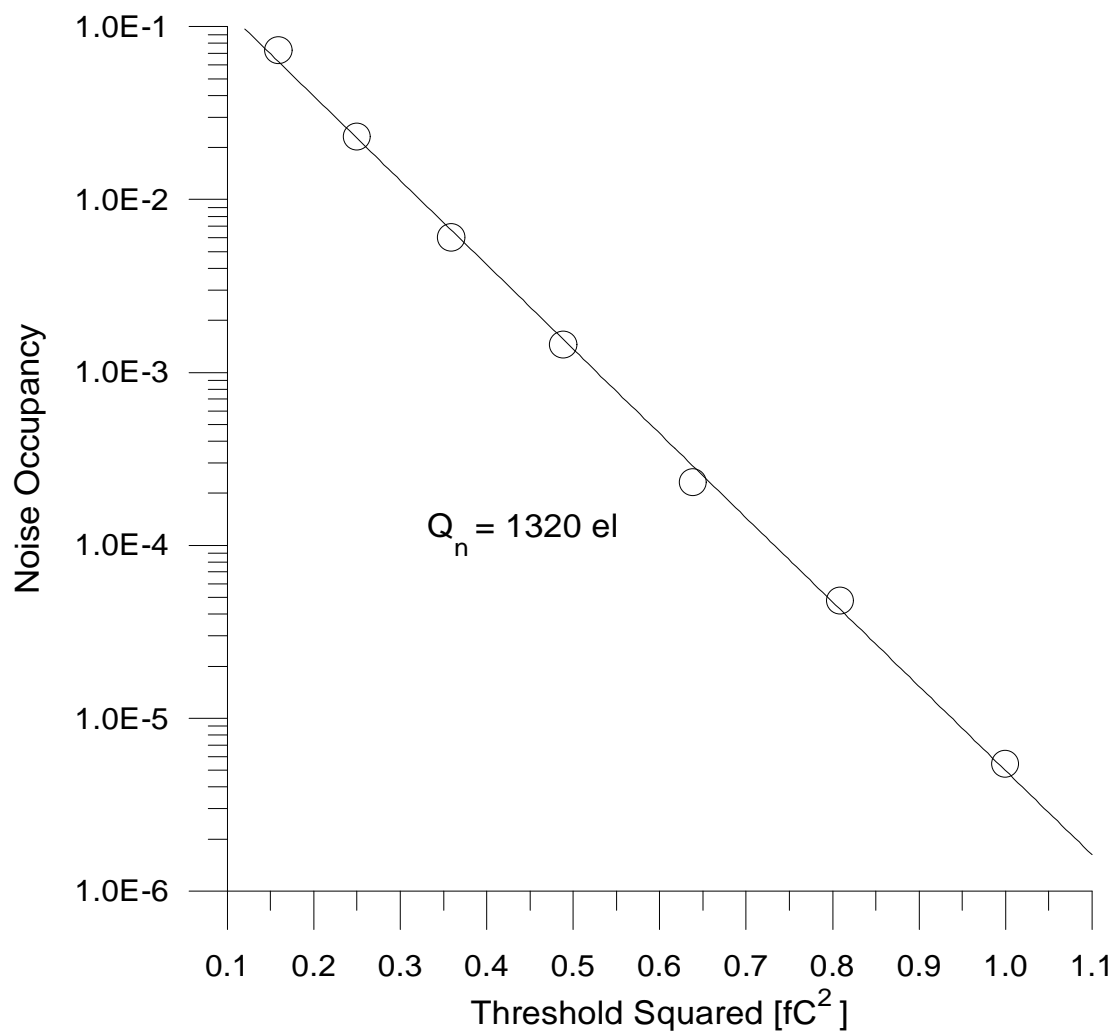
Baseline fluctuations, digital cross-talk

$\Rightarrow$ deviations from straight line plot
(gaussian noise)

CAFE Noise Before and After Irradiation

Measured on full-size modules (12 cm strips)

ATT7 and ATT8 use old ATLAS baseline detector configuration:

n-strip on n-bulk, AC coupled (fab. by Hamamatsu)

    ATT7   detector uniformly irradiated to 10^{14} cm^{-2} (MIP equiv)
                      CAFEs irradiated to 10^{14} cm^{-2} (MIP equiv)

    ATT8   CAFEs from run 2
                    non-irradiated reference module

Noise measured on complete modules (ATT7 at about -10 $^\circ$C)

measurement site	ATT7 chip 0	ATT7 chip 1	ATT8 chip 0	ATT8 chip1
LBNL, 28-Jun-96	1440 el	1380 el	1375 el	1435 el
H8 beam line, 15-Jul-96	1470 el	1380 el	1350 el	1410 el
H8 beam line, 7-Aug-96	1400 el	1375 el	1400 el	1375 el

Electronic calibration (~ 10% absolute accuracy)

CAFE Timing Performance

1. Chips from run 1 measured on test boards

- **irradiated to 10^{14} cm^{-2} (MIP equiv)**

Time Walk   16 ns (1.25 - 10 fC) at 1 fC threshold
1.25 - 4 fC: 12 ns
4 fC - 10 fC: 4 ns

Jitter at 1.25 fC $\approx$ 4 ns FWHM

Total time diistribution (99% efficiency)
confined within about 18 ns.

2. Chips from Run 2 measured on test boards (pre-rad)

C_{load}= 15 pF, 1 fC threshold, jitter as above
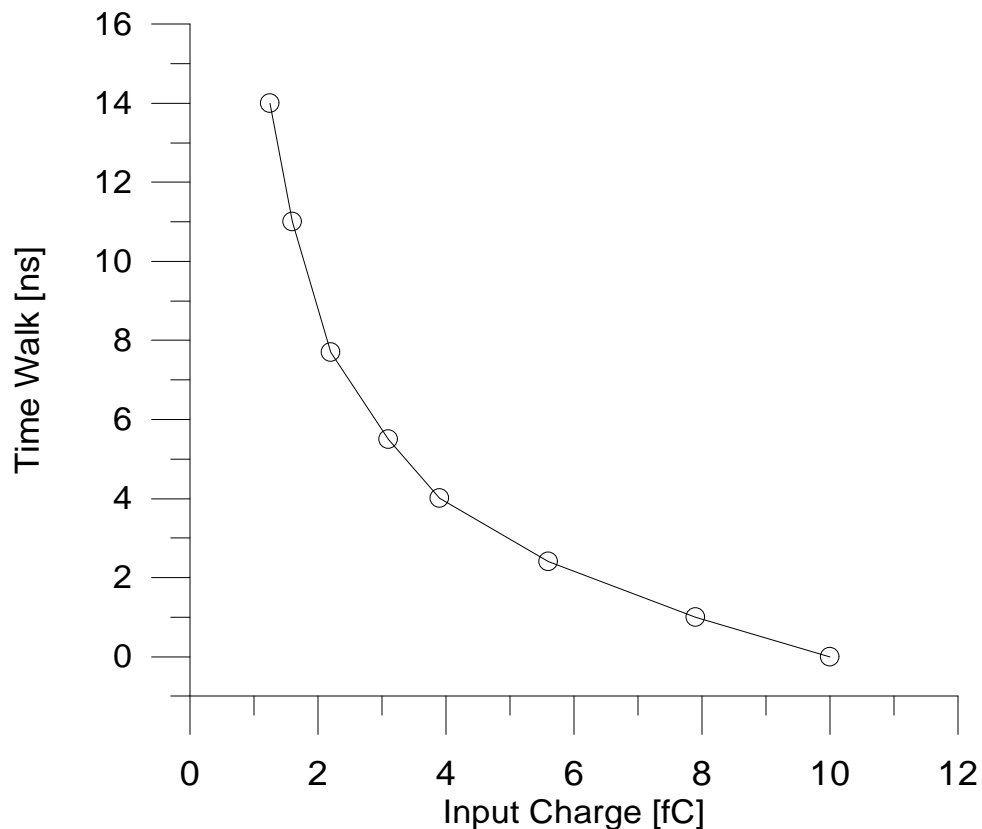
Test Beam Data

Tracking Efficiency vs. Occupancy for Full-Length Modules

non-irradiated module

ATT8 EFFICIENCY & OCCUPANCY
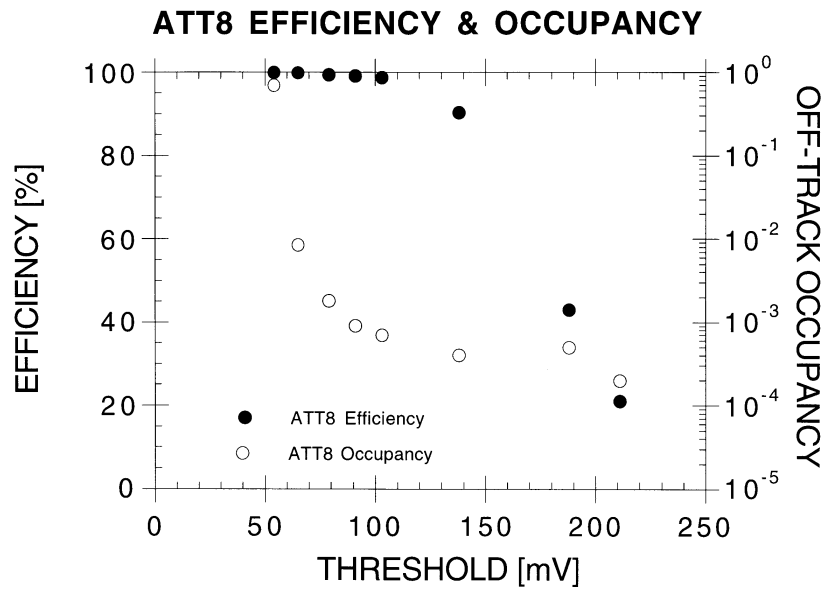
irradiated module ($\Phi = 10^{14}$ cm^{-2})

ATT7 EFFICIENCY & OCCUPANCY
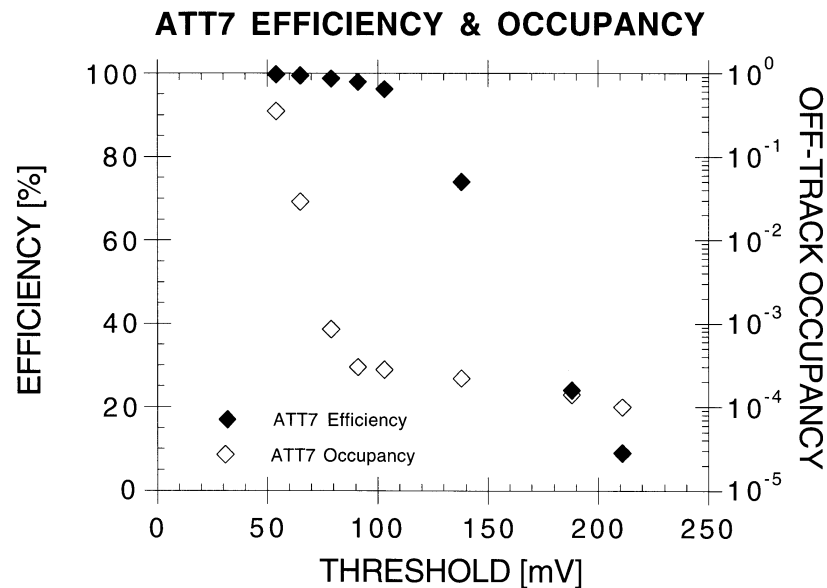
Two-Dimensional Detectors

1. Two-Dimensional Projective Devices

Example: Crossed strips on opposite sides of Si wafer
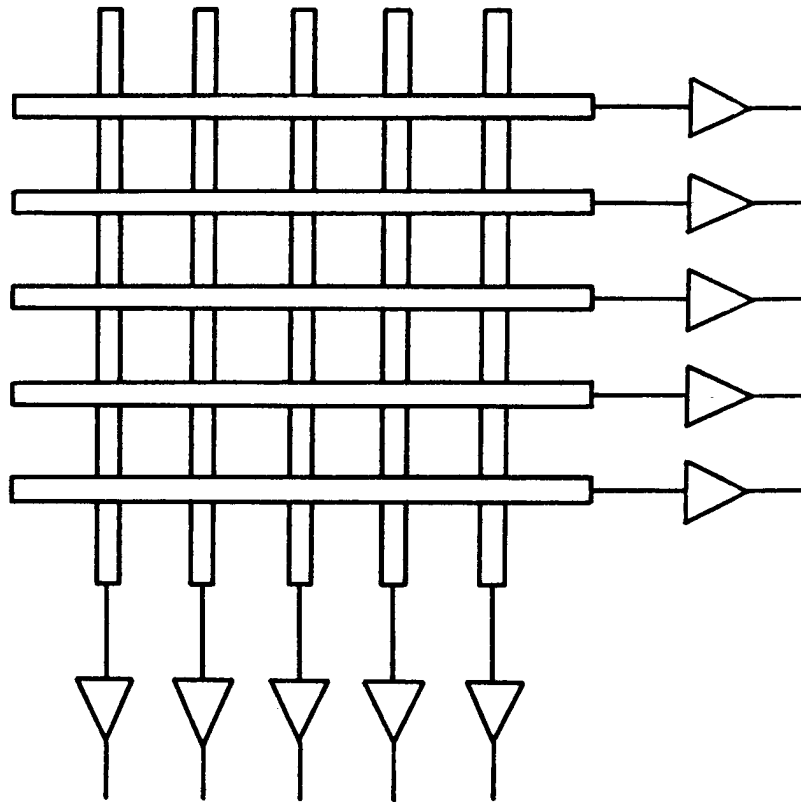
n readout channels $\Rightarrow$ n^2 resolution elements

Problem: ambiguities with multiple hits

n hits in acceptance field $\Rightarrow$ n x-coordinates

n y-coordinates

$\Rightarrow$ n^2 combinations

of which
$n^2 - n$ are "ghosts"

"Ghosting" can be reduced by small angle stereo at the expense of longitudinal resolution.

2. Non-Projective 2D Arrays

a) CCDs (talk by Chris Damerell) - limitations: readout time
radiation resistance

b) Random–Access Pixel Arrays

Amplifier per pixel

Address + signal lines read out individually addressed,
i.e. single, pixels

detector
array

2D contact
grid

amplifier/
readout
array
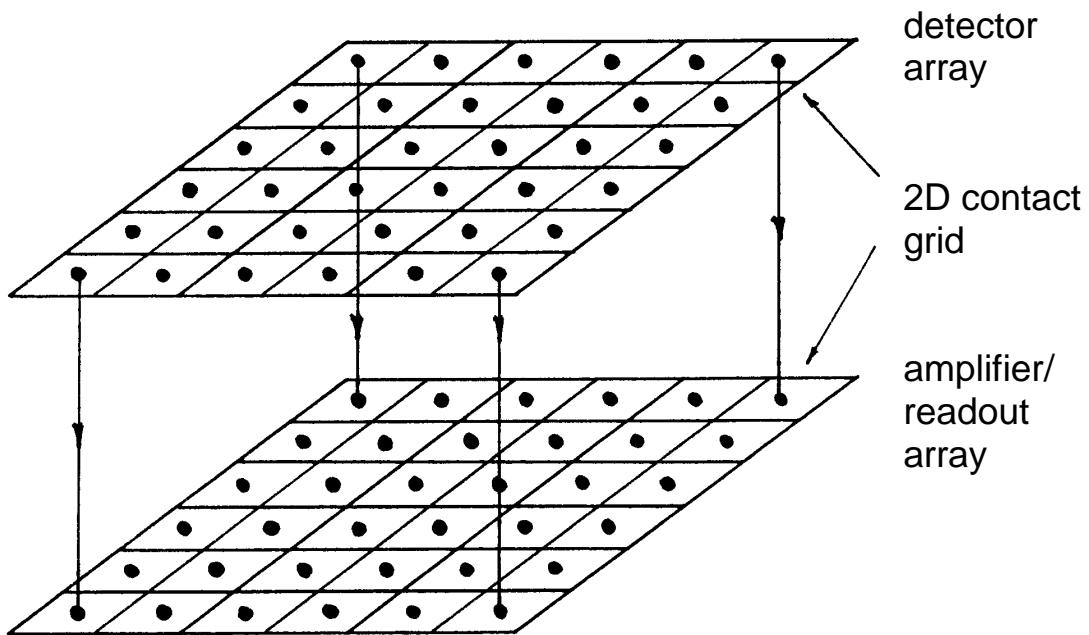
2D contact via "bump bonds"

INCIDENT RADIATION

DETECTOR
CHIP

BUMP
BONDING

AMPLIFIER/
READOUT
CHIP

OUTPUTS
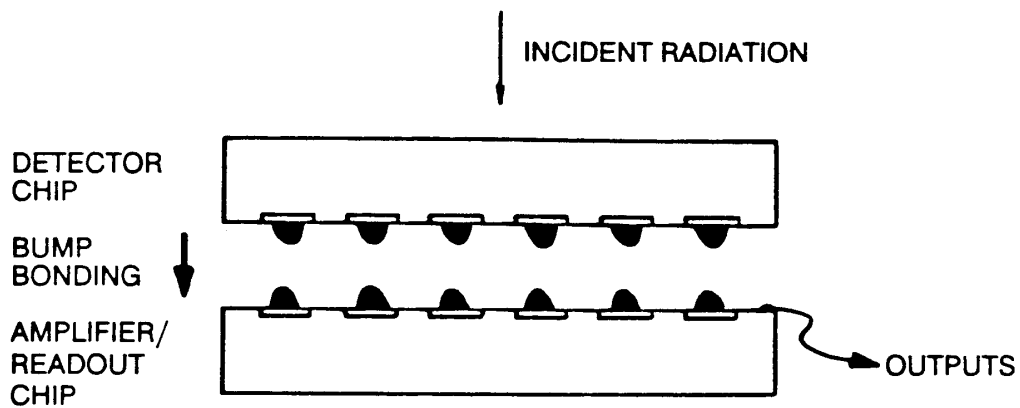
# ATLAS Pixel Detectors
(LBNL, K. Einsweiler, et al.)
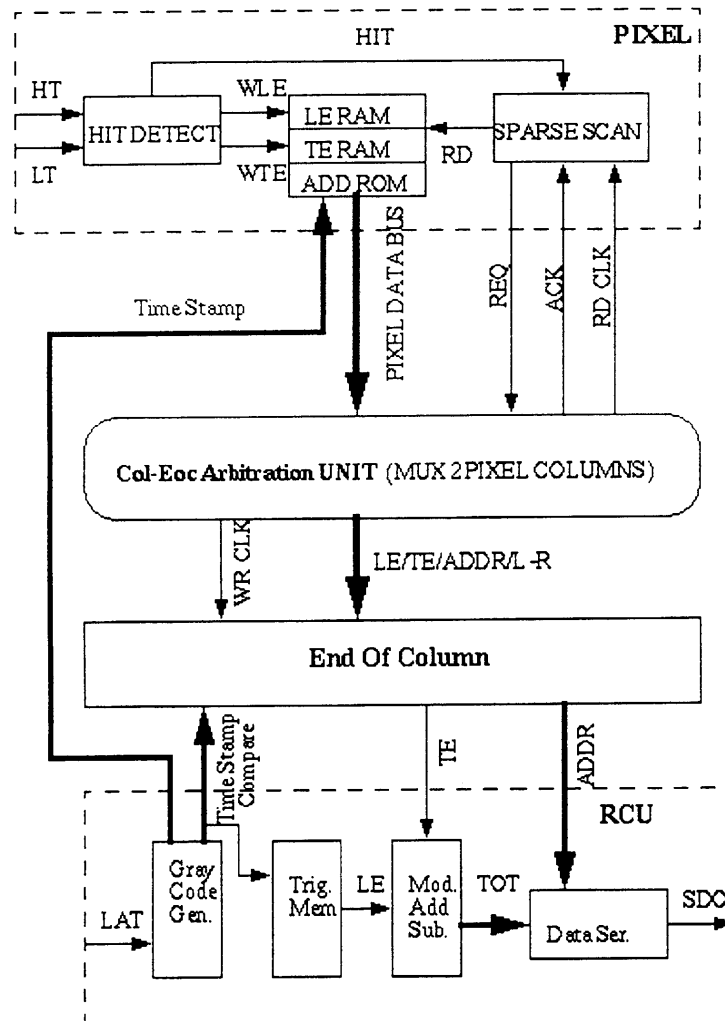
Quiescent state: no clocks or switching in pixel array

When pixel is struck: pixel address is sent to column buffer at chip periphery and time stamped

Receipt of trigger: check to see which addresses are in selected time bin and selectively read out pixels.

Peripheral buffer must be sufficiently large to accommodate all hits (incl. jets) within trigger latency time.

Block Diagram of Pixel Cell
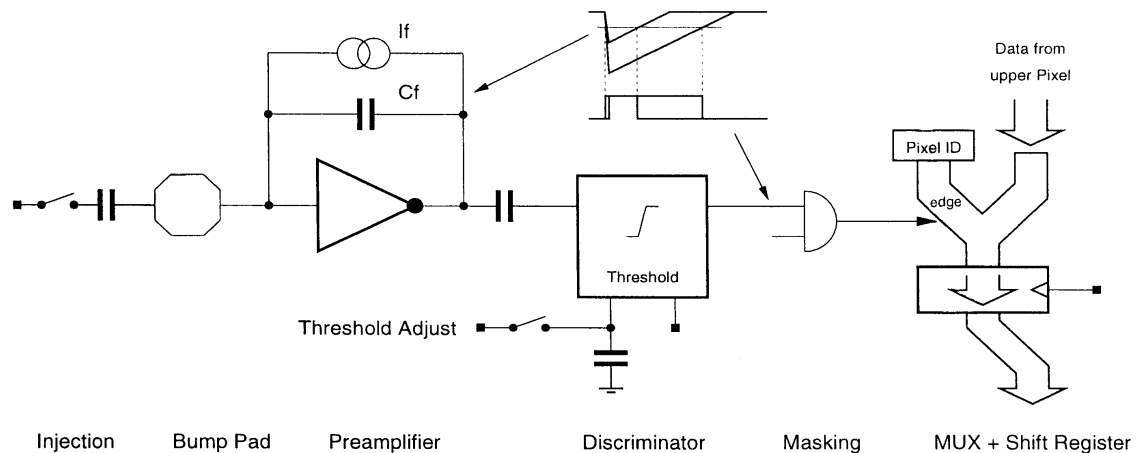
Linear discharge of preamplifier feedback capacitor provides linear
time-over-threshold digitization for readout of analog information.

Pixel size: 50 μm x 300 μm

Power per pixel: < 40 μW

Final chip: 24 columns x 160 pixels (3840 pixels)

Module size: 16.4 x 60.4 mm^2

16 front-end chips per module

61440 pixels per module

Thresholds are trimmed pixel by pixel to maintain uniformity after radiation damage (software, automated).
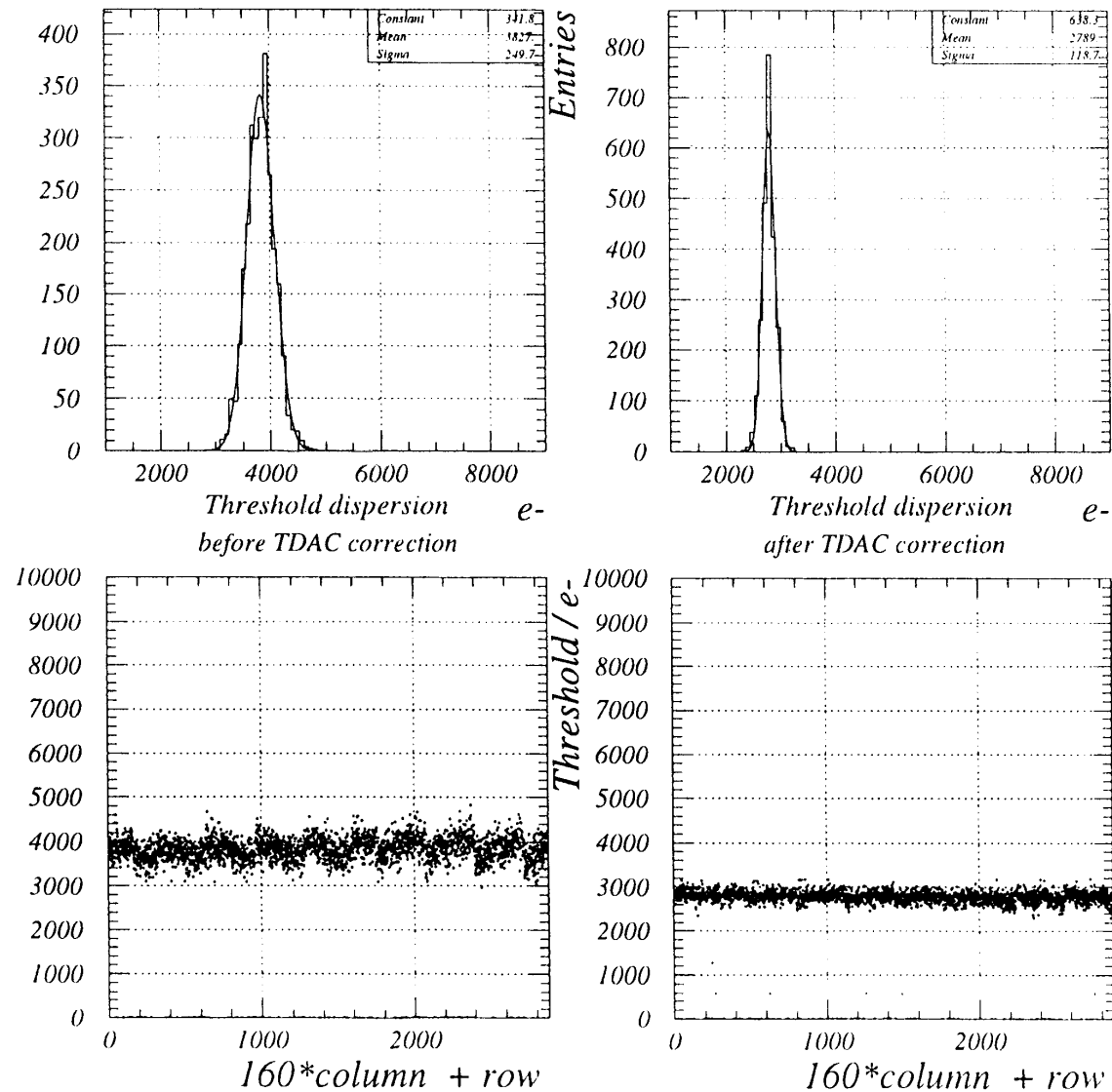
Test Beam Results

Track through single pixel
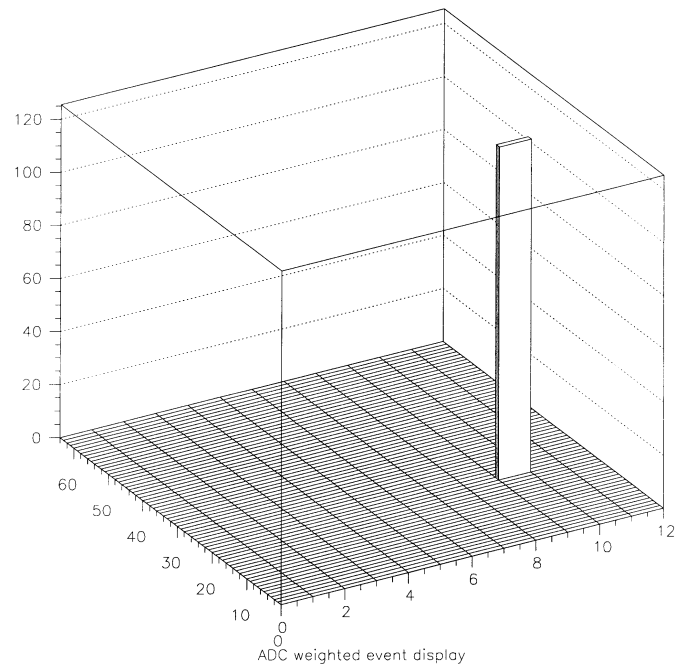
Charge sharing
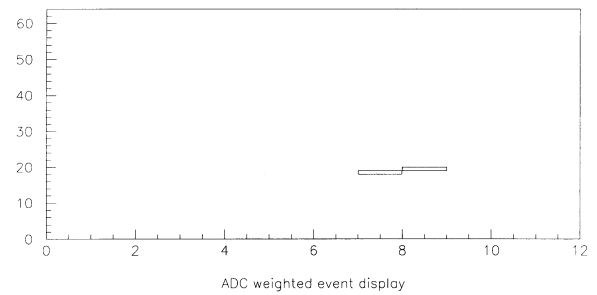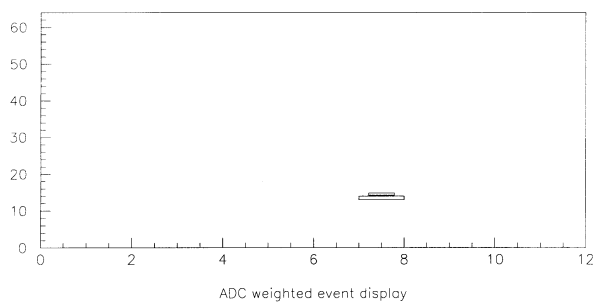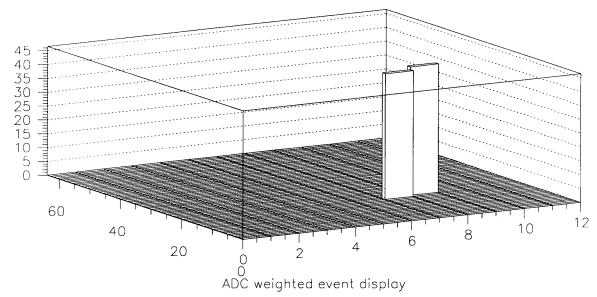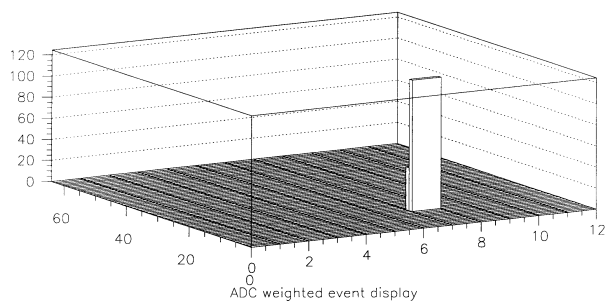
Advantages of pixels at LHC

2D segmentation
⇒ Pattern recognition at small radii

Low capacitance
⇒ high S/N

⇒ allows degradation of both detector signal and
electronic noise due to radiation damage

small detector elements
⇒ detector bias current per element still small
after radiation damage

Drawback:

Engineering complexity order of magnitude greater than
previous chips

Questions

What is the ultimate limit of radiation resistance?

detectors
other materials? diamond, SiC?
cryogenic operation?

electronics
CMOS beyond 100 Mrad?
cryogenic operation?